3/12/85 07

NASA TECHNICAL NOTE

NASA TN D-3074

c.1

NASA TN D-3074

AN INVESTIGATION OF HEAT TRANSFER WITHIN REGIONS OF SEPARATED FLOW AT A MACH NUMBER OF 6.0

by Paul F. Holloway, James R. Sterrett, and Helen S. Creekmore

Langley Research Center
Langley Station, Hampton, Va.

NATIONAL AERONAUTICS AND SPACE ADMINISTRATION • WASHINGTON, D. C. • NOVEMBER 1965

AN INVESTIGATION OF HEAT TRANSFER WITHIN REGIONS OF SEPARATED FLOW AT A MACH NUMBER OF 6.0

By Paul F. Holloway, James R. Sterrett,
and Helen S. Creekmore

Langley Research Center
Langley Station, Hampton, Va.

NATIONAL AERONAUTICS AND SPACE ADMINISTRATION

For sale by the Clearinghouse for Federal Scientific and Technical Information
Springfield, Virginia 22151 – Price $3.00

AN INVESTIGATION OF HEAT TRANSFER WITHIN REGIONS OF SEPARATED FLOW AT A MACH NUMBER OF 6.0

By Paul F. Holloway, James R. Sterrett,
and Helen S. Creekmore
Langley Research Center

SUMMARY

An extensive systematic investigation of the heat transfer associated with regions of laminar, transitional, and turbulent separation has been conducted on sharp- and blunt-leading-edge flat plates at a Mach number of 6.0 over a free-stream unit Reynolds number range of approximately 1×10^6 to 8×10^6 per foot. Separated regions were forced by forward- and rearward-facing steps, and by 10°, 20°, 30°, and 40° wedges located in several longitudinal positions on the plate.

It has been shown that upon proper classification of the several types of separated flow, the trends of the heating rates within the regions of separation may be characterized by typical distributions which are essentially independent of the model geometry (except to the extent that the model-geometry variations affect the location of transition). In particular, the local heating in the separation region is less than or greater than that on the flat plate without separation for the case of pure laminar or turbulent separation, respectively.

Methods are not available which can give a complete explanation of the mechanism of separation and the resulting effects on many of the important aerodynamic parameters such as heat transfer. However, it has been shown that careful classification of the type of separation and application of existing methods of prediction will yield reasonable predictions of the magnitudes and trends of many of the important heat-transfer parameters in the separation region and on the surface of the wedges placed on the flat plate.

INTRODUCTION

Boundary-layer separation is a common phenomenon in aerodynamics that will occur on any surface where the pressure rise and pressure gradient are sufficiently large. The importance of this phenomenon has long been recognized and results of many theoretical and experimental investigations of the problem are available in the literature. (See, for example, refs. 1 to 13.) The complexity of the separation flow field has, however, prevented a complete solution to the

problem of prediction of separation effects on the various aerodynamic parameters. The importance of the problem has been increased by the current interest in flares and control surfaces for stabilization and aerodynamic control of various flight configurations at hypersonic speeds.

The importance of transition on the behavior of parameters within a separation region has been recognized (see ref. 3) and has led to the classification of regions of separation into three types: (1) pure laminar, (2) transitional, and (3) turbulent. The effects of these types of separation on heat transfer are not as well documented as those on pressure distributions, particularly at high supersonic and hypersonic speeds. The experimental laminar heat-transfer results of references 14 and 15 have agreed very well with Chapman's prediction of the average heat transfer in a region of laminar separated flow (ref. 16). However, very little information is available at hypersonic velocities for the cases of transitional and turbulent separation. More experimental data are needed for separated boundary layers, particularly for transitional and turbulent separation to provide a check on the validity and range of applicability of the theoretical methods of prediction available and to act as a guide for a more generalized theoretical approach to the problem of predictions of heat transfer within the separated region.

Much of the previous experimental work on separation has been conducted on flat plates. Analyses of these results has led to questions concerned with the three-dimensional-flow effects in separation. A discussion of three-dimensional effects is out of the scope of this paper; however, such a discussion is given in reference 2. In reference 2, it is pointed out that although more research on this subject is needed, two-dimensional-flow models often yield results which may be utilized to give estimations of flow parameters for other more practical geometries which are not two dimensional in nature. It is also pointed out that the detailed physical process of separation is probably three dimensional even for essentially two-dimensional models. Although flat-plate studies have their limitations, such studies offer the opportunity to investigate experimentally complex problems under conditions where many variables may be easily changed.

The purpose of this paper is to present the results of an extensive, systematic, experimental investigation of the heat transfer in regions of laminar, transitional, and turbulent separation obtained on an unswept flat plate at a free-stream Mach number of 6.0 with a ratio of wall temperature to stagnation temperature of approximately 0.55. The experiments were conducted in two wind tunnels which together had a free-stream unit Reynolds number range of approximately 1×10^6 to 8×10^6 per foot. Model geometries tested were forward- and rearward-facing steps and 10°, 20°, 30°, and 40° wedges. The tests were conducted on an unswept flat plate with three degrees of leading-edge bluntness (including a sharp leading edge). Tests were conducted in the Langley 20-inch Mach 6 tunnel and in the Langley variable-density Mach 6.2 blowdown jet.

Both local and average heat-transfer parameters are presented, and the effects of classification of the separated regions into laminar, transitional, and turbulent are discussed. Also, peak heating in the separated regions and on the wedges is discussed. Finally, the results are compared with several theoretical and semiempirical methods of prediction.

SYMBOLS

A_1, A_2	coefficients of T' equation (see appendix A)
C_f	local skin-friction coefficient
C_F	average skin-friction coefficient
c_p	specific heat of air at constant pressure
C_p	pressure coefficient defined on local conditions, $\frac{p_w - p_o}{q_o}$
c_w	specific heat of wall material
h	local heat-transfer coefficient
H	step height
k	vertical height of roughness above plate
K_3	correlation function in heating-rate equation due to pressure gradient (see ref. 24)
M	Mach number
N_{Pr}	Prandtl number
N_{St}	local Stanton number (see eq. (4)) based on free-stream conditions
p	pressure
q	dynamic pressure
$\dot{q}$	experimental heating rate
$\dot{q}_t$	stagnation heating rate calculated for a sphere with 1-foot radius (see ref. 22)
$\bar{\dot{q}}$	integrated experimental heating rate, $\int_{x_1}^{x_2} \dot{q}\, dx$
r	recovery factor (see eq. (3))
R	Reynolds number, $\frac{\rho u x}{\mu}$

R_∞ free-stream Reynolds number per foot, $\frac{\rho_\infty u_\infty}{\mu_\infty}$

$R_{\infty,d}$ free-stream Reynolds number based on distance from leading edge of plate to beginning of step or wedge, $\frac{\rho_\infty u_\infty x_d}{\mu_\infty}$

$R_{\infty,x}$ free-stream Reynolds number based on distance from leading edge, $\frac{\rho_\infty u_\infty x}{\mu_\infty}$

$R_{o,d}$ Reynolds number based on conditions at outer edge of boundary layer upstream of disturbance effects and on distance from leading edge of plate to beginning of step or wedge, $\frac{\rho_o u_o x_d}{\mu_o}$

s lateral spacing of roughness elements (fig. 1(c))

l longitudinal surface length of wedges

t average diameter (thickness) of leading edge

T temperature

T' reference temperature

u velocity component of flow parallel to surface of plate

x longitudinal distance along plate measured from leading edge

x_d longitudinal distance from leading edge to beginning of disturbance (step or wedge)

x_j longitudinal surface distance from junction of wedge leading edge and plate (positive values measured downstream along wedge, negative values measured upstream of wedge along plate)

α angle of attack, positive values indicate compression on instrumented surface

β leading-edge wedge angle

γ ratio of specific heats of air

θ_w local wall thickness

μ viscosity

ρ density

τ time

ϕ	wedge angle

Subscripts:

d	disturbance (wedge or step)
fp	flat-plate conditions
j	junction of wedge and plate
lam	laminar
max	maximum measured value
o	local conditions at outer edge of attached boundary layer or at outer edge of separation
p	plateau conditions for laminar separation, or first peak condition for turbulent separation
r	recovery
s	separation
t	stagnation
T'	based on reference temperature
trans	transition
turb	turbulent
v	virtual origin
w	wall (local)
x	distance from leading edge
∞	free stream
ϕ=0	wedge angle equals zero
1	beginning of separation
2	beginning of step

Primes denote parameters evaluated at reference temperature T'.

APPARATUS AND TEST METHODS

Wind Tunnel

The test program was conducted in the Langley 20-inch Mach 6 tunnel and in the Langley variable-density Mach 6.2 blowdown jet (referred to in figures as tunnels 1 and 2, respectively). The Langley 20-inch Mach 6 tunnel is the intermittent type exhausting to the atmosphere through a diffuser augmented by an air ejector. Tests were run with tunnel stagnation pressures of 365, 440, and 515 pounds per square inch absolute with stagnation temperatures of approximately 940° R to 1040° R. The models were essentially isothermal at room temperature and had a T_w/T_t variation of 0.53 to 0.59. A more detailed description of the tunnel is given in reference 6.

In order to extend the test Reynolds number range below that obtainable in the 20-inch Mach 6 tunnel, additional tests were conducted in the variable-density Mach 6.2 blowdown jet. However, tests for a given model configuration and Reynolds number were not duplicated in the two tunnels. This tunnel is also of the intermittent type exhausting to a 40,000-cubic-foot sphere which can be pumped to pressures as low as 1 millimeter of mercury absolute. Tests were run with tunnel stagnation pressures of approximately 65, 115, 165, 215, 265, 365, and 515 pounds per square inch absolute with stagnation temperatures of 840° R to 1020° R. A more detailed description of the tunnel is given in reference 17.

Models

The models consisted of unswept flat plates constructed from stainless steel. Each plate was 9 inches wide and approximately 11 inches long. Plate number 1 was a continuous plate with a sharp leading edge ($t = 0.0015$ inch) mounted on a support plate as shown in figure 1(a). The remaining models consisted of plate number 2 with interchangeable leading edges (fig. 1(b)). Leading-edge piece A was sharp and $t = 0.0015$ inch. Leading-edge pieces B and C were blunt and $t = 0.120$ inch and $t = 0.375$ inch, respectively. In order to trip the boundary layer and obtain turbulent separation data, several sharp leading edges ($t < 0.004$ inch) were tested with various size roughness located 2 inches from the leading edge. (See ref. 18 for effect of roughness.) The spheres were glued into small spherical segment indentations in the leading-edge piece. The location, spacing, height above the plate, and diameter of the spheres is given in figure 1(c) along with a sketch of the model assembly consisting of plate number 2, a leading-edge piece, and the support plate.

After completion of the test program in the 20-inch Mach 6 tunnel, the model assembly, as shown in figure 1(b) (that is, the plate 2 assembly), was cut down to overall dimensions of $7\frac{1}{2}$ inches wide and $10\frac{1}{2}$ inches long to be tested in the smaller variable-density Mach 6.2 blowdown jet.

The forward-facing steps utilized in these tests had a span of 7 inches and a chord of 1.15 inches. (See fig. 1(a).) For most of the tests, the step

height was 0.25 inch. However, a limited quantity of data has been obtained on steps of height 0.125 inch and 0.40 inch. For the tests on plate 1, the step locations along the plate were varied and were at distances x_d from the leading edge of the plate to the leading edge of the step of 2.94, 6.70, and 9.44 inches. Two longitudinal positions were used for the tests of plate 2 with x_d = 6.69 and 9.58 inches. The rearward-facing step was located at a distance of x_d = 2.9 inches. The step was built into the sharp-leading-edge piece as shown in figure 1(d). Two step heights were tested, H = 0.125 and 0.250 inch.

Four wedge angle ramps (10°, 20°, 30°, and 40°) were tested with a span of 7 inches and a wedge (ramp) surface length of 1.5 inches. (See fig. 1(a).) The following table gives the distances in inches from the leading edge of the plate to the leading edge of the wedge for the four wedge angles tested.

Wedge angle, ϕ, deg	x_d, plate 1			x_d, plate 2
	Forward	Middle	Rear	Middle
10	2.98	6.71	9.47	6.44
20	3.02	6.77	9.53	6.44
30	3.13	6.88	9.63	6.50
40	3.31	7.04	9.78	6.81

Two models of each plate were constructed - one instrumented with 0.050-inch inside-diameter pressure orifices and the other with 30-gage iron-constantan thermocouples. The instrumentation on plate 1 began at a distance of 1.35 inches from the leading edge, and on plate 2 at a distance of 3.25 inches from the leading edge. (See fig. 1(e).) The 0.25- and 0.40-inch forward-facing steps and the wedges were instrumented similarly. (Instrumentation was located only on the upper surface of the forward-facing step.) The 0.125-inch forward-facing step was not instrumented. All instrumentation was located chordwise along the center line of the models. The undersurface of each plate instrumented with thermocouples was slotted along the center line to a width of 0.6 inch and had a surface skin thickness of approximately 0.020 inch on the plates and 0.032 inch on the wedges and steps in order to minimize the lateral heat conduction in the skin.

The back of the wedges and steps from which the thermocouple leads were taken was always shielded from the flow.

Test Methods and Techniques

For most tests, the models were positioned at a nominal angle of attack of 0°. However, some tests were conducted in the 20-inch Mach 6 tunnel with the model with the forward-facing step at a nominal angle of attack of 8° compression and this condition resulted in a local free-stream Mach number upstream of

the disturbance of 4.9 for the sharp-leading-edge models. The accuracy of angle of attack was $\pm 1/4^{\circ}$. However, the angle of attack is considered to be invariant for each group of tests since the mounting was not altered.

The approximate ratio of wall temperature to free-stream temperature outside the attached boundary layer for the heat-transfer tests is given in the following table:

Leading edge	α, deg	Approximate T_w/T_o
A	0	4.5
A	8	3.3
B,C	0	1.7

The free-stream unit Reynolds numbers tested in the 20-inch Mach 6 tunnel were approximately 5.6×10^6, 6.9×10^6, and 8.0×10^6 per foot. The free-stream unit Reynolds numbers tested in the Mach 6.2 blowdown jet were approximately 7.7×10^6, 5.6×10^6, 4.2×10^6, 2.7×10^6, 2.0×10^6, and 1.2×10^6 per foot.

Pressure tests.- Pressure distributions along the center line of the plates were obtained in both tunnels over the test Reynolds number range. In the 20-inch Mach 6 tunnel the local static pressures on the plates were measured by connecting the orifices to pressure-switching devices which in turn connected the orifice in sequence to electrical pressure transducers. The electrical outputs from the transducers were recorded on a digital readout recorder. Each pressure-switching device was connected to two transducers with ranges of 1 and 5 pounds per square inch absolute.

In the variable-density Mach 6.2 blowdown jet, the orifices were connected directly to the transducers and the pressure readings were recorded as described. All pressure tests were run on the same support system as was used for the heat-transfer tests.

Heat-transfer tests.- The aerodynamic heating was determined by the transient calorimetry technique by which the rate of heat storage in the model skin is measured. The models, originally at room temperature or slightly cooler, were suddenly exposed to the airflow by quick injection from a sheltered position beyond the tunnel wall. Injection was accomplished in less than 0.25 second and the model remained in the tunnel for approximately 4 seconds. Unpublished results of tests in the Langley 20-inch tunnel on sharp-leading-edge plates with and without end plates have indicated virtually no effect of end plates on heat transfer within turbulent separation regions for the type of models utilized in this investigation. (Note that all instrumentation is located on the model center line.) End plates were not used in this investigation so that schlieren and shadowgraphs of the flow might be obtained.

Optical methods.- During the pressure and heat-transfer tests in the 20-inch Mach 6 tunnel, shadowgraphs and schlieren photographs were often taken to aid in determining the extent of the regions of separated flow.

DATA REDUCTION

The electrical outputs from the thermocouples were recorded on a high-speed digital readout recorder. The reading from each thermocouple was recorded at 0.025-second interval, converted to a binary digital system, and recorded on magnetic tape. The temperature-time data were fitted to a second-degree curve by the method of least squares, and the time derivative of temperature was computed on a card-programed computer.

The tunnel stagnation temperature range was approximately 840° R to 1040° R and the wall temperature of the plate was approximately 550° R. Because of the short time required for the injection of the model, the plates were considered to have been subjected to a step function in the applied heat-transfer coefficient. The thin-skin equation used to calculate the local surface heating rate was

$$\dot{q} = c_w \rho_w \theta_w \frac{dT_w}{d\tau} \tag{1}$$

The measured local heat-transfer coefficient was then calculated by the relation

$$h = \frac{\dot{q}}{T_r - T_w} \tag{2}$$

in which conduction effects are neglected and where T_r is the calculated recovery temperature defined as

$$T_r = T_o\left(1 + M_o^2 r \frac{\gamma - 1}{2}\right) \tag{3}$$

where T_w is the measured wall temperature, and M_o is the local Mach number outside the boundary layer calculated from the measured pressure distribution (a normal shock-pressure loss for the blunt-leading-edge models and no pressure loss for the sharp-leading-edge models being assumed). This method was considered adequate since the measured heat-transfer coefficient is rather insensitive to small errors in M_o. The recovery temperature T_r was calculated by assuming a recovery factor equal to 0.824 in the laminar region and 0.879 in the turbulent region. The Stanton number was calculated by the use of the equation:

$$N_{St} = \frac{h}{\rho_\infty u_\infty c_{p,\infty}} \tag{4}$$

based on free-stream conditions ahead of the model. (Note that both measured or calculated Stanton numbers are always based on free-stream conditions ahead of the model.)

The experimental heat-transfer parameters $\dot{q}$, h, and N_{St} presented in this report were determined by reading the slope of the temperature-time curve at a time approximately 0.05 second after the model was in position in the 20-inch tunnel and 0.20 second after the model was in position in the variable-density Mach 6.2 blowdown jet. The maximum surface temperature increase on the plates and steps was generally less than 15° and on the wedges generally less than 25°. The nearly isothermal conditions of the tests kept the lateral conduction to a minimum.

RESULTS AND DISCUSSION

It has been shown previously by several investigators (for example, ref. 3) that a meaningful analysis of the pressures in a separated region on a flat plate can be obtained for separation forced by many geometric shapes if the flow is properly classified as laminar, transitional, or turbulent. For example, the plateau pressure for laminar separation and the first peak pressure for turbulent separation are nearly independent of the geometry of the disturbance that forces the separation of the boundary layer at supersonic and hypersonic speeds. (See also ref. 19.) The variation of these laminar- and turbulent-separation pressure parameters with Mach number as determined by equations taken from reference 19 are presented in figure 2. The equations of reference 19 fit a summary of experimental data taken without any or moderate surface cooling. (Surface cooling, of course, affects the boundary layer, and experimental data have shown that large surface cooling has an effect on separation. See, for example, refs. 2 and 11.) In figure 2, examples of pressure distributions illustrating typical laminar and turbulent separation cases taken from reference 6 are presented. It has been shown in reference 6 that the first peak pressure for the case of transitional separation can vary from slightly above that for pure laminar separation to a value approximately equal to that for turbulent separation depending upon the position of transition relative to the separation point.

The heating-rate distribution in separated-flow regions obtained for several model geometries over a wide range of Reynolds number is presented in the following sections. By using a classification system for the heat-transfer data similar to that previously established for pressure results, a meaningful analysis of the separation-heating-rate results may also be obtained.

Typical Separation Heat-Transfer Distributions

Characteristic examples of the heating-rate distributions for the three types of separation as determined by the location of boundary-layer transition (ref. 3) are presented in figure 3. The model used to obtain these data was a sharp-leading-edge flat plate with a forward-facing step. The faired

heating-rate distributions for the flat plate without the step are shown for comparison. The pressure distributions and schlieren photographs of the flow field are also shown in figure 3. Values of the laminar plateau pressure and the turbulent peak pressure calculated from the equations of reference 19 (assuming $M_o = 6.0$) are indicated on the pressure plots of figures 3(a) to 3(c) to aid in classifying the types of separation.

A comparison of the measured pressure data in figure 3(a) with the calculated laminar plateau value is sufficient to classify the separation region as laminar in nature. As mentioned earlier, however, the value of the peak pressure within a separation region is not always sufficient to determine whether the flow in that region is transitional or turbulent. The peak pressure value measured in figure 3(b) indicates that the separation could be turbulent in nature. Additional certainty of this turbulent nature was available from the study of reference 18 which indicated that the flow on this plate (without the step) with the roughness trip employed and at the same test Reynolds number was turbulent over the full extent of the instrumented area.

Finally, the separation data shown in figure 3(c) was classified as transitional based on the heating-rate distribution on the plate without the step, the experimental pressure distribution on the plate with the step, the length of the separation region indicated by the schlieren photograph, and by the heating-rate distribution with the step. The pressures in the separated region first increase to a value similar to that expected for laminar separation and then increase to much higher values, which are, however, below the expected peak pressure for turbulent separation. This pressure distribution is characteristic of one type of transitional separation as described in reference 3.

Detailed study of the various experimental data obtained in this investigation has indicated that one of the more simple ways to detect and classify separation is to observe the local heating-rate distributions in the separated region relative to the distribution obtained on the same model under similar conditions without the geometry which forces the separation. Therefore, for the remainder of this report, the separated flow is classified as "pure laminar," turbulent, or transitional according to the following definitive conditions based on the separated heating-rate distributions (the reattachment region being neglected):

(1) Pure-laminar separated flow: The local heating rates in regions of laminar separation decrease below those heating rates obtained under similar conditions on a plate with attached flow once separation has occurred and remain less than the equivalent attached case on a smooth plate throughout the separation region as shown in figure 3(a). This definition is supported by the previous work of Nicoll (ref. 14) and Larson (ref. 15) for cavity-type separation models and by the work of Miller, et al. (ref. 12), for outwardly deflected control surfaces. Not too much importance should be attached to the absolute value of the lowest heating rate since theoretically the skin friction drops to zero at the separation point (see, for example, ref. 20) and the lowest heat-transfer values obtained are, at least partially, a function of the stability of the separated flow with time.

(2) Turbulent separated flow: Upon separation, the local heating rates increase rapidly above those obtained on the reference plate, peak, and then decrease slightly with increasing distance from the separation point (that is, increasing Reynolds number) as shown in figure 3(b). Near the base of the step, where the pressures increase, the heating rates peak again. (See, for example, refs. 3 and 21.) The points in the distribution referred to as the first peak heating rate and the second peak heating rate for turbulent separated flow are indicated in figure 3(b). This trend of heating-rate distributions for turbulent separation is similar to that already established for pressure distributions in regions of turbulent separation by Chapman, et al., in reference 3; that is, the local pressures upon separation increase rapidly to a peak value without experiencing any small initial pressure rise similar to that obtained for transitional separation.

(3) Transitional separated flow: It has been established in previous pressure work (see, for example, ref. 3) that the pressure distribution within a region of transitional separation is strongly dependent upon the location of the transition region in relation to the separation and reattachment points. If the beginning of transition is near reattachment, the resulting separation pressure distribution will be approximately that expected for laminar separation. If the transition region is near the separation point, the separation pressure distribution will be similar to that expected for turbulent separation. Analysis of the results of reference 3 indicates that if the beginning of transition is downstream of separation and the end of transition is upstream of reattachment, the pressures will first increase to a plateau pressure; then upon transition the pressures increase rapidly (but less quickly than for turbulent separation) and finally peak as is typical of turbulent separation.

In the same manner, if the beginning of transition is downstream of separation and the end of transition is upstream of reattachment, the heat-transfer distribution within the separation region may be divided into three distinct areas. An example of this type of transitional separation is shown in figure 3(c). In region 1, the local heating rates follow the trend noted as characteristic of laminar separation, that is, decreasing and remaining below the attached flow values prior to the occurrence of transition. In region 2, the heating rates increase rapidly until a peak occurs that signals the approximate end of transition. (This region is considered to be bounded by the approximate beginning and ending of transition.) Finally, in region 3, the local heating rates follow the trends noted as characteristic of turbulent flow. When the beginning of fully developed turbulent flow is located sufficiently far upstream of reattachment, first- and second-peak heating rates will be obtained as is the case for turbulent separation. These peak values are indicated in figure 3(c).

Other examples of the variation in heating-rate distributions obtainable for transitional separation as determined by the location of transition relative to the separation and reattachment points are presented in figures 3(d) and 3(e). Apparently, in figure 3(d) the end of transition is near the reattachment point and the distribution shown in region 3 of figure 3(c) is not obtained. In figure 3(e), the beginning of transition is apparently near the separation point and the trends noted in regions 1 and 3 of figure 3(c) are not obtained.

(However, the instrumentation does not extend sufficiently far upstream to rule out the existence of the trends indicated in region 1 of figure 3(c).) For the cases of transitional separation similar to those shown in figures 3(d) and 3(e) (that is, when the end of transition is sufficiently far downstream that the distribution of region 3 does not occur), the highest heating rate is referred to as the peak heating rate for transitional separation. These peak heating rates are indicated in figures 3(d) and 3(e).

Heat Transfer Associated With Steps

Forward-facing steps.- In examining the heat transfer in a region of transitional separation, it must be remembered that many factors are known to influence the position of transition. Therefore, care must be taken in determining the position of transition under the various conditions. The data presented in figures 4 to 8 present additional separated heating-rate distributions obtained under many conditions over a wide range of Reynolds numbers; however, if properly classified, the data follow the trends previously discussed. The faired data presented in these figures represent the flat-plate heating-rate distributions for similar free-stream conditions to those for which the separation data were obtained. The theoretical laminar heating-rate distributions obtained by the reference temperature method reviewed in appendix A of this report are shown in figures 4 to 8 for comparison purposes. Also presented in the figure for reference is the calculated stagnation heating rate of a 1-foot-radius sphere at the same free-stream conditions as determined by the method of reference 22. In each case, the heating rates in the attached regions for the configurations with steps agree well with the flat-plate data at the same Reynolds number prior to separation and agree reasonably well with the laminar theory prior to transition.

Figure 4 presents the effect of step location on the separation heating-rate distributions for a sharp-leading-edge ($t = 0.0015$ inch) model at local Mach numbers of 6.0 and 4.9 and at three unit free-stream Reynolds numbers (the step height is 0.25 inch). In figure 4(a), with the model at an angle of attack of 0° ($M_o = 6.0$), the separation regions are transitional in nature for the step in the front and middle position at the three Reynolds numbers of the test. The trends of distributions (fig. 4(a)) within the regions of separation are the same as those previously discussed for transitional separation (fig. 3(c)). With the step in the rear position, it is difficult to classify the flow because it is borderline between transitional and turbulent conditions. In figure 4(b) with the model at an angle of attack of 8° ($M_o = 4.9$), the separation regions are transitional for the case of the step forward. (See fig. 3(e).) The heating-rate distribution for the turbulent separation with the step in the middle and rearward positions is similar to that discussed in figure 3(b).

In order to obtain additional data on heating-rate variation within regions of turbulent separation, tests were run with various size boundary-layer trips located 2 inches from the sharp leading edge of the model with the 0.25-inch step located in the rearward position. The results of these tests are presented in figure 5. The trips utilized were the three-dimensional controlled-surface-roughness (spheres) leading-edge pieces used in the investigation reported in

reference 18. From figure 5, the forward movement of the "virtual origin" of turbulent flow (see ref. 18) as caused by the increasing roughness height is seen to have had virtually no effect on the extent or magnitude of heating of the separation region.

The separated heating-rate distributions are presented in figure 6 for the models with varied leading-edge bluntness and with the 0.25-inch step in the rearward position at 0° and 8° (compression) angle of attack at the maximum unit free-stream Reynolds number. The separation data for the sharp leading edge ($t = 0.0015$ inch) in figures 6(a) and 6(b) are turbulent in nature. For both angles of attack, the heating-rate distributions follow the trends presented as typical of turbulent separation. The 8° (compression) angle of attack yields a higher local unit Reynolds number (an increase of approximately 39 percent) and caused the transition to move forward on the plate.

The effects of blunting the leading edge to a thickness diameter of 0.12 inch (fig. 6) is to reduce the local Reynolds number at the edge of the boundary layer sufficiently to give laminar flow over the smooth plate at both angles of attack. The laminar theoretical heating-rate distribution was calculated by assuming a normal-shock pressure loss and that the flow had expanded back to free-stream pressure. The resulting separation regions obtained for the model with the 1/4-inch forward-facing step are transitional in nature, the beginning of transition being located significantly far forward of reattachment. Each heating-rate distribution follows the expected trends for transitional separation.

Further blunting of the leading edge to a thickness diameter of 0.375 inch apparently caused transition to occur earlier than it did for the thickness of 0.120 inch. In figure 6(a) at an angle of attack of 0°, the flow is laminar over the full length of the smooth plate. The model with the step yields transitional separation which agrees well with the expected trends. However, at an angle of attack of 8° compression, in figure 6(b), transition apparently occurs early on the smooth plate (with no step), fully developed turbulent flow being obtained near the trailing edge of the model. The mechanism by which transition could occur on a model with a $t = 0.375$ inch leading edge but not occur on a model with a $t = 0.12$ inch leading edge at similar test conditions is not fully understood; further investigation of bluntness effects on natural transition at hypersonic Mach numbers seems to be warranted. The separated region shown in figure 6(b) for an angle of attack of 8° and $t = 0.375$ inch is also transitional in nature, but the end of transition is near the separation point so that the heating-rate distribution follows more nearly the trend expected for turbulent separation.

Figure 7 presents the variation in separation heating rates with the three degrees of bluntness over the full test Reynolds number range. For all but the lowest Reynolds number, the separation regions of figure 7(a) are transitional in nature and follow the expected trends. At the lowest free-stream Reynolds number of 1.2×10^6 per foot, the separation region for the sharp leading edge is laminar in nature and the local heating rates remain below the smooth-plate values as expected. For the 0.12-inch-diameter leading edge, in figure 7(b), the increased blunting results in transitional separation only at the maximum

free-stream Reynolds number of approximately 7.8×10^6. Laminar separation regions were obtained for all other Reynolds numbers. In each case, the distributions follow the typical trends.

Again in figure 7(c) for the 0.375-inch-diameter leading edge, the increased blunting results in transitional separation occurring earlier than it did for the 0.12-inch-diameter leading edge. Transitional separation regions were obtained for $R_\infty = 7.7 \times 10^6$, 5.6×10^6, 4.1×10^6 per foot. Laminar separation regions were obtained for the lower Reynolds numbers (below $R_\infty = 4.1 \times 10^6$). The heating-rate distributions agree with the typical trends presented previously.

The effects of step-height variation on the magnitude of the separation heating rates and on the extent of the separation region for the sharp-leading-edge model are shown in figure 8. In figure 8(a), the data for the 0.125-inch step might be classified as either laminar or transitional in nature whereas the data for the 0.25-inch step are definitely transitional in nature. When the step height was increased from 0.125 inch to 0.25 inch, the resulting peak separation heating rates for the 0.25-inch step are approximately 5 to 6 times as large as those for the 0.125-inch step.

With the steps located in the rear position and the model at an angle of attack of 0° (fig. 8(b)), the steps create regions of transitional separation which at maximum Reynolds number are very close to turbulent conditions. The separation regions associated with the 0.40-inch step are somewhat larger than those associated with the 0.25-inch step.

With the steps located in the rear position and the model at 8° (compression) angle of attack, as shown in figure 8(c), the separation regions are all turbulent in nature. The separation region resulting from 0.40-inch step is larger than that resulting from the 0.25-inch step, but there is less difference between the two regions for turbulent separation than was found in figures 8(a) and 8(b) for transitional separation.

Rearward-facing steps.- Two rearward-facing steps (with heights of 0.125 inch and 0.25 inch located at $x_d = 2.9$ inches) were tested at free-stream Reynolds numbers of approximately 1.3×10^6 and 2.8×10^6 per foot. The heating-rate distributions for the rearward-facing steps are presented in figure 9. Also presented for comparison are the distributions obtained on a sharp-leading-edge smooth plate at comparable free-stream conditions and the theoretical laminar heating-rate distribution for a smooth plate. In figure 9(a) for the 0.125-inch step, the separated regions are laminar for both Reynolds numbers. The heating rates are initially less than the attached flow values and gradually recover back to slightly less than the attached-flow values near the approximate reattachment region as indicated by the schlieren photographs. For the separated heating rates for the 0.25-inch step in figure 9(b), the heating rates in the reattachment region exceeded the attached flow values found on the smooth plate and remain greater than these reference values. It has been shown in reference 23 that these two types of distribution are to be expected for models with rearward-facing steps at supersonic Mach numbers with various Reynolds numbers. The present investigators believe that when the

maximum heating values near reattachment and downstream of reattachment are much larger than the values for the smooth plate, transition from laminar to turbulent flow has occurred or is occurring. As evidence of this effect, there is also plotted in the figure the turbulent heating-rate distribution found on the same plate without a step in the same tunnel at approximately the same Reynolds number with a roughness trip of $k = 0.080$ inch located 2.0 inches from the leading edge. (See ref. 18.) Comparison of the 0.25-inch step data at $R_\infty = 2.7 \times 10^6$ per foot with the turbulent plate data shows rather conclusively that transition to turbulent flow has occurred near the reattachment region for these conditions. An example of rearward-facing steps being used to promote transition is also given in reference 3.

Transition was not given as an explanation of the difference between the two types of distributions in reference 23. Rather, the value of $\frac{x_d}{H\sqrt{R_{o,d}}}$ was represented as the parameter which determines the relation of the heating rates downstream of reattachment to those at similar conditions on a smooth plate. Maximum heating-rate values were found in reference 23 to be less than the smooth-plate values when $\frac{x_d}{H\sqrt{R_{o,d}}} > 0.067$ and greater than the smooth-plate values when $\frac{x_d}{H\sqrt{R_{o,d}}} < 0.067$. The values of this parameter for the present investigation are given in figure 9 where it can be seen that values of $\frac{x_d}{H\sqrt{R_{o,d}}} < 0.0197$ caused the heating-rate values in the reattachment region to be greater than the smooth-plate values. The parameter $\frac{x_d}{H\sqrt{R_{o,d}}}$, therefore, appears to be ineffective in predicting the results of the present investigation. Analysis of the present results would indicate that any significant increase in heat transfer downstream of a rearward-facing step would be associated with the promotion of transition caused by the step. (See also ref. 3.)

Average heating rates.- Chapman's analysis of the ratio of the average heating rate in a laminar separation region to the average heating rate for laminar attached flow (ref. 16) has been shown to give good predictions of the available experimental results for cavity type of separation models. In particular, the results of Larson in reference 15 and of Nicoll of reference 14 give excellent agreement between the experimental results and Chapman's prediction. Figure 10 presents the ratio of the measured integrated heating rate in the separated region to the measured integrated heating rate for attached flow under similar free-stream conditions. The slight differences in the free-stream total pressure and temperature have been considered by a correction factor $(\dot{q}_t)_{fp}/(\dot{q}_t)_s$. The integrated heating rates have been obtained for the separation region only, the reattachment and the heating on the face of the step being neglected. The experimental heating rates are plotted as a function of the Reynolds number based on conditions at the edge of the boundary layer on

the smooth plate and the distance from the leading edge of the model to the beginning of the step. For the blunt-leading-edge plates, the local flow was assumed to have passed through a normal shock, and resulted in a nominal Mach number of 3.16.

The solid symbols on the left of figure 10 represent the pure laminar separation data obtained in this investigation. The solid line represents the value of the ratio as predicted by the theoretical analysis of Chapman. The theory is seen to predict the experimental data reasonably well. In particular, the numerical average of the current experimental results agrees very well with the prediction. (An approximate correction to these experimental values to account for the pressure rise due to separation would be to divide these values by $\sqrt{p_w/p_o}$ as discussed in references 12 and 24. However, it would make only a small difference for these particular cases since the value of $\sqrt{p_w/p_o}$ is only about 10 percent above unity.) Hence, a theory that was derived for laminar separation within a cavity, also gives a reasonably good prediction of the integrated heating ratios for laminar separation forced by a forward-facing step.

The open symbols shown in the middle of figure 10 represent the transitional separation data. The integrated heating-rate ratios for transitional separation increase rapidly with increasing Reynolds number from the laminar value of approximately 0.5 to a peak value on the order of 2 or greater. The scatter of the transitional data is thought to be at least partially due to the difference in the transition position caused by the bluntness of the leading edge and by the presence of the step (as compared to the transition position for the smooth plate).

The solid symbols on the right of figure 10 represent the turbulent separation data. Also shown in this figure are theoretical predictions of the integrated heating-rate ratio for turbulent separation based on a rather arbitrary assumption. This assumption is that the local Stanton number remains constant streamwise across the separation point. (See appendix B for more details.) Therefore,

$$\left(\frac{h}{\rho_o u_o C_{p,o}}\right)_{\text{Before separation}} = \left(\frac{h}{\rho_o u_o C_{p,o}}\right)_{\text{Edge of separation region}} \tag{5}$$

The values of ρ_o and u_o at the edge of the separation region can be estimated from nonviscous equations if the static pressure in the separation region is known and may be predicted by the equation

$$C_{p,p} = 0.13 - \frac{1.5}{M_o^2} + \frac{9.1}{M_o^3} \tag{6}$$

which is taken from reference 6 for this Mach number range. Comparison of the prediction with the experimental data indicates that this simple method of prediction gives a good approximation of the magnitude of the experimental results.

The maximum values of the transitional separation data in the ratio form shown in figure 10 are due, at least in part, to the laminar or near-laminar average heating rates for the smooth flat plate which were used to nondimensionalize the separation data; that is, the separation forced by the step can move the transition region forward. Therefore, to gain a better insight into the true relative magnitudes of the integrated heating rates for the three types of separation, figure 11 presents the integrated heating rates for separation in dimensional form as a function of $R_{o,d}$.

In figure 11(a), the separation data obtained with models at an angle of attack of 0° are presented. Examination of this figure indicates that once transitional separation occurs, the integrated heating rates increase rapidly with Reynolds number and reach a peak for the case of turbulent separation. For the case of 8° compression angle of attack, the data obtained (fig. 11(b)) were all turbulent in nature.

Local Stanton number distribution for turbulent separation.- It has been shown in figure 10 that the simple assumption that the local Stanton number remains constant streamwise across the separation point together with the assumption that the pressure in the separated region is that given by equation (6) gives a good prediction of the magnitude of the integrated heating-rate ratio for turbulent separated flow. In figure 12, this method of prediction is compared with the streamwise local Stanton number distribution (based on experimental data) for turbulent separation.

Figure 12(a) presents the turbulent separation data for an angle of attack of 0° and for $R_\infty \approx 8 \times 10^6$ per foot. In order to move the beginning of turbulent flow further forward (ref. 18), various height roughness elements were also placed 2 inches from the leading edge for most of the data shown in this figure. The theoretical calculations of Stanton number based on attached turbulent flow shown in the figure were obtained by the methods reviewed in reference 18 and in appendix A of this paper. As was done in reference 18, when the roughness height was sufficiently high so that the beginning of transition was near the roughness position, the theoretical distributions have been calculated by assuming that the boundary-layer virtual origin is located at the roughness position. In figures 12(b) to 12(d) the Stanton numbers based on experimental data are compared with the theoretical prediction for the 0.25-inch step and the 0.40-inch step model at an angle of attack of 8°, for several step locations, and several free-stream Reynolds numbers with and without roughness. As would be expected, the prediction of the separated-flow heat-transfer coefficient (eqs. (5) and (6)) does not give any approximation of the trends of the N_{St} variation within the separation region. However, the comparison of the calculations and data shows that this method of prediction gives an approximation of the magnitudes of local Stanton numbers to be expected within a region of turbulent separation.

Peak Stanton numbers for transitional and turbulent separation.- Another parameter of interest is the peak Stanton number which occurs in the region of separated flow. In figure 13, the peak Stanton numbers in regions of transitional and turbulent separation caused by a forward-facing step are plotted as

a function of Reynolds number based on local undisturbed conditions and the distance from the leading edge of the model to the step. The data of figure 13(a) show that the peak Stanton number for transitional separation increases rapidly with increasing Reynolds number and reaches a peak value slightly greater than that for turbulent separation. The peak Stanton numbers for turbulent separation (second peak heating as defined in fig. 3(b)) decrease with increasing Reynolds number. In figure 13(b), the first peak Stanton numbers for turbulent separation (see fig. 3(b)) show the same decrease in $(N_{St})_{max}$ with increasing Reynolds number found for the second peak Stanton number in turbulent flow. Also in figure 13(b) the first peak Stanton numbers for transitional separation with the beginning of fully developed turbulence sufficiently far upstream of the step (see fig. 3(c)) show the same increase of $(N_{St})_{max}$ with increasing Reynolds number.

Larson in reference 15 has shown for supersonic conditions that although the variation of average Stanton number for turbulent attached flow with Reynolds number follows the expected trend of $N_{St} \propto (R_{o,x})^{-1/5}$, the variation of average Stanton number for turbulent separated flow with Reynolds number shows an increased dependence on Reynolds number with $N_{St} \propto (R_{o,x})^{-2/5}$. In figure 13, lines are presented in the regions for the peak Stanton number in turbulent separated flow that follow the slope given by the assumption that $N_{St,peak} \propto (R_{o,x})^{-2/5}$. Comparison of these slopes with the experimental data shows that within the reasonable limits of data scatter, the peak Stanton number for turbulent separation also varies as a function of $(R_{o,x})^{-2/5}$.

It was shown in reference 18 that the assumption of $N_{St} \propto R_{o,x}$ gave a reasonably good prediction of the Stanton number variation for attached transitional flow. Therefore, also shown in figure 13 in the region of peak heating for transitional separation are the lines with the slope obtained by assuming $N_{St,peak} \propto (R_{o,x})$ for transitional separation. Comparison of these slopes with the data shows that within the reasonable limits of data scatter, the peak Stanton number for transitional separation increases directly with increasing Reynolds number.

The peak values of Stanton number obtained in transitional and turbulent separation regions forced by wedges are also shown in figure 13(a). Comparison of these data indicates that the peak values are smaller for the wedges than for the step. However, the peak Stanton number does increase with increasing wedge angle.

Heat Transfer Associated With Wedge Surfaces

The results presented in figures 14 to 22 represent the heating-rate data obtained when various angle wedges were mounted on the plate for a significant Reynolds number range. Also included in the figures are the faired curves representing data obtained on the flat plate without the wedge under similar

free-stream conditions. Some typical examples of these data are also plotted in figure 23 in the form of the variation of the laminar correlation parameter $N_{St}\sqrt{R_{\infty,x}}$ with the longitudinal distance from the leading edge.

In figure 23, for laminar attached flow on the plate, the parameter $N_{St}\sqrt{R_{\infty,x}}$ has a nearly constant value which is approximately equal to the theoretical laminar value shown at the left of the figure. (See ref. 24 for the calculation method.) Laminar or transitional separation regions occur for the model geometries shown in figure 23 except for the sharp-leading-edge model with a 20° wedge at free-stream Reynolds numbers greater than 4×10^6 per foot. That is, when the flow becomes transitional sufficiently far forward of the 20° wedge (fig. 23(b), $R_\infty > 4 \times 10^6$ per foot), the boundary layer is able to turn the 20° wedge angle without separating. The increase in heating rates forward of the wedge in this case is due to the beginning of transition. An inspection of the data in figures 14 to 23 shows that when the wedges force separation, the heating-rate distributions in the separation region ahead of the wedge are above or below that for the basic plate depending upon the type of separation (laminar, transitional, or turbulent) in a manner similar to that indicated earlier for separation forced by steps. A more detailed examination of the heat-transfer results for various wedge angles is given in the following sections.

10° wedge.- In figure 14(a), the heating-rate distributions are presented for three longitudinal wedge positions and at three free-stream unit Reynolds numbers. In figures 14(a) and 24(d) due to an oversight in test procedure, the x position of data where any tailed symbols on the wedge are used could not be determined. However, either the set of tailed symbols or the tailless symbols are the correct values. It is believed that the tailless symbols represent the correct data. The heating-rate distributions of figure 14(a) do not indicate that the flow separates when the wedge was located in the rear position for any of the three Reynolds numbers. When the wedge was located in the middle position, there was a small region of laminar separation that caused a decrease in heating rates compared with those for the smooth plate. The 10° wedge in the forward position caused a relatively large region of laminar separation in which the heating-rate distributions follow the trends noted as typical for laminar separation. Figure 14(b) represents the heating-rate distributions obtained on the sharp-leading-edge model with the 10° wedge mounted in the middle position on the plate over a lower Reynolds number range. In figure 14(b), the wedge forces laminar separation for the two lower Reynolds numbers.

The heating-rate distributions obtained on two blunt-leading-edge models with the 10° wedge mounted in the middle position are presented in figure 15. The effects of blunting the leading edge to 0.12 inch (fig. 15(a)) as compared with the sharp-leading-edge data of figure 14 is seen to cause a substantial increase in the extent of the separation region for $R_\infty = 7.6 \times 10^6$, 5.5×10^6, and 4.1×10^6 per foot. The heating-rate distributions for the 0.375-inch-diameter leading-edge model are shown in figure 15(b). For each Reynolds number tested, laminar separation is evident with the expected heating-rate trends.

20° wedge.- In figure 16(a), the heating-rate distributions are presented for three longitudinal wedge positions and at three free-stream unit Reynolds numbers. As was found for the 10° wedge, the heat-transfer distributions did not indicate any appreciable separation when the wedge was located in the rear position where transitional or turbulent boundary-layer conditions existed for the flat plate.

Figure 16(b) presents the heating-rate distributions obtained on the sharp-leading-edge model with the 20° wedge in the middle position over the lower Reynolds number range. For $R_\infty = 4.46 \times 10^6$, separation is not clearly evident from the data. However, it was visually noted from the schlieren screen that when the junction of the wedge was located very close to the beginning of transition, the flow sometimes fluctuated between separated and nonseparated conditions. At $R_\infty = 2.87 \times 10^6$ and $R_\infty = 1.30 \times 10^6$, regions of transitional and laminar separation, respectively, were obtained.

The heating-rate distributions obtained on two blunt-leading-edge models with the 20° wedge mounted in the middle position are presented in figure 17. For all Reynolds numbers, the separation regions are laminar or transitional and very near laminar conditions, and follow the expected trends. Increasing the bluntness to 0.375-inch diameter as shown in figure 17(b) results in a smaller separation region than was obtained on the 0.12-inch-diameter leading-edge model at comparable free-stream conditions.

30° wedge.- In figure 18 the heating-rate distributions are similar to those found on the 20° wedge with the exception of the separation region being more extensive for the 30° wedge than for the 20° wedge and the transition region being farther forward for the 30° wedge than for the 20° wedge. In general, the separation regions obtained with the two blunt-leading-edge models in figure 19 are transitional and more extensive for the 0.12-inch-diameter leading-edge model than for the 0.375-inch-diameter leading-edge model.

40° wedge.- The effects of wedge location and free-stream Reynolds number variation on a sharp-leading-edge model with a 40° wedge are shown in figure 20. The 40° wedge is seen to cause very extensive separation on the model under each condition investigated. In each case, the separation region is transitional in nature, and the transitional region is further forward than for the smaller angle wedges under otherwise similar conditions. The effects of blunting the leading edge on a model with a 40° wedge in the middle position are shown in figure 21. In each case, the transitional separation extends forward of the instrumentation location.

30° wedge and 40° wedge with roughness.- In an attempt to obtain turbulent separation forward of the 30° wedge and 40° wedge, the models were run with a sharp leading edge having roughness heights of 0.080 inch located 2 inches from the leading edge. For both free-stream Reynolds numbers tested (fig. 22), the flow did not separate appreciably on the 30° wedge. The 40° wedge, however, did force separation of a turbulent nature. The heating-rate distributions within this region of turbulent separation are similar to those presented for the forward-facing step with the exception that no second peak heating rate was found for the 40° wedge as was found for the step. It has been shown that the

assumption that the Stanton number is constant streamwise across the separation point for turbulent separation will result in an approximation of the heat transfer within the turbulent separation region for separation forced by the forward-facing steps. (See figs. 10 and 12.) Also shown in figure 22 is the heating-rate level predicted by this assumption as based on the experimental attached heating-rate level prior to separation. Figure 22 shows reasonably good agreement between the data obtained by this method of prediction and the data for the turbulent separation forced by a 40° wedge.

Stanton number distributions on wedges.- Stanton number distributions based on experimental data along the wedges for the sharp-leading-edge model are shown in figure 24. Some experimental data on the plate forward of the wedges are also presented for comparison with the laminar attached-flow theory for the smooth plate to provide information on the nature of the flow forward of the wedges. Figure 24 includes theoretical calculations of the turbulent Stanton number distribution on the wedges computed by the reference-temperature method by assuming that the boundary-layer virtual origin for the flow over the wedge began at the junction of the wedge and the plate. (Similar assumptions were also made in refs. 10 and 11.) For these calculations, the local Mach number and pressures on the wedge were calculated by assuming nonviscous conditions. (See appendix B for more details.) A nominal value of stagnation temperature of 500° F was used in the calculations. Both the experimental and theoretical Stanton numbers have been based on free-stream flow conditions. An overall inspection of these figures indicates that when the flow is turbulent (or nearly turbulent) at the beginning of the wedge and separation does not occur, this calculation method gives a good prediction of the Stanton numbers on the wedge. (See, for example, fig. 24(a) with the wedge in the rear position and $R_\infty = 8.12 \times 10^6$ per foot.) As the Reynolds number at the wedge position decreases in such a way that transitional separation occurs, the experimental data show that the peak Stanton number on the wedges moves rearward along the wedge and causes increasing discrepancies between data and the trends and values predicted by the turbulent calculations. (See, for example, fig. 24(a) with the wedge in the forward position, and $R_\infty = 7.97 \times 10^6$.) This trend might be expected since the flow is now separated and reattachment occurs along the wedge surface, fully developed turbulent flow generally beginning downstream of the wedge-plate junction. Although the local Stanton numbers vary considerably from those predicted by the theory for the lower Reynolds numbers, these calculations continue to give an approximation of the peak Stanton number until laminar or near-laminar conditions exist at the rear of the wedge.

The 40° wedge always causes separation of the flow and the data of figure 24(e) show that the Stanton number on the wedge always increases with increasing distance from the wedge-plate junction. These trends would be expected from a consideration of the flow mechanism involved; for example, the very large region of separation caused by the 40° wedge as compared with the flow field found on the lower wedge angles causes the local pressure on the wedge surface to increase substantially with increasing distance from the wedge-plate junction. (See the schlieren photographs of fig. 25.) It should be stressed here that the surface distance of the wedges l is a constant in these tests for all wedge angles.

To gain a better understanding of the physical meaning that can be attributed to the applicability of the calculations by the method of appendix B to the experimental data, figure 26 compares the approximate measured peak pressure ratios obtained on the wedges with the theoretical shock values for the test Reynolds number range. Analysis of this figure shows that although the peak pressures are a function of Reynolds number the predictions obtained by assuming the local flow to be attached and inviscid agree reasonably well with the experimental peak pressures at the lower wedge angles. As the wedge angle becomes larger, the values of the peak pressures become increasingly larger functions of Reynolds number; for example, the measured values for the 40° wedge vary considerably from the values obtained by assuming attached and inviscid flow except in a very narrow Reynolds number range. Therefore, the turbulent heat-transfer calculation method presented here which makes use of pressures calculated by inviscid equations loses much of its physical meaning for the 40° wedge angle and for the 30° wedge angle at the lower Reynolds numbers.

The Stanton number distributions on the wedges for the blunted leading-edge plates are compared with the turbulent theoretical calculations in figure 27. For calculations of the Stanton number distribution on the wedges mounted on the blunt-leading-edge plate, the local flow over the plate forward of the wedges was first assumed to have passed through a normal shock at the leading edge with a resulting nominal Mach number of 3.16 and then the Stanton number distributions were calculated by the method of appendix B. An inspection of the figures shows results similar to those obtained with the sharp-leading-edge plate; that is, the best agreement of data and theory is obtained when the flow upstream of the wedge is turbulent or transitional. For laminar conditions upstream of the wedge, the theory gives an approximation of the maximum Stanton number on the 20° and 30° wedges (see figs. 27(a) and 27(b)), even though the trend of the distribution is not predicted. When laminar conditions extend to approximately the end of the wedge (see, for example, fig. 27(c), $R_\infty = 1.09 \times 10^6$), the theory overpredicts the heating on the wedges.

A parameter that is of particular interest is the maximum heat transfer on the wedges. Figure 28 presents the maximum Stanton number based on experimental data measured on the wedge surface for both sharp- and blunt-leading-edge models as a function of free-stream Reynolds number based on the distance from the leading edge of the model to the beginning of the wedge. Transition has occurred before the end of the wedge for most of the data in this figure. The exceptions are the 10° wedge data at the low Reynolds numbers which are made solid to indicate that they represent laminar or very near laminar conditions. The peak Stanton number increases with increasing Reynolds number until the flow becomes sufficiently transitional that the peak Stanton number decreases with increasing Reynolds number. In general, for wedge angles greater than 10°, the flow along the wedge has become sufficiently transitional at the lowest Reynolds number that the peak Stanton number decreases with increasing Reynolds number. The prediction of the maximum Stanton numbers on wedges is difficult; however, in the following discussion it will be shown that if the proper classifications of the flow are made, reasonable estimations of the values and trends can be obtained.

The results of reference 12 have shown that the method of Bertram and Feller in reference 24 gives a good prediction of the heating rates on wedges for pure laminar flow at high Mach numbers (of the order of 14). This method was originally derived in reference 24 by using the hypersonic similarity theory to predict the heat transfer on plates at angle of attack. The maximum Stanton number on wedges calculated by this method for laminar flow using the equation

$$N_{St} = N_{St,\phi=0} K_3 \sqrt{\frac{p_w}{p_{w,\phi=0}}} \tag{7}$$

are shown in figure 28. In this equation, K_3 is a function of the pressure gradient over the wedge; however, for the calculations shown in figure 28, K_3 was taken as unity. The pressure ratio $\frac{p_w}{p_{w,\phi=0}}$ was taken as the theoretical inviscid two-dimensional value. The results of a comparison of these calculations with the 10° wedge experimental data in figure 28 for laminar conditions show that the theory gives a reasonably fair prediction of the data for both the sharp- and blunt-leading-edge models.

Because of the agreement obtained between this method and the data in figure 28, equation (7) is also used in figures 24(d) and 27(c) to calculate the local Stanton number on the wedges for several cases where the flow is still laminar at the rear of the wedge. Two values of K_3 were used, 1.0 and 1.4, the latter being the approximate value obtained from the experimental pressure data. (However, it should be mentioned that the experimental pressure distributions obtained were not sufficient to obtain a very exact value of this parameter because of the small number of orifices and the inaccuracy of the pressure measurement at the lowest pressure.) The measured pressures were also used in equation (7) to evaluate the parameter $\frac{p_w}{p_{w,\phi=0}}$. A reasonably good prediction of the local Stanton numbers on the wedge is obtained by these calculations, but the agreement is not as satisfactory as that obtained in reference 12.

Also shown in figures 24(d) and 27(c) is the theoretical laminar Stanton number distribution for $R_\infty = 1.1 \times 10^6$ per foot obtained by assuming that the boundary layer begins at the leading edge of the wedge and that the local Mach number is that value obtained by taking the local flow through a 10° turning angle. This method of prediction greatly overpredicts the experimental results for the blunt-leading-edge plate and does not give nearly as good prediction as those obtained from equation (7).

Since the flow was transitional or turbulent at the beginning of the wedge for most of the 20° wedge data presented, the approximate peak Stanton number distribution for a 20° wedge obtained by converting the turbulent flat-plate theory for $\phi = 0°$ (as obtained by the method reviewed in appendix A of this paper) to a value for $\phi = 20°$ is shown in figure 28. It was assumed that the local Stanton number remains constant across the junction of

the plate and the wedge. (Calculations were similar to those of equation (5) and appendix B.) This method underpredicts the experimental results considerably.

As was mentioned earlier, the calculations of Stanton number distribution on the wedge surfaces for turbulent flow, the virtual origin assumed to begin at the wedge-plate junction, in general gave a good approximation of the peak Stanton number on the wedge although the trends of the prediction of the local distributions did not agree with those of the data. The maximum Stanton number on the wedges in the region where the thermocouples are located as predicted by this method are shown as a crosshatched region in figure 29. In figure 29(a), this method is seen to give a good approximation of the maximum Stanton number based on experimental data for the 10°, 20°, and 30° wedges for the sharp leading edge. For the 40° wedge the theory slightly underpredicts the experimental results. For the blunt-leading-edge results of figure 29(b), the theory best predicts the data for the 20° wedge. For the 10° wedge, the theory overpredicts the maximum Stanton number primarily because of the laminar or near laminar conditions of the local flow field on the wedge. For the 30° wedge, the theory slightly underpredicts the experimental results, although the theory does give a good representation of the trend of the data with increasing Reynolds number.

Calculation of Stanton numbers on wedges from experimental data.- The Stanton numbers on the wedges based on experimental data which have been presented in this report were determined by assuming a Mach number which was calculated from experimental pressure data and an assumed total pressure of that for the flat plate undisturbed by the wedge. This assumption results in an assumed local Mach number of the flow of slightly greater magnitude than the actual flow conditions. Another technique would be to obtain the total pressure conditions by assuming that the flow along the wedge is inviscid, the resulting local Mach number being determined by this total pressure and the experimental local pressure data. The results of figure 29 are replotted in figure 30 under this assumption. Neither of the techniques used in figures 29 or 30 is strictly correct particularly for the case of separated flow. However, the two techniques should give the upper and lower bounds of the Stanton numbers based on experimental data. The data of figure 30 show the best agreement with theoretical predictions. However, comparison of figures 29 and 30 shows that there is little difference (less than 10 percent) in the values of the N_{St} calculated by the two techniques.

CONCLUSIONS

An extensive experimental investigation of heat transfer within regions of separated flow forced by forward- and rearward-facing steps and by 10°, 20°, 30°, and 40° wedges on sharp- and blunt-leading-edge flat-plate models over a unit free-stream Reynolds number range of approximately 1×10^6 to 8×10^6 per foot and at a free-stream Mach number of 6 with a wall-stagnation temperature ratio of approximately 0.55 has yielded the following conclusions:

1. The trends of heating rates within regions of laminar, transitional, and turbulent separation may be characterized by typical distributions, generally independent of model geometry, except to the extent that the model-geometry variations affect the location of transition. That is, for the case of pure laminar or turbulent separation, the local heating rate in the separated region is, respectively, less than or greater than that for a flat plate without separation. For transitional separation, the local heating rates decrease below the flat-plate values until transition occurs and then increase rapidly to values above those of the flat plate.

2. The ratio of the integrated heating rate in a separated region forced by a forward-facing step to the integrated heating rate in the same region with attached flow can vary from approximately 0.5 for laminar separation to 2 or greater for transitional or turbulent separation.

3. Although incomplete knowledge of the separation mechanism has prevented the development of theoretical heat-transfer calculations based on firm rational conditions, a meaningful analysis of the data can be made if the flow is first classified as pure laminar, transitional, or turbulent. Trends and values of many of the heat-transfer parameters can then be made by using existing heat-transfer calculations based on the reference-temperature method. The integrated heating-rate ratio for laminar separation is well predicted by Chapman's theory. The magnitude of the integrated heating-rate ratio for turbulent separation is predicted by the assumption that the local Stanton number remains constant streamwise across the separation region when the local velocity and density outside the separated region were obtained from previous turbulent separation equations. The assumptions of constant local Stanton number across the separation point and of pressures within the separation region equivalent to those predicted by previous turbulent separation studies also give fair predictions of the values of the local Stanton numbers in regions of turbulent separation forced by forward-facing steps. However, the theory underpredicts the maximum local values very near the step where the pressures are high.

4. The experimental data show a large variation of the local heating values and the location of the maximum heating rates on the surface of wedges at various angles depending upon the position of transition. The assumption that the virtual origin of the boundary layer is located at the junction of the wedge and the plate gives a very good approximation of the local Stanton number distribution on a wedge for turbulent conditions without separation when the pressure on the wedge is taken as the theoretical inviscid two-dimensional value. For transitional flow nearing laminar conditions with separation upstream of the wedge, this assumption gives a good approximation of the maximum heating rate even though the location of this maximum heating rate on the wedge is not predicted. For laminar conditions, a previous equation derived from the hypersonic similarity theory for plates at angles of attack predicts reasonably well the heat transfer on wedges.

Langley Research Center,
National Aeronautics and Space Administration,
Langley Station, Hampton, Va., June 22, 1965.

APPENDIX A

REVIEW OF HEAT-TRANSFER EQUATIONS FOR FLAT PLATE

There are many methods available for the theoretical calculation of the Stanton number on a flat plate. In this analysis, the T' method of Monaghan (refs. 25 and 26) has been employed. From reference 27 the T' equation may be written as

$$T' = A_1 T_w + T_o\left(1 - A_1 + A_2 \frac{\gamma - 1}{2} M_o^2\right) \tag{A1}$$

The Stanton number may be determined from the modified Reynolds analogy

$$N_{St,T'} = \frac{1}{2} \frac{C_{f,T'}}{(N_{Pr})^{2/3}} \tag{A2}$$

where the Prandtl number N_{Pr} is based on T' conditions.

Laminar Boundary Layer

For the case of a laminar boundary layer, the coefficients of equation (A1) (see ref. 25) become

$$\left.\begin{aligned} A_1 &= 1 - 0.468(N_{Pr})^{1/3} \\ A_2 &= \left(1 - A_1 - 0.273 N_{Pr}\right)(N_{Pr})^{1/2} \end{aligned}\right\} \tag{A3}$$

By using the Blasius equation for laminar flow, equation (A2) becomes

$$N_{St} = \frac{0.332\sqrt{C'}}{\sqrt{R_{o,x}}(N_{Pr})^{2/3}} \tag{A4}$$

where N_{St} is based on free-stream conditions for direct comparison with data and the conversion parameter from T' reference conditions to free-stream conditions C' is given by

$$C' = \frac{\mu'}{\mu_o} \frac{T_o}{T'} \tag{A5}$$

APPENDIX A

Turbulent Boundary Layer

For the case of a turbulent boundary layer, the coefficients of equation (A1) (see ref. 28) become

$$\left.\begin{aligned} A_1 &= 0.54 \\ A_2 &= 0.142 \end{aligned}\right\} \tag{A6}$$

The Karman-Schoenherr equations were used to determine the local skin-friction coefficient as follows. (See ref. 29 for a plot of these parameters and further discussion.)

$$\frac{0.242}{\sqrt{C_{F,T'}}} = \log_{10}\left(R_{x,T'}\right)\left(C_{F,T'}\right) \tag{A7}$$

where

$$R_{x,T'} = \frac{\rho' u_o x_v}{\mu'} \tag{A8}$$

$$\frac{C_{f,T'}}{C_{F,T'}} = \frac{1}{1 + 3.59\sqrt{C_{F,T'}}} \tag{A9}$$

and $C_{f,T'}$ may be converted to free-stream conditions as follows:

$$C_f = \frac{C_{f,T'}}{T'/T_o} \tag{A10}$$

and finally the Stanton number is determined by modifying equation (A2), by basing N_{St} on free-stream conditions so that

$$N_{St} = \frac{1}{2}\frac{C_f}{\left(N_{Pr}\right)^{2/3}} \tag{A11}$$

where C_f is determined by equation (A10). The distance x_v of equation (A8) is defined as the distance from the virtual origin. In this paper, the virtual origin for the flat plate with undisturbed flow was defined as the point at which laminar flow ends as determined by the surface heat-transfer rates. (See ref. 29 and ref. 18, for further discussion.) For the flat plate with roughness, the virtual origin was assumed to be located at the roughness position. (See ref. 18.)

APPENDIX B

CALCULATION AND CONVERSION OF STANTON NUMBERS BASED ON LOCAL TURBULENT CONDITIONS TO FREE-STREAM CONDITIONS

This appendix gives an example of the method used for the calculation and conversion of Stanton numbers based on local turbulent conditions to free-stream conditions for wedges and for separation forced by steps.

Turbulent Stanton Number Distribution on Wedges

Consider a flat-plate—wedge model combination with regions of flow as indicated below

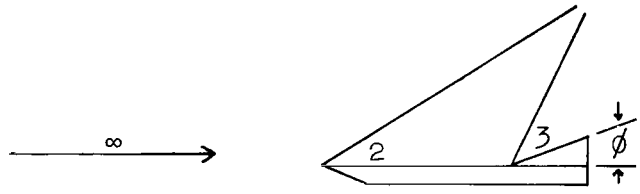

In order to calculate the turbulent Stanton number distribution on wedges the boundary-layer "virtual origin" is assumed to be located at the wedge-plate junction. The local Reynolds number based on the distance from the virtual origin in region 3 can be written in terms of the known conditions in region 2 as

$$R_{o,v} = \frac{\rho_3 u_3 x_v}{\mu_3} = R_{o,2}\left(\frac{\rho_3 u_3}{\rho_2 u_2}\frac{\mu_2}{\mu_3}\right)x_v \tag{B1}$$

where $R_{o,2}$ is the unit Reynolds number per foot at the outer edge of the undisturbed boundary layer in region 2. (The subscripts 2 and 3 denote regions 2 and 3 indicated on sketch.)

If γ is assumed to be 1.4 and the Sutherland viscosity equation is used, equation (B1) can be rewritten in the form

$$R_{o,v} = x_v R_{o,2}\frac{p_3}{p_2}\frac{M_3}{M_2}\left(\frac{T_2}{T_3}\right)^2\frac{T_3 + 198.6}{T_2 + 198.6} \tag{B2}$$

where T is given in $^{\circ}R$. Finally, by combining equation (B2) with the equations presented in appendix A for a turbulent boundary layer, Stanton number can be determined at any x_v position based on conditions in region 3 (shock equations or tables being used to solve equation (B2)). (See, for example, ref. 30.)

The Stanton number calculations based on conditions in region 3 can then be converted to free-stream conditions for direct comparison with experimental data as follows:

$$\left(N_{St}\right)_{\text{region } 3} = \frac{h}{\rho_3 u_3 C_p} \tag{B3}$$

therefore,

$$N_{St,\infty} = \frac{h}{\rho_3 u_3 C_p} \frac{\rho_3 u_3}{\rho_\infty u_\infty} \tag{B4}$$

if it is assumed that the specific heat is constant in all regions. Equation (B4) may be rewritten in terms of pressure, temperature, and Mach number as

$$N_{St,\infty} = \left(N_{St}\right)_{\text{region } 3} \frac{p_3}{p_\infty}\left(\frac{T_\infty}{T_3}\right)^{1/2} \frac{M_3}{M_\infty} \tag{B5}$$

For the case of a blunt-leading-edge plate, the Mach number and Reynolds number in region 2 were determined by assuming that all local flow had passed through a normal shock and that the static pressure in region 2 was constant and equal to the free-stream pressure.

Stanton Number in Regions of Separation

For the prediction of Stanton numbers in a separated region forward of a step or wedge, equation (B5) was also used. However, the wedge angle ϕ was replaced by the separation angle of the flow as predicted by equation (6) in order to determine the conditions in region 3. Equation (B2) was not used under these conditions. Rather, it was assumed that the local Stanton number remained constant across regions 2 and 3 (see eq. (5)). Therefore, the local Stanton number was calculated for region 2 at the separation point by the methods reviewed in appendix A. The local distribution of Stanton number within the separation region is then found by the normal dependence of N_{St} on Reynolds number where the local Reynolds number is assumed to be that along a wedge whose angle is equal to the separation angle.

REFERENCES

1. Crocco, Luigi: Considerations on the Shock-Boundary Layer Interaction. Proc. Conf. on High-Speed Aeronautics, Antonio Ferri, Nicholas J. Hoff, and Paul A. Libbey, eds., Polytechnic Inst. of Brooklyn, c.1955, pp. 75-112.

2. Kaufman, Louis G., II; Hartofilis, Stavros A.; Evans, William J.; Oman, Richard A.; Meckler, Lawrence H.; and Weiss, Daniel: A Review of Hypersonic Flow Separation and Control Characteristics. ASD TDR 62-168, U.S. Air Force, Mar. 1962.

3. Chapman, Dean R.; Kuehn, Donald M.; and Larson, Howard K.: Investigation of Separated Flows in Supersonic and Subsonic Streams With Emphasis on the Effect of Transition. NACA Rept. 1356, 1958.

4. Kuehn, Donald M.: Experimental Investigation of the Pressure Rise Required for the Incipient Separation of Turbulent Boundary Layers in Two-Dimensional Supersonic Flow. NASA MEMO 1-21-59A, 1959.

5. Love, Eugene S.: Pressure Rise Associated With Shock-Induced Boundary-Layer Separation. NACA TN 3601, 1955.

6. Sterrett, James R.; and Emery, James C.: Extension of Boundary-Layer-Separation Criteria to a Mach Number of 6.5 by Utilizing Flat Plates With Forward-Facing Steps. NASA TN D-618, 1960.

7. Sterrett, James R.; and Emery, James C.: Experimental Separation Studies for Two-Dimensional Wedges and Curved Surfaces at Mach Numbers of 4.8 to 6.2. NASA TN D-1014, 1962.

8. Erdos, John; and Pallone, Adrian: Shock-Boundary Layer Interaction and Flow Separation RAD-TR-61-23, Res. and Advanced Develop. Div., AVCO Corp., Aug. 15, 1961.

9. Bogdonoff, S. M.; and Vas, I. E.: Some Experiments on Hypersonic Separated Flows. ARS J., vol. 32, no. 10, Oct. 1962, pp. 1564-1572.

10. Becker, John V.; and Korycinski, Peter F.: Heat Transfer and Pressure Distribution at a Mach Number of 6.8 on Bodies With Conical Flares and Extensive Flow Separation. NASA TN D-1260, 1962.

11. Schaefer, John W.; and Ferguson, Harold: Investigation of Separation and Associated Heat Transfer and Pressure Distribution on Cone-Cylinder-Flare Configurations at Mach Five. ARS J., vol. 32, no. 5, May 1962, pp. 762-769.

12. Miller, D. S.; Hijman, R.; and Childs, M. E.: Mach 8 to 22 Studies of Flow Separations Due to Deflected Control Surfaces. AIAA J., vol. 2, no. 2, Feb. 1964, pp. 312-321.

13. Carlson, Walter O.: Heat Transfer in Laminar Separated and Wake Flow Regions. 1959 Heat Transfer Fluid Mech. Inst. (Univ. of Calif.), Stanford Univ. Press, June 1959, pp. 140-155.

14. Nicoll, Kenneth M.: A Study of Laminar Hypersonic Cavity Flows. AIAA J., vol. 2, no. 9, Sept. 1964, pp. 1535-1541.

15. Larson, Howard K.: Heat Transfer in Separated Flows. J. Aero/Space Sci., vol. 26, no. 11, Nov. 1959, pp. 731-738.

16. Chapman, Dean R.: A Theoretical Analysis of Heat Transfer in Regions of Separated Flow. NACA TN 3792, 1956.

17. Jones, Robert A.; and Gallagher, James J.: Heat-Transfer and Pressure Distributions of a 60° Swept Delta Wing With Dihedral at a Mach Number of 6 and Angles of Attack From 0° to 52°. NASA TM X-544, 1961.

18. Holloway, Paul F.; and Sterrett, James R.: Effect of Controlled Surface Roughness on Boundary-Layer Transition and Heat Transfer at Mach Numbers of 4.8 and 6.0. NASA TN D-2054, 1964.

19. Sterrett, J. R.; and Holloway, P. F.: On the Effect of Transition on Parameters Within a Separation Region at Hypersonic Speeds - With Emphasis on Heat Transfer. Symposium on Fully Separated Flows, Arthur G. Hansen, ed., Am. Soc. Mech. Engrs., May 1964, pp. 15-26.

20. Hakkinen, R. J.; Greber, I.; Trilling, L.; and Abarbanel, S. S.: The Interaction of an Oblique Shock Wave With a Laminar Boundary Layer. NASA MEMO 2-18-59W, 1959.

21. McDonald, R. D.; Vinson, P. W.; and Mayes, J. F.: A Study of Three Hypersonic Missile Control Devices. Rept. OR 3978, Martin-Marietta Corp., June 1964.

22. Lees, Lester: Laminar Heat Transfer Over Blunt-Nosed Bodies at Hypersonic Flight Speeds. Jet Propulsion, vol. 26, no. 4, Apr. 1956, pp. 259-269, 274.

23. Rom, Josef; and Seginer, Arnan: Laminar Heat Transfer to a Two-Dimensional Backward Facing Step From the High-Enthalpy Supersonic Flow in the Shock Tube. AIAA J., vol. 2, no. 2, Feb. 1964, pp. 251-255.

24. Bertram, Mitchel H.; and Feller, William V.: A Simple Method for Determining Heat Transfer, Skin Friction, and Boundary-Layer Thickness for Hypersonic Laminar Boundary-Layer Flows in a Pressure Gradient. NASA MEMO 5-24-59L, 1959.

25. Monaghan, R. J.: An Approximate Solution of the Compressible Laminar Boundary Layer on a Flat Plate. R. & M. No. 2760, British A.R.C., 1953.

26. Rubesin, M. W.; and Johnson, H. A.: A Critical Review of Skin-Friction and Heat-Transfer Solutions of the Laminar Boundary Layer of a Flat Plate. Trans. A.S.M.E., vol. 71, no. 4, May 1949, pp. 383-388.

27. Bertram, Mitchel H.: Calculations of Compressible Average Turbulent Skin Friction. NASA TR R-123, 1962.

28. Monaghan, R. J.: On the Behavior of Boundary Layers at Supersonic Speeds. Fifth International Aeronautical Conference (Los Angeles, Calif., June 20-23, 1955), Inst. Aero. Soc. Inc., 1955, pp. 277-315.

29. Peterson, John B., Jr.: A Comparison of Experimental and Theoretical Results for the Compressible Turbulent-Boundary-Layer Skin Friction With Zero Pressure Gradient. NASA TN D-1795, 1963.

30. Ames Research Staff: Equations, Tables, and Charts for Compressible Flow. NACA Rept. 1135, 1953. (Supersedes NACA TN 1428.)

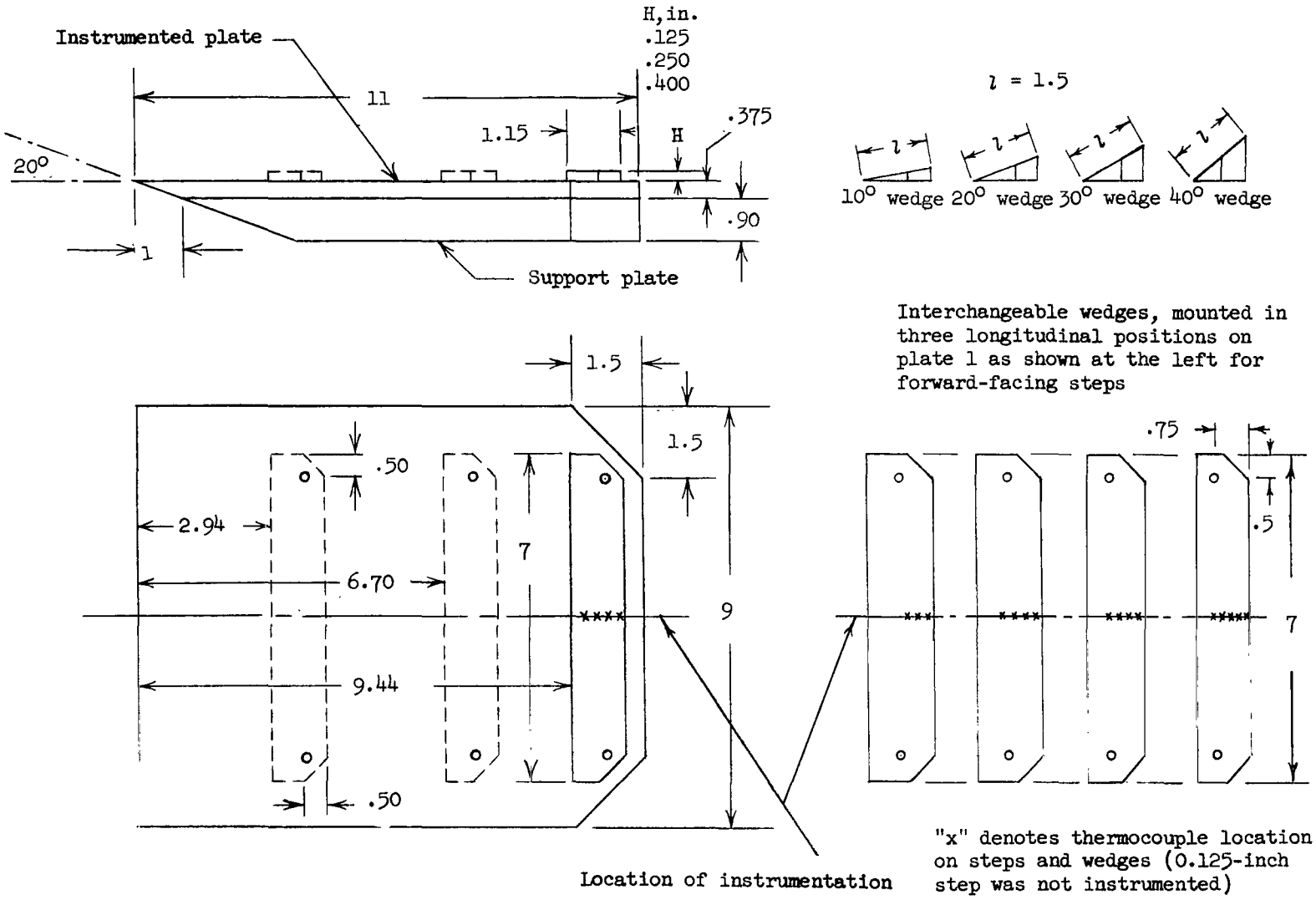

(a) Plate one model assembly, with forward-facing steps or wedges, t = 0.0015 inch.

Figure 1. Models. All linear dimensions are in inches.

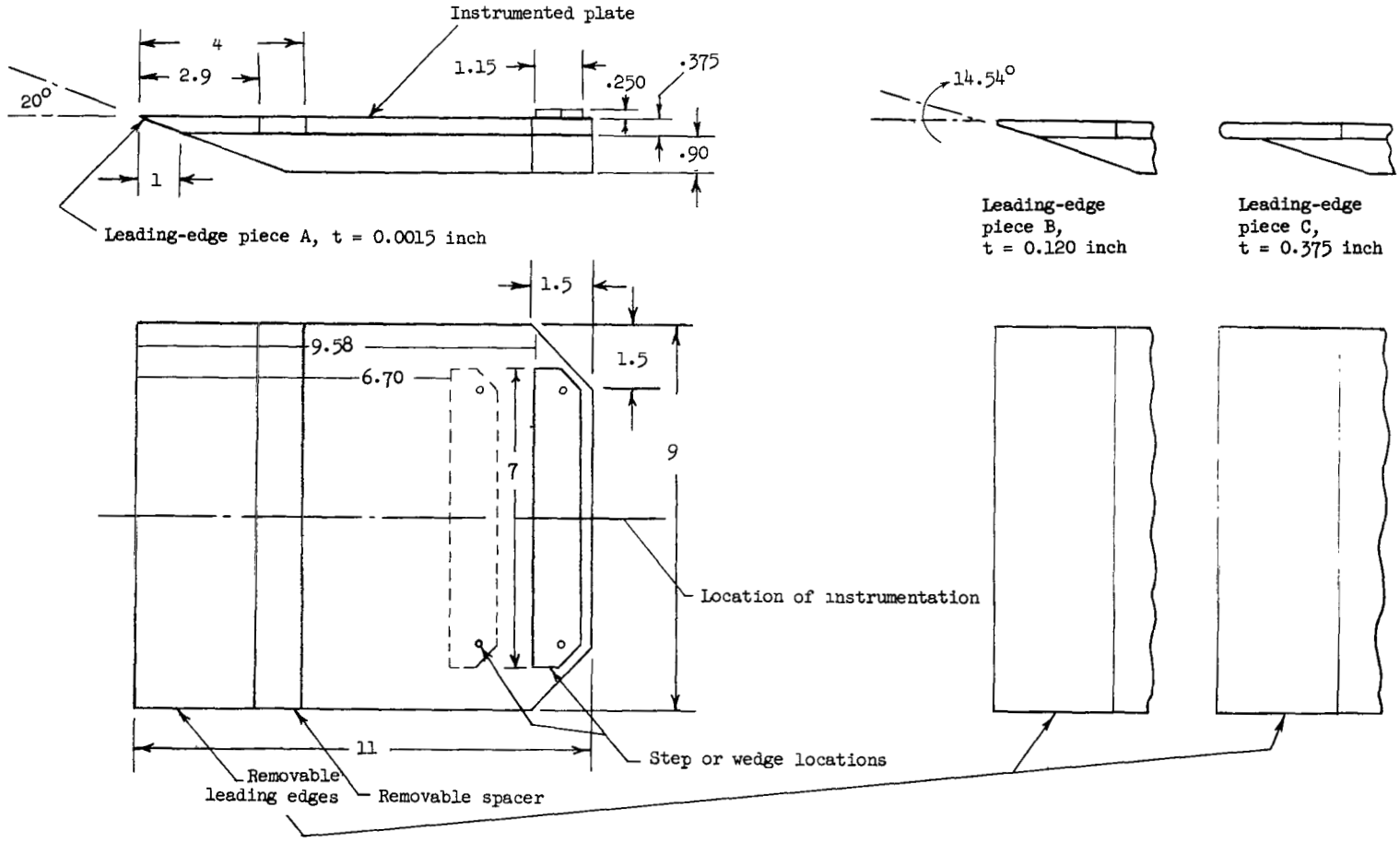

(b) Plate two model assembly with forward-facing steps or wedges and with three degrees of leading-edge bluntness.

Figure 1.- Continued.

Characteristics of spheres

k, inch	Diameter, inch	s, inch
0	0	
.036	.046	.200
.052	.063	.200
.064	.078	.312
.080	.093	.312
.109	.125	.312

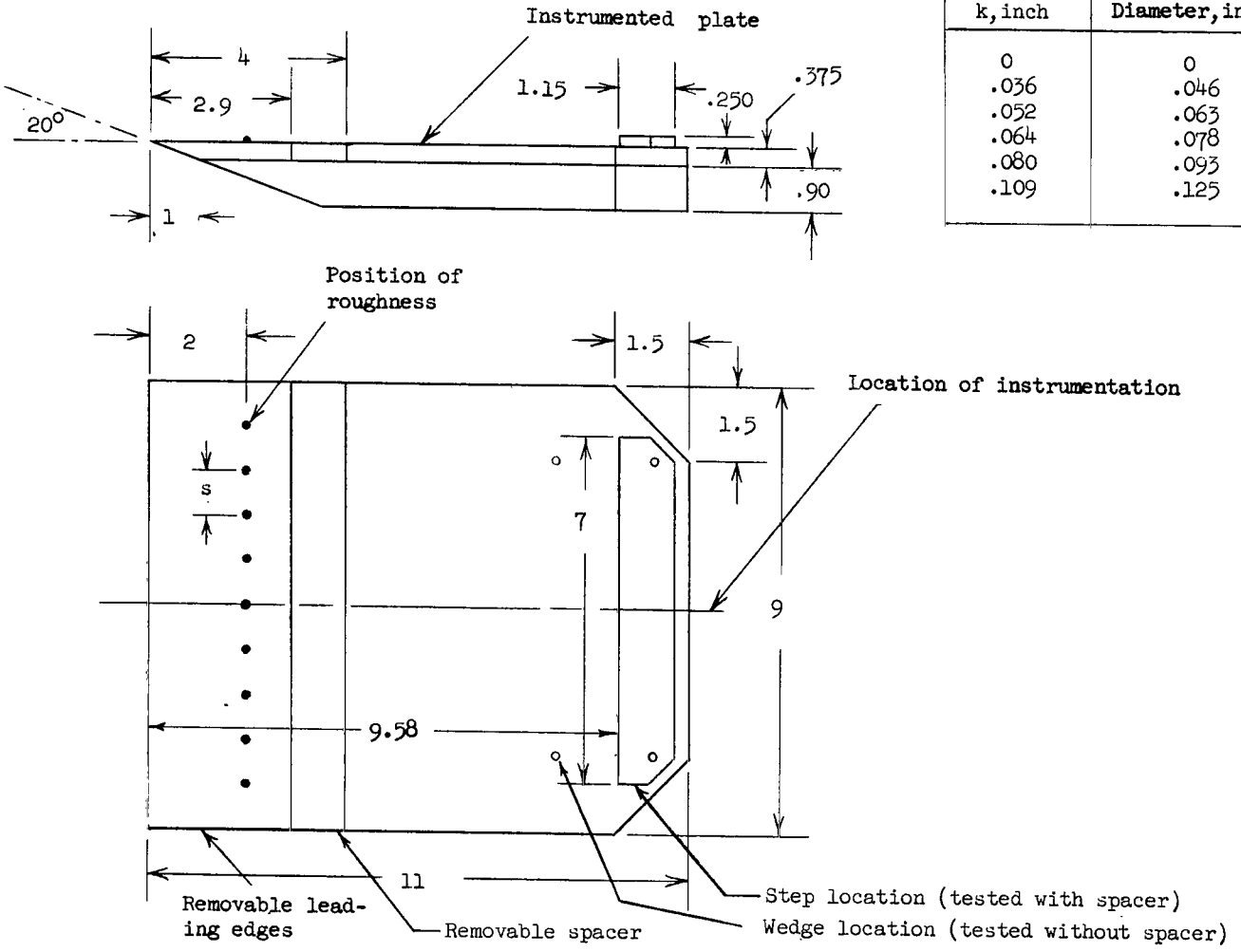

(c) Plate two model assembly with forward-facing steps or wedges and with roughness, $t < 0.004$ inch.

Figure 1.- Continued.

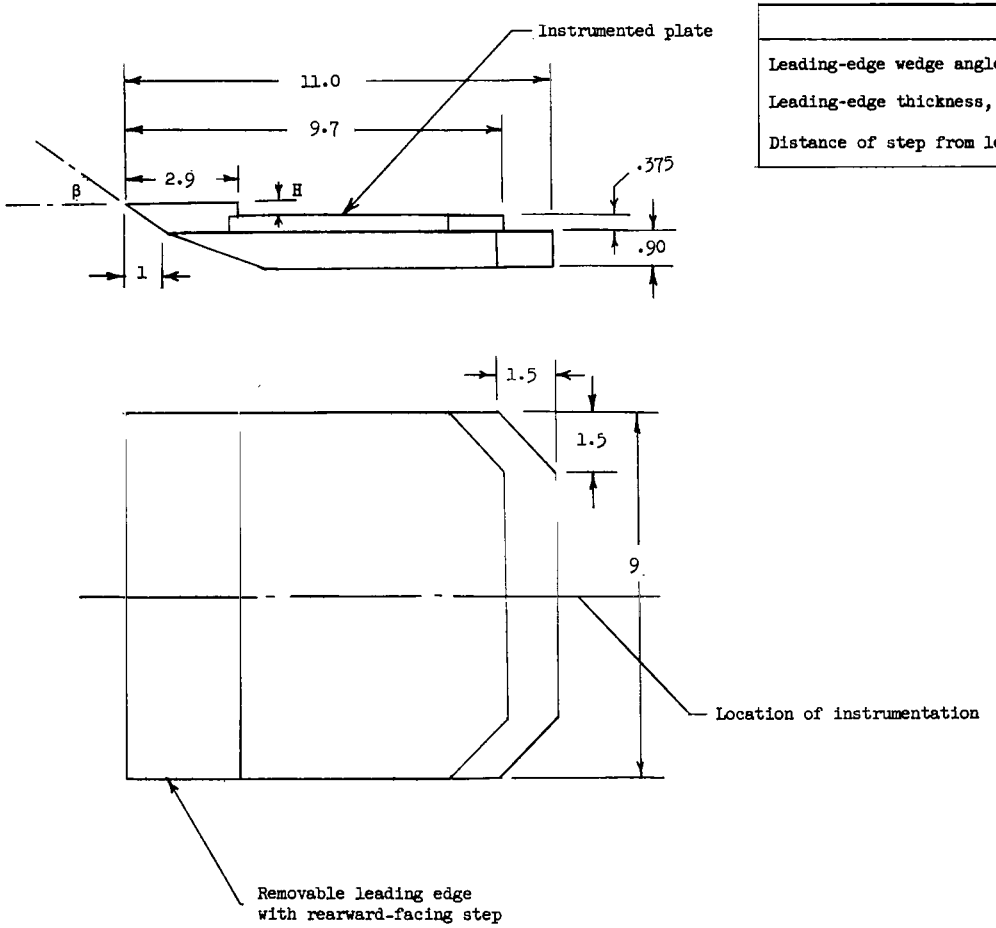

	H = .125 inch	H = .250 inch
Leading-edge wedge angle, β, deg	26.6	32.0
Leading-edge thickness, t, in.	.0020	.0015
Distance of step from leading edge, x_d, in.	2.9	2.9

(d) Plate two model assembly with rearward-facing steps.

Figure 1.- Continued.

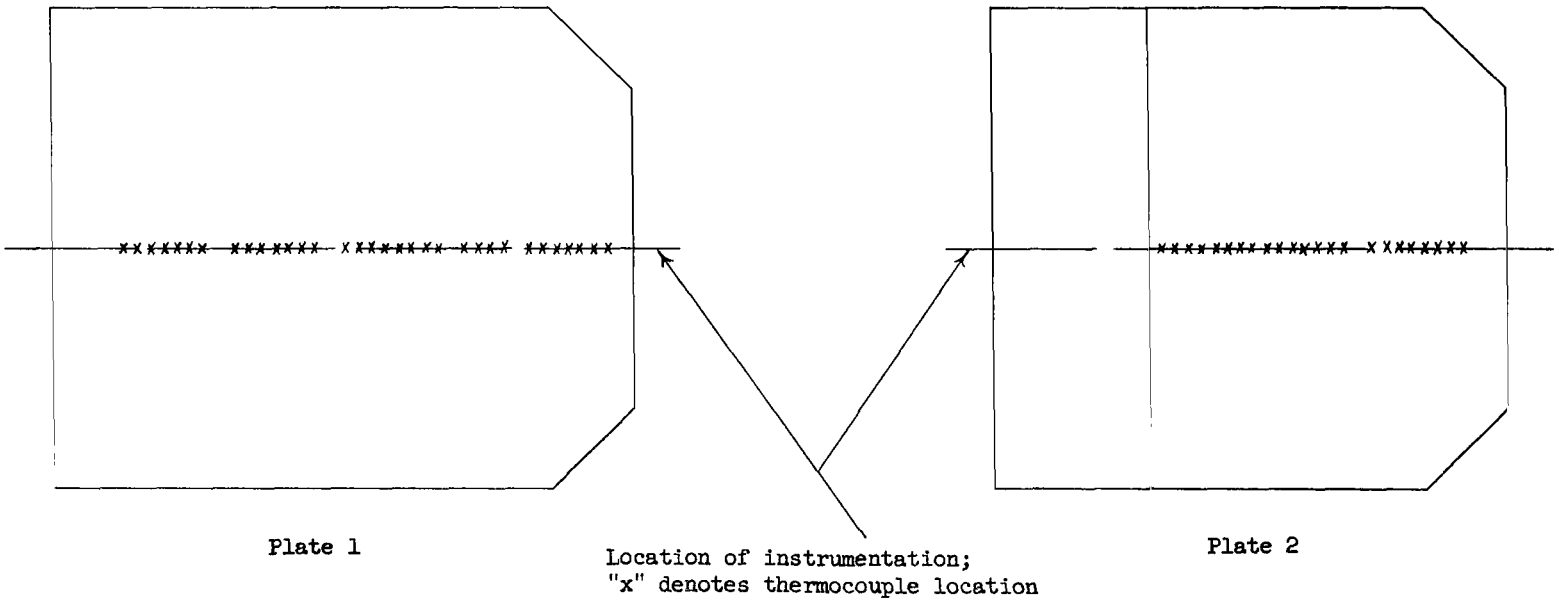

(e) Location of heat-transfer instrumentation on plates 1 and 2.

Figure 1.- Concluded.

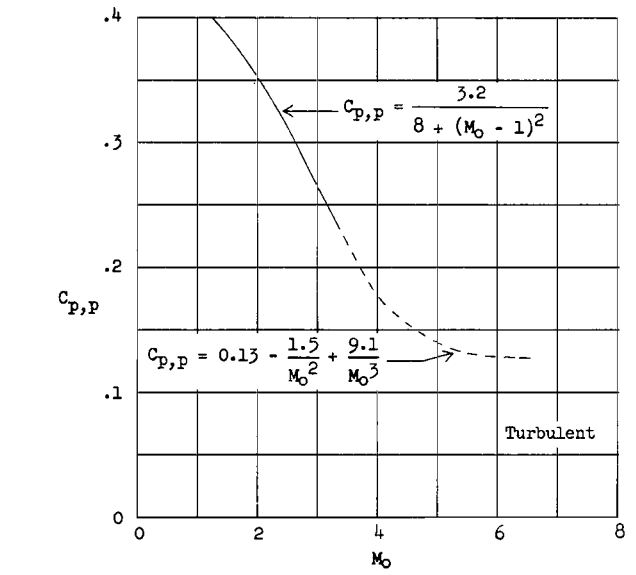

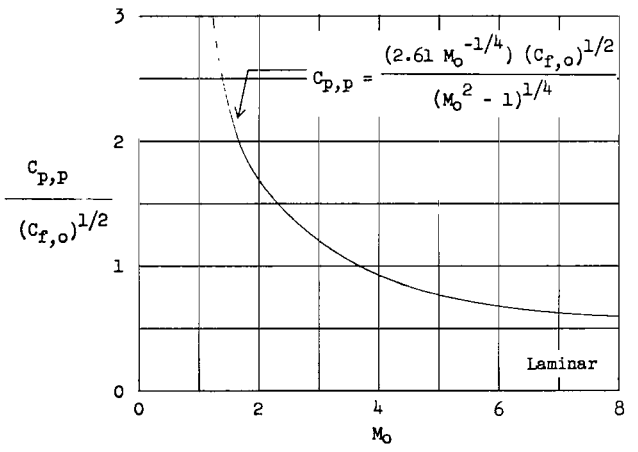

(a) Variation of separation pressure parameters with Mach number. (See ref. 19.)

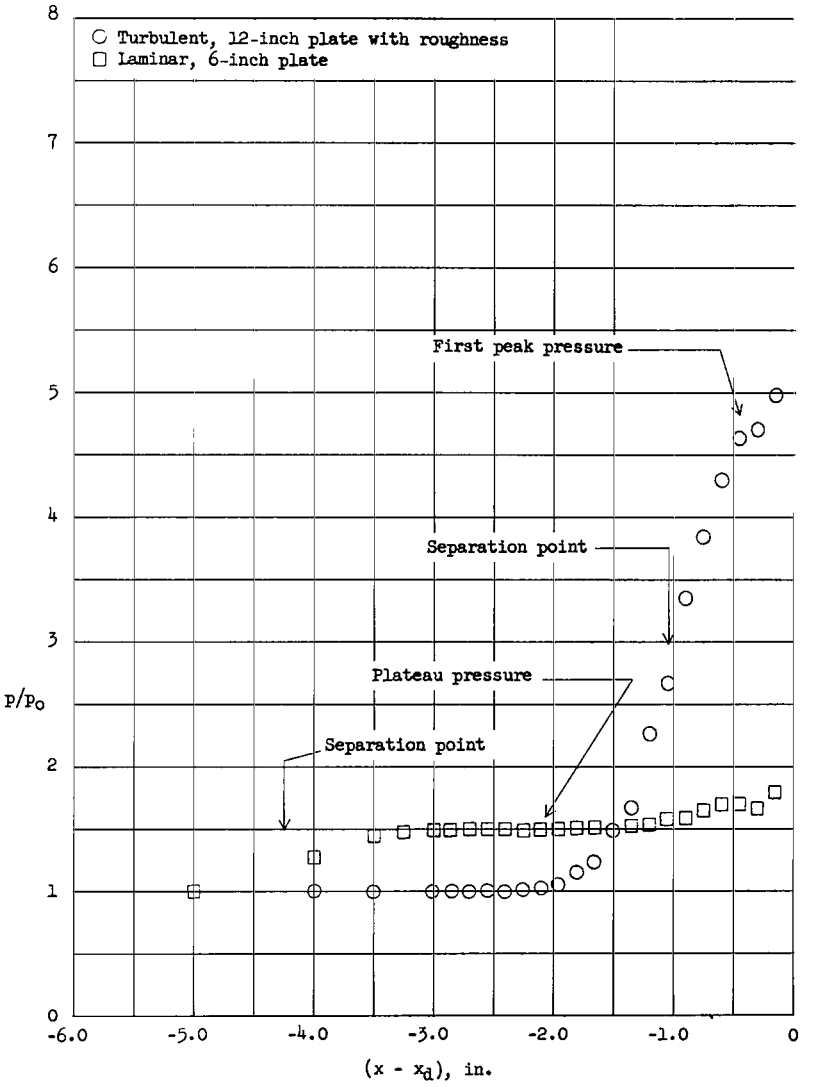

(b) Pressure distributions for typical laminar and turbulent separation cases forced by forward-facing steps. H = 0.250 inch; $M_o \approx 6.3$. (From ref. 6.)

Figure 2.- Pressures associated with different types of separation on a flat plate.

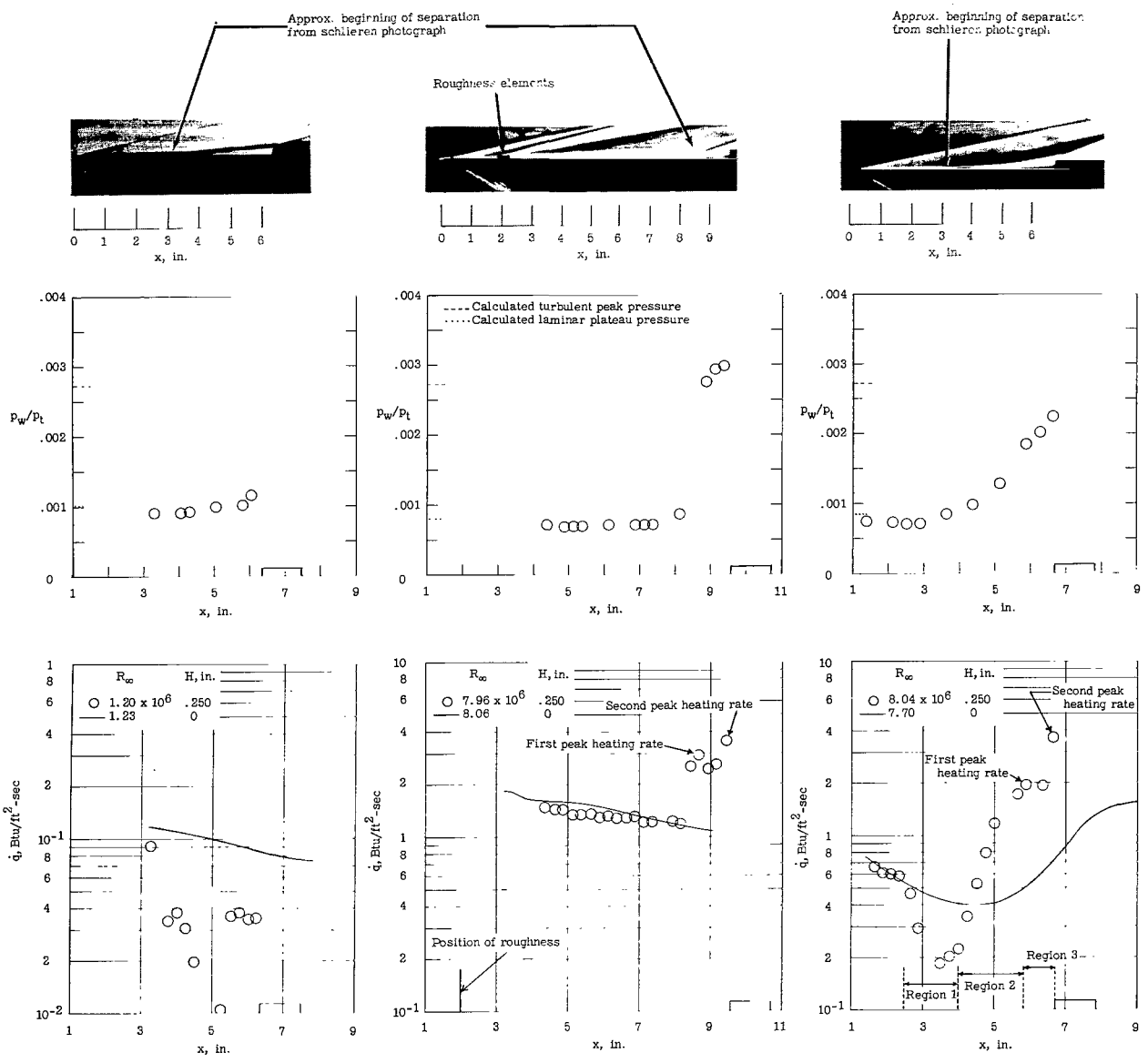

L-65-157

(a) Laminar separation; $R_\infty \approx 1.2 \times 10^6$. (b) Turbulent separation; $R_\infty \approx 8.0 \times 10^6$. (c) Transitional separation; $R_\infty \approx 8.0 \times 10^6$.

Figure 3.- Typical heating-rate distribution associated with forward-facing steps for laminar, turbulent, and transitional separation for a sharp-leading-edge model. $\alpha = 0^0$.

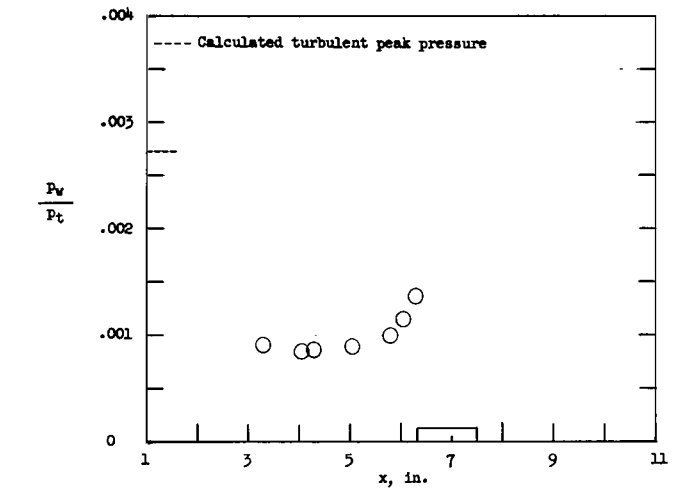

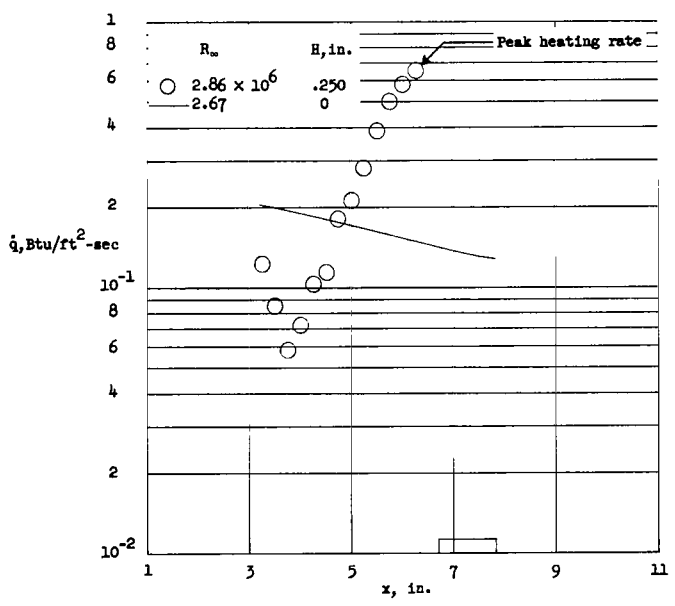

(d) Transitional separation; $R_\infty \approx 2.8 \times 10^6$.

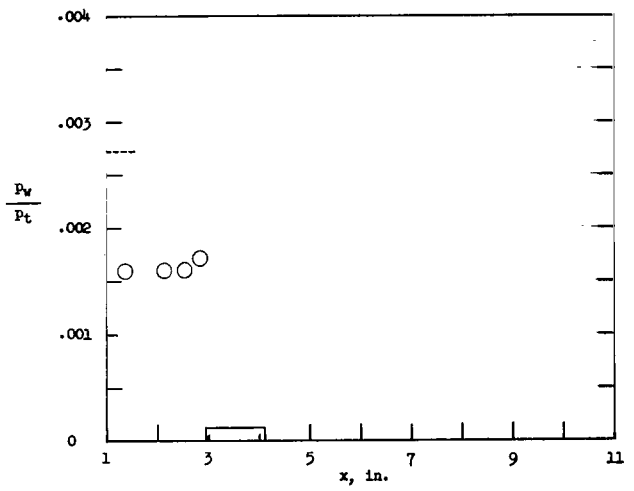

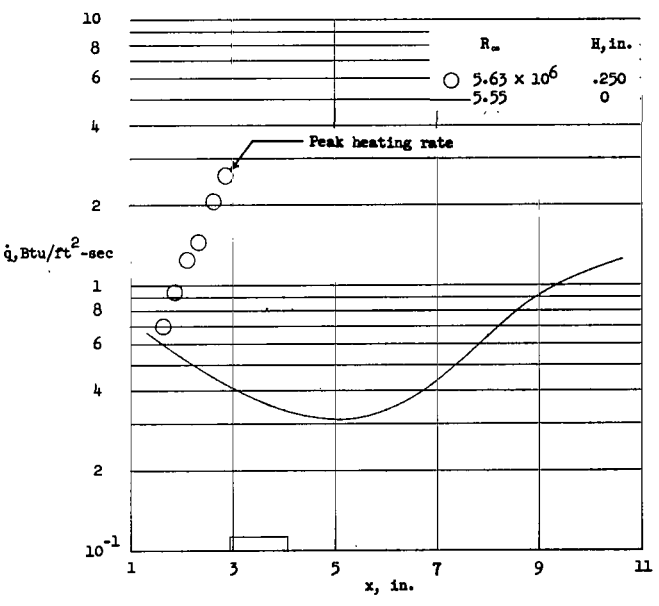

(e) Transitional separation; $R_\infty \approx 5.6 \times 10^6$.

Figure 3.- Concluded.

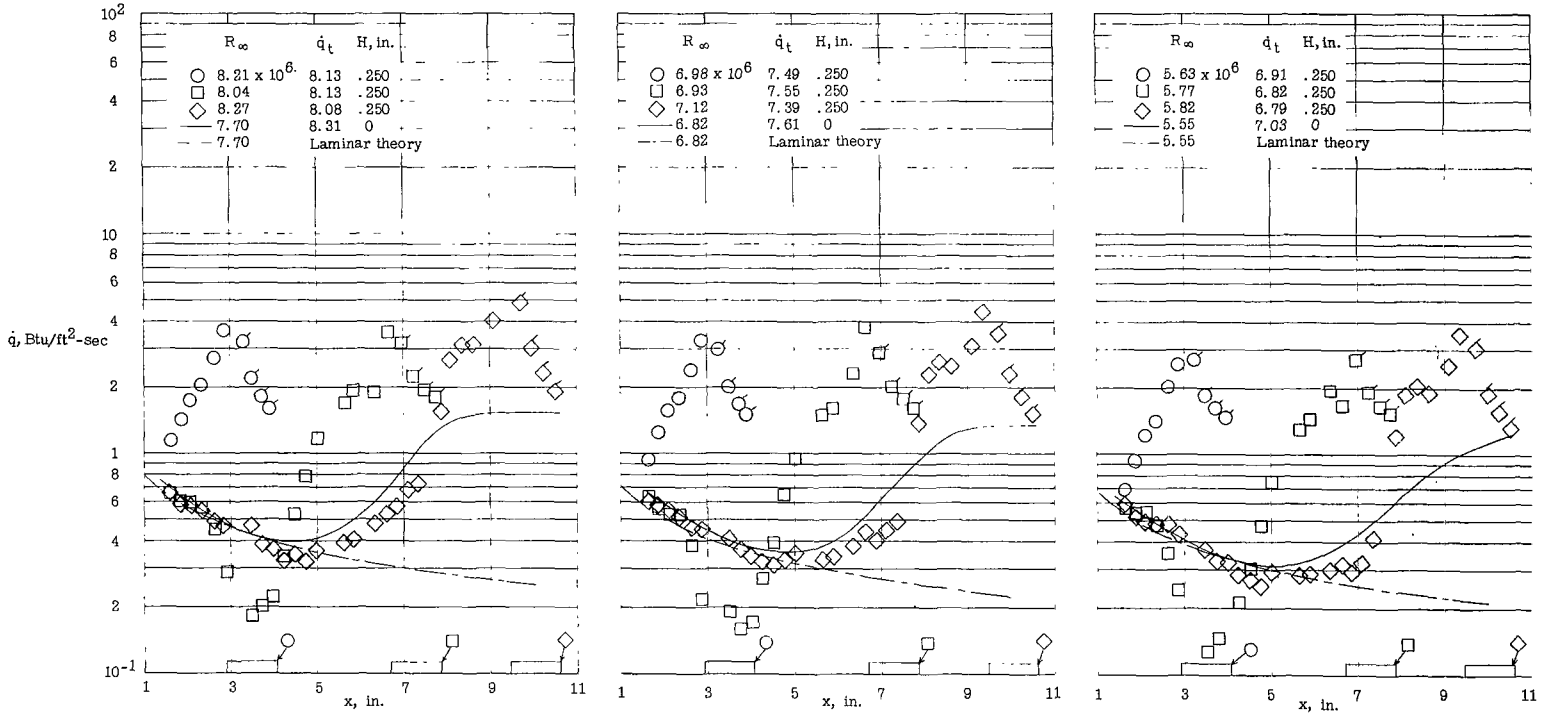

(a) $\alpha = 0^0$.

Figure 4.- Effects of step location and Reynolds number on heat transfer within a separated region forced by forward-facing steps for a sharp-leading-edge model. t = 0.0015 inch; H = 0.250 inch; plate 1; tunnel 1. Flagged symbols denote data on upper step surface.

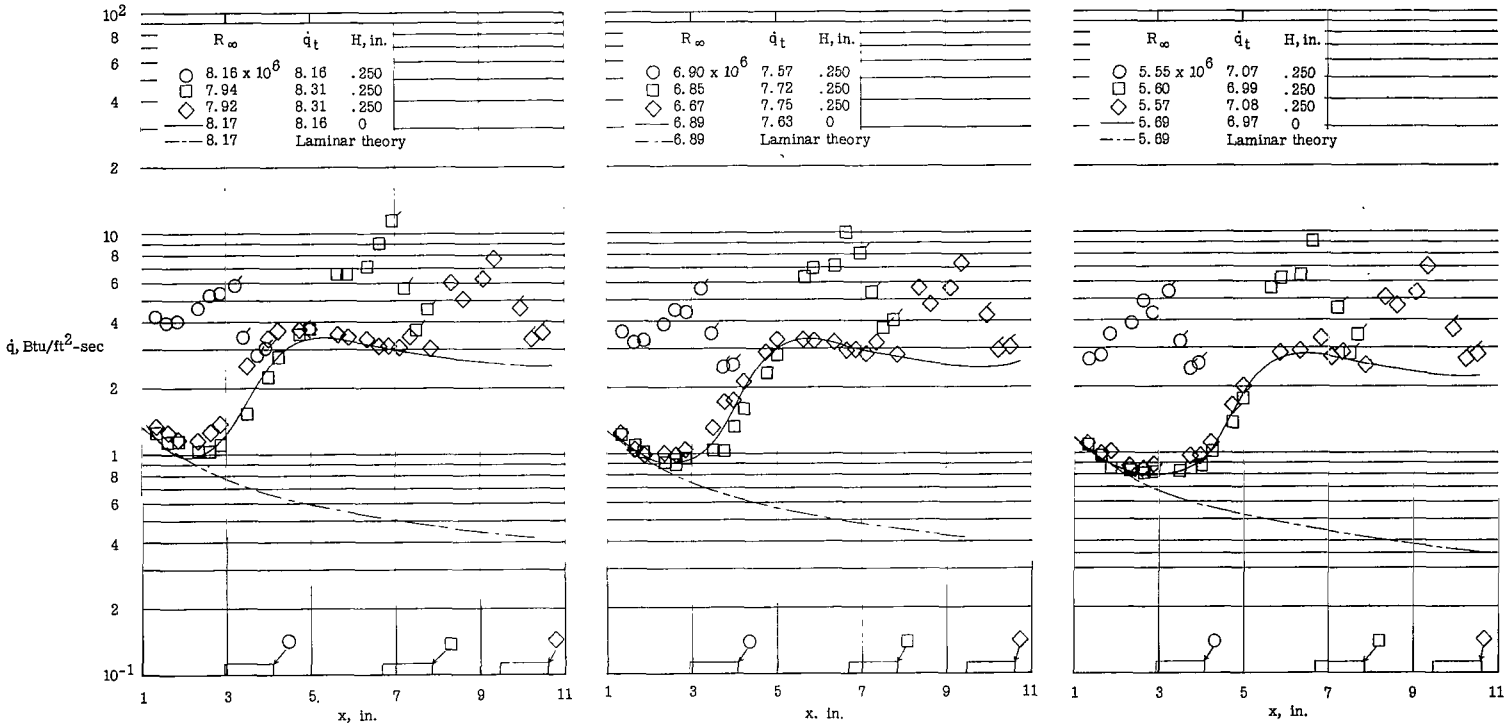

(b) $\alpha = 8^0$.

Figure 4.- Concluded.

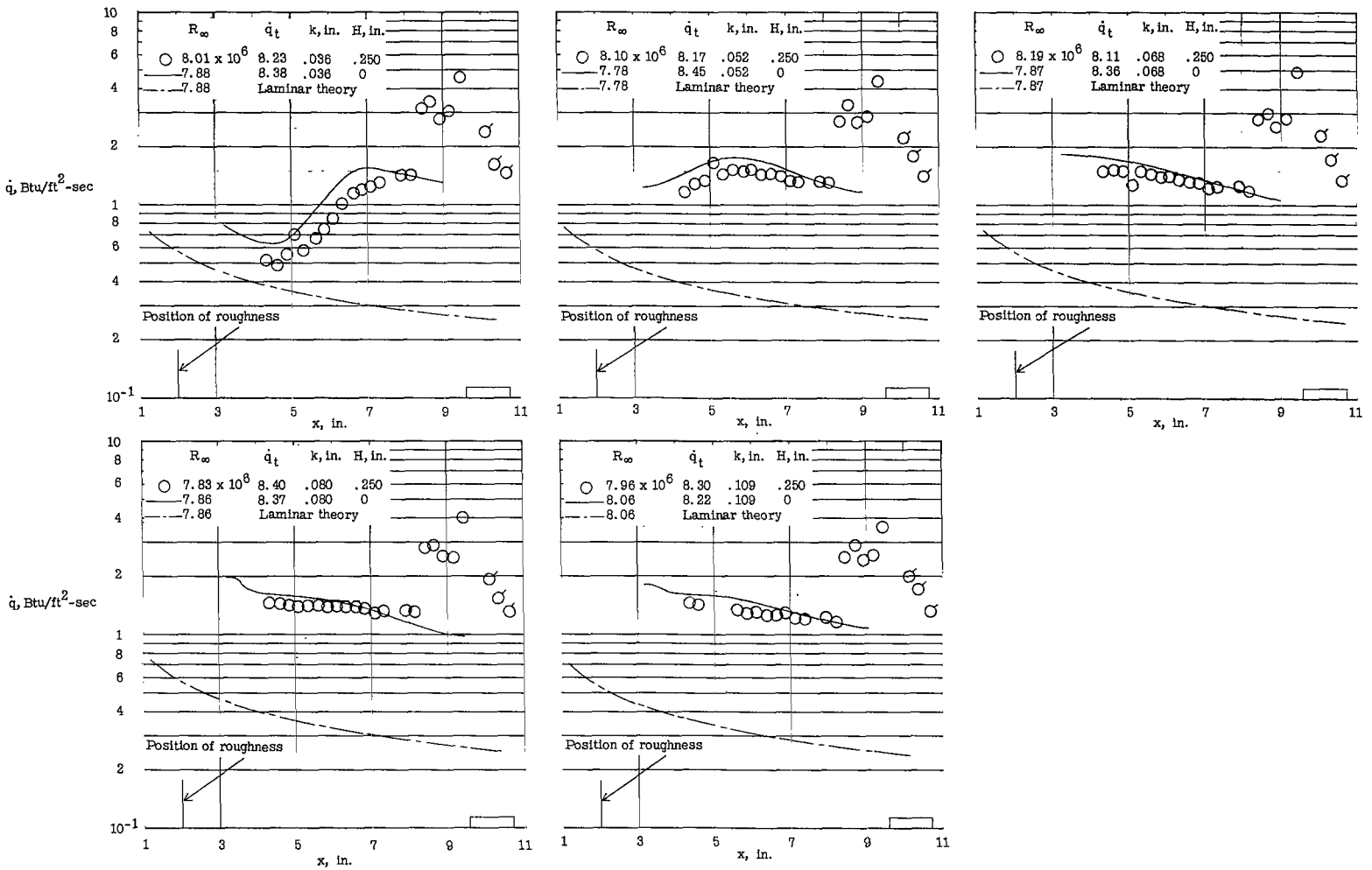

(a) $\alpha = 0^0$.

Figure 5.- Heat transfer within regions of turbulent separation forced by forward-facing steps. $t < 0.004$ inch; $H = 0.250$ inch; $R_\infty \approx 8 \times 10^6$ per foot; $x_d = 9.58$ inches; plate 2; tunnel 1. Flagged symbols denote data on upper step surface.

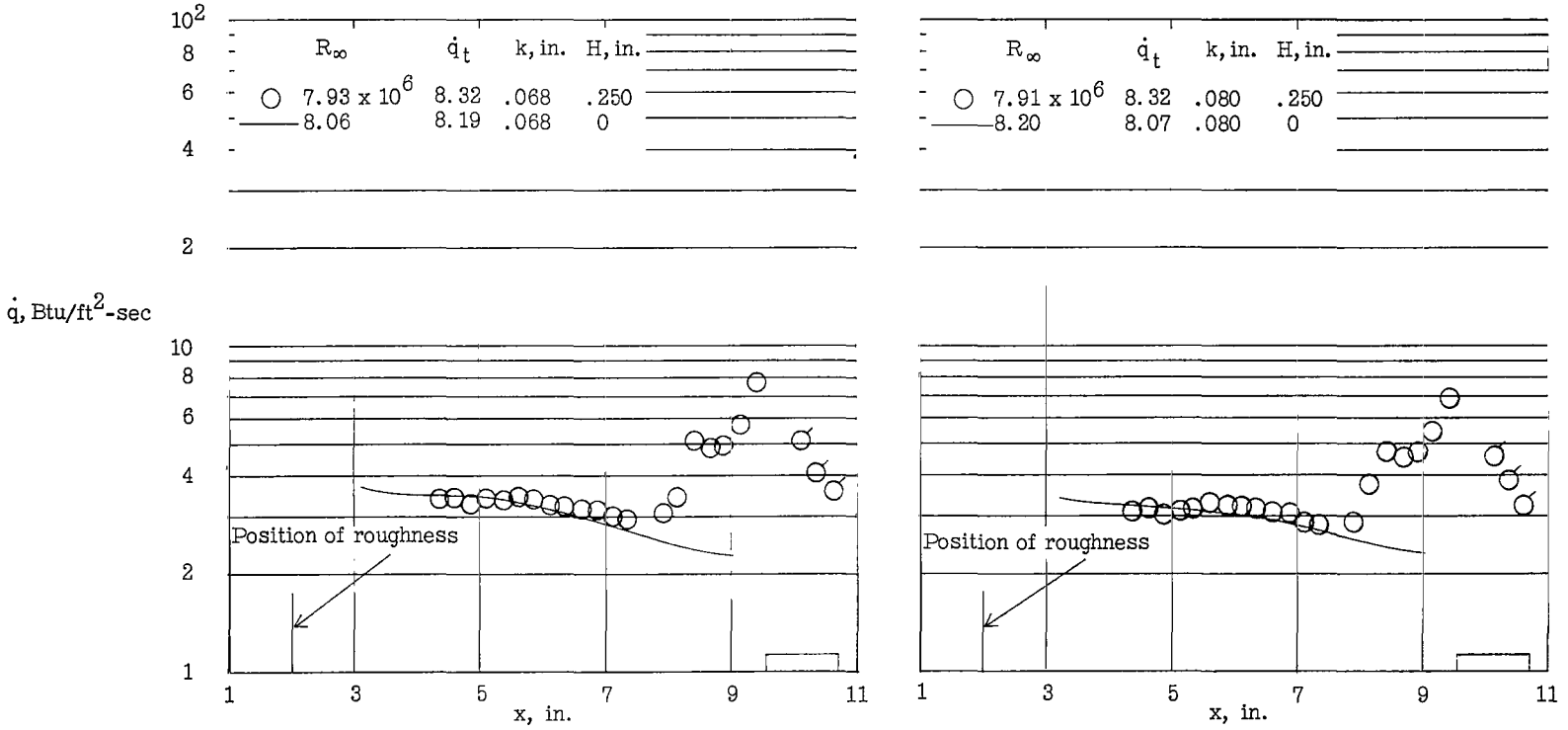

(b) $\alpha = 8^0$.

Figure 5.- Concluded.

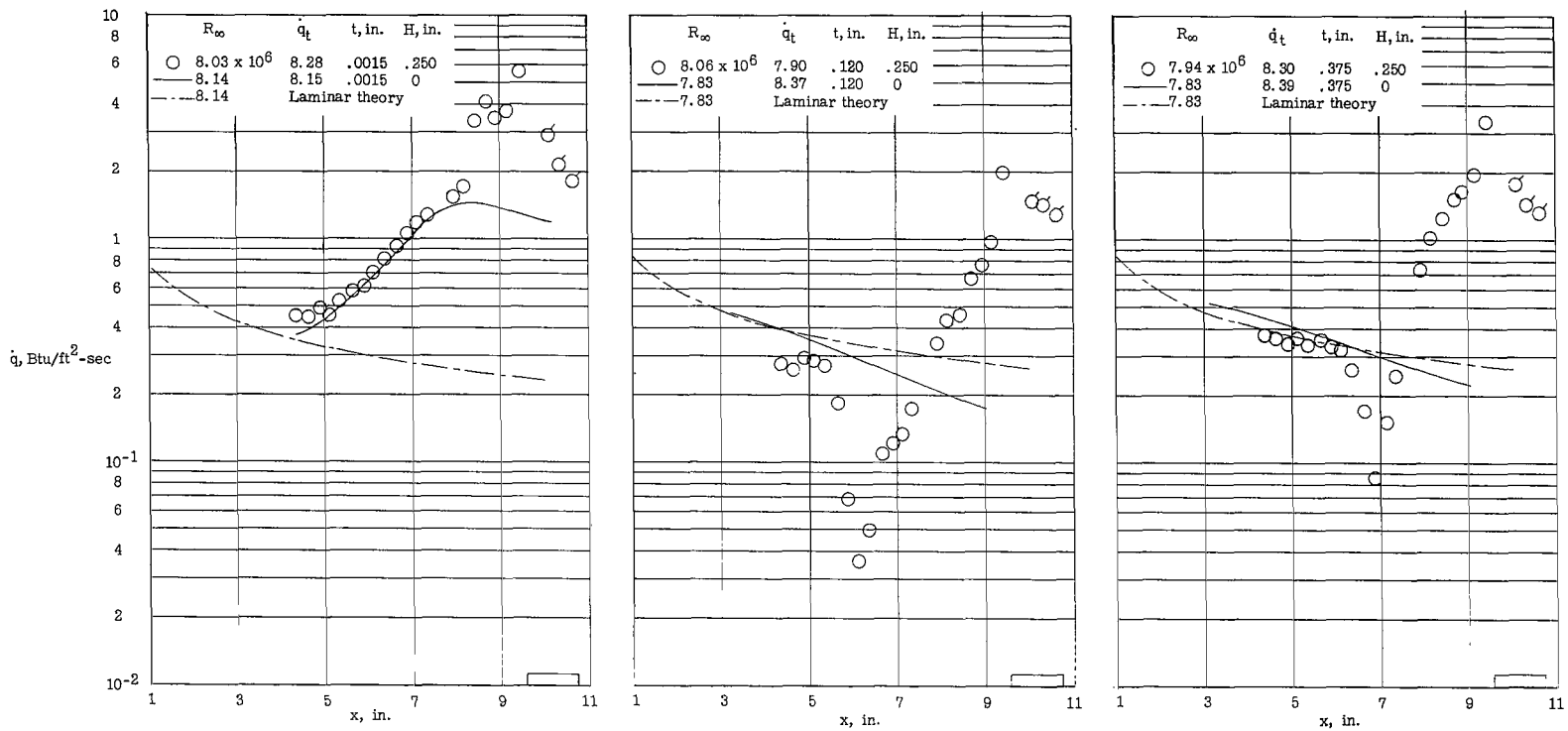

(a) $\alpha = 0^0$.

Figure 6.- Effects of leading-edge bluntness on heat transfer within regions of separation forced by forward-facing steps. $R_\infty \approx 8 \times 10^6$ per foot; x_d = 9.58 inches; H = 0.250 inch; plate 2; tunnel 1. Flagged symbols denote data on upper step surface.

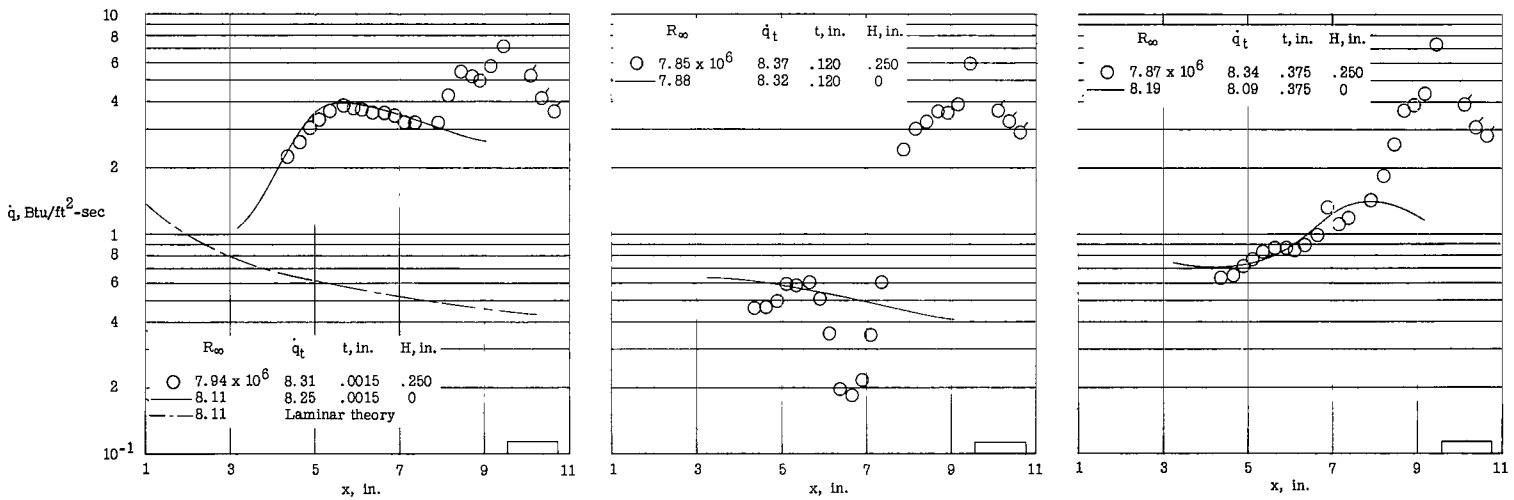

(b) $\alpha = 8^0$.

Figure 6.- Concluded.

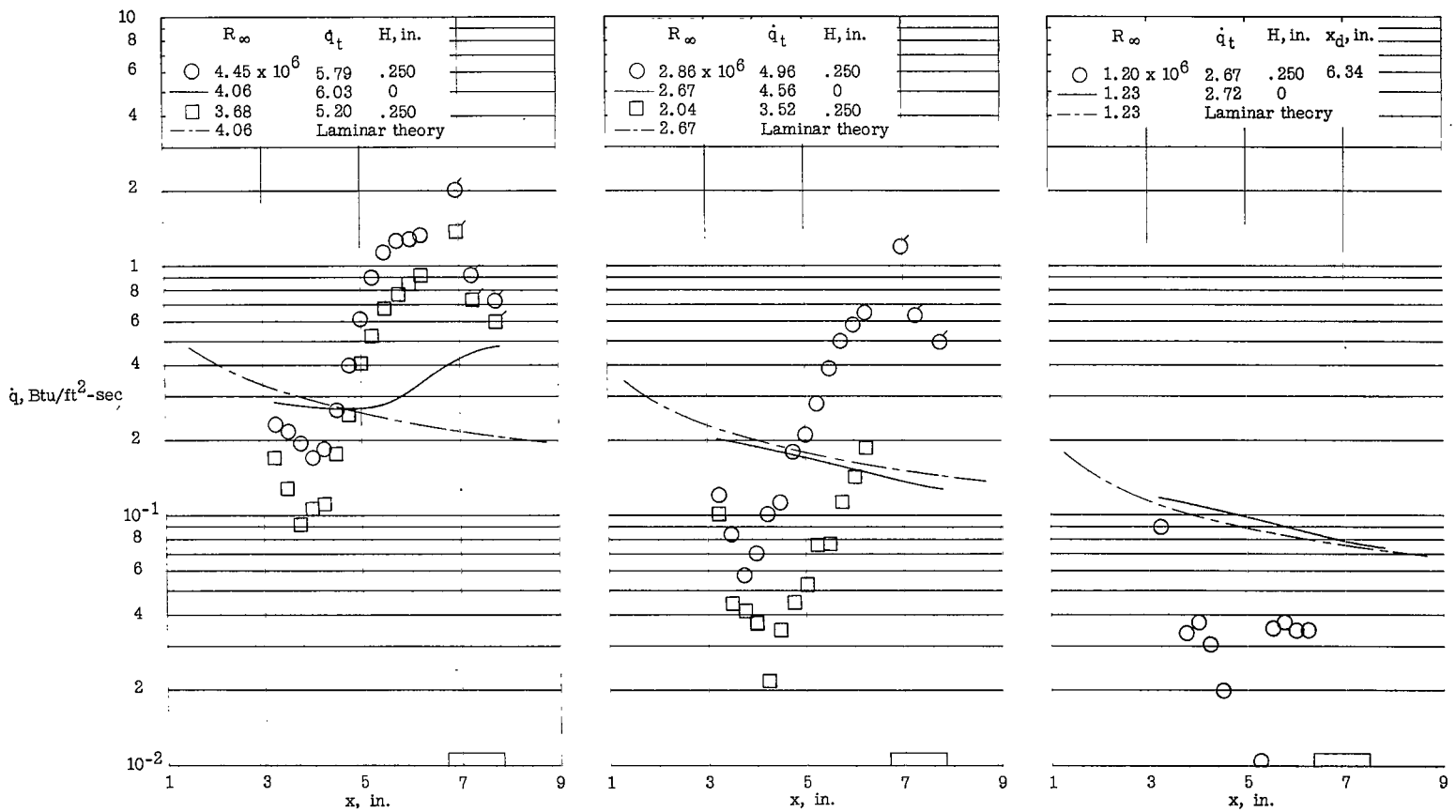

(a) t = 0.0015 inch.

Figure 7.- Effects of leading-edge bluntness on heat transfer within regions of separation forced by forward-facing steps for the full test Reynolds number range. $\alpha = 0^0$; x_d = 6.7 inches; H = 0.25 inch; plate 2; tunnel 2. Flagged symbols denote data on upper step surface.

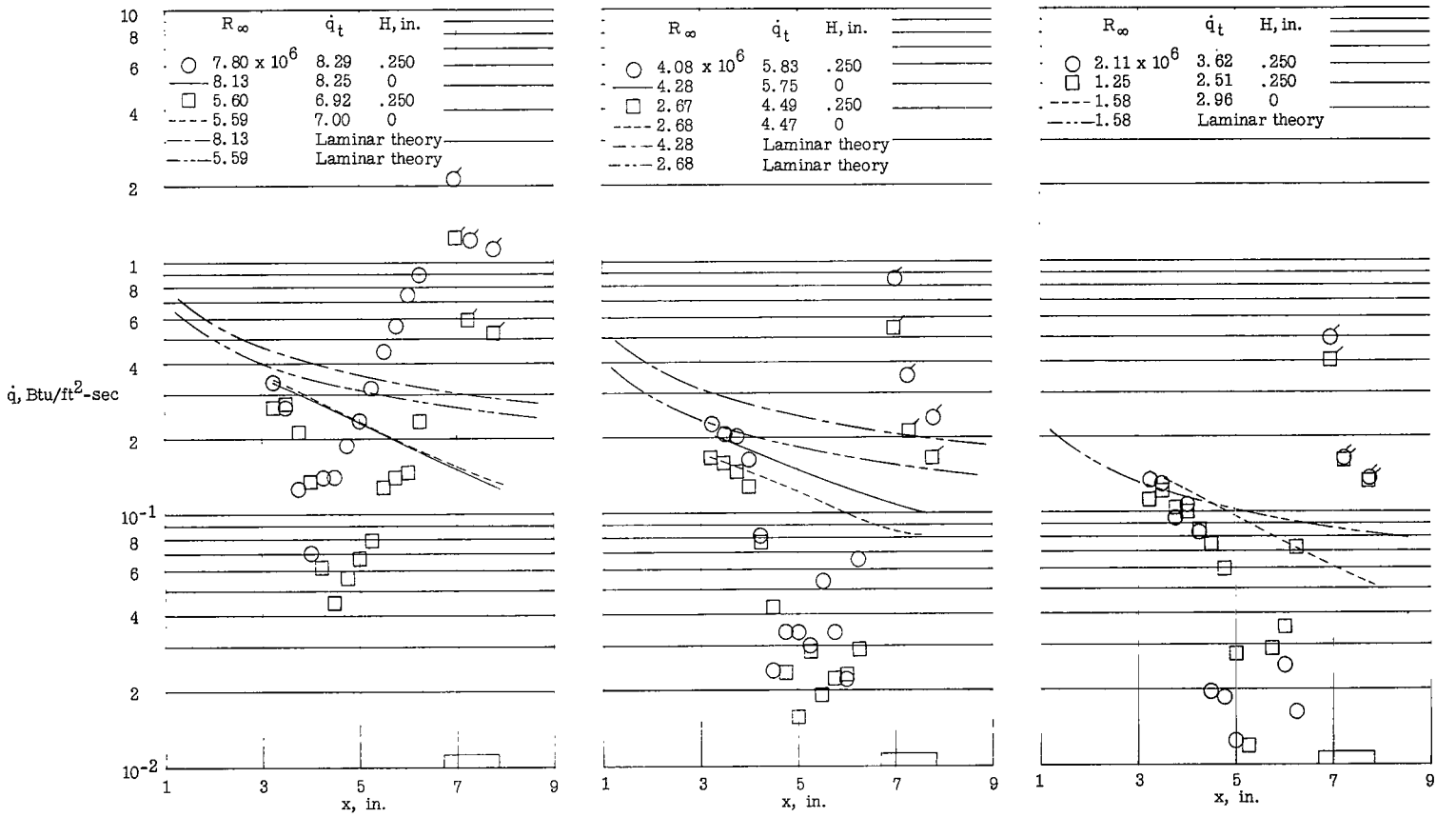

(b) t = 0.120 inch.

Figure 7.- Continued.

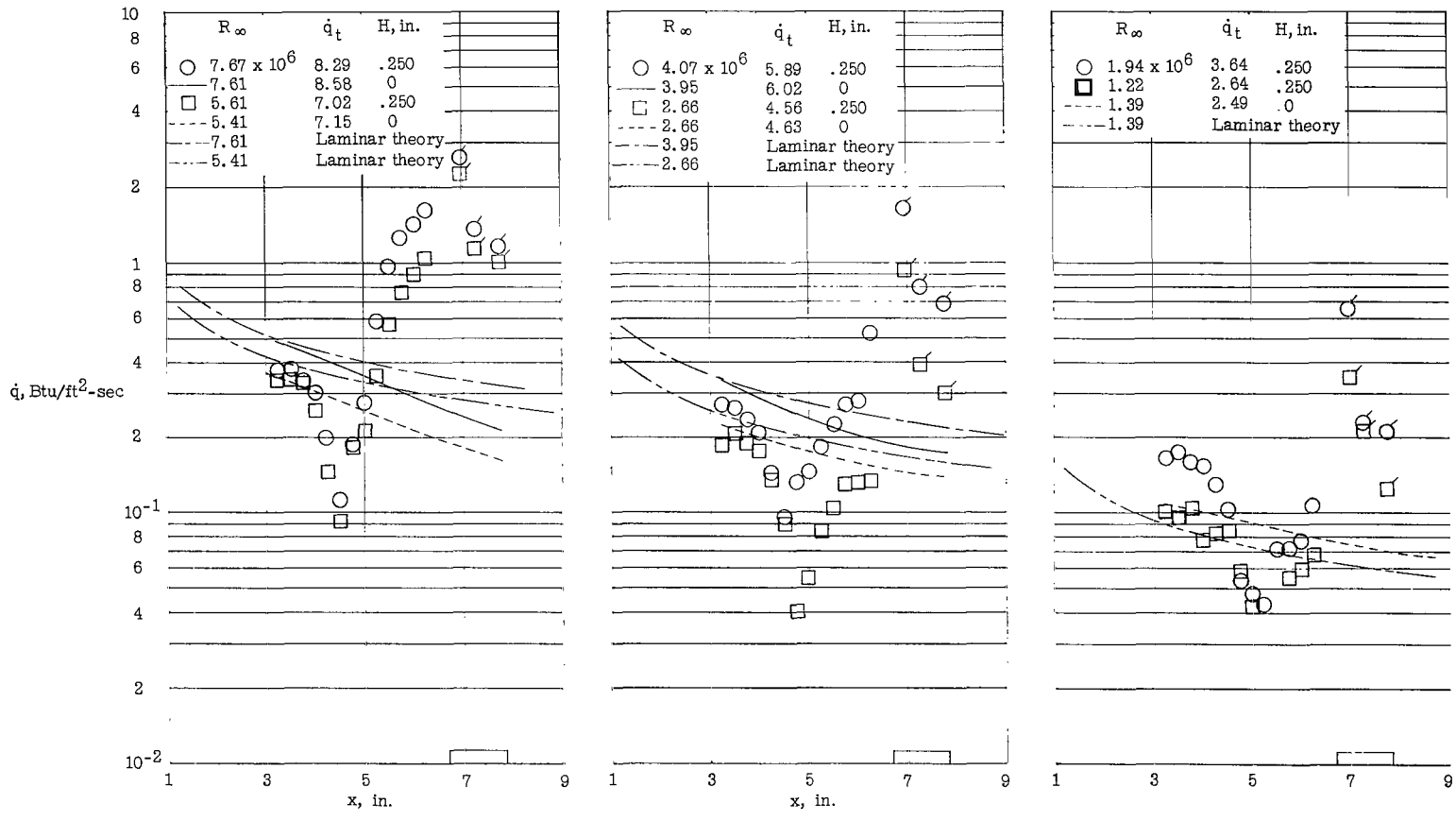

(c) t = 0.375 inch.

Figure 7.- Concluded.

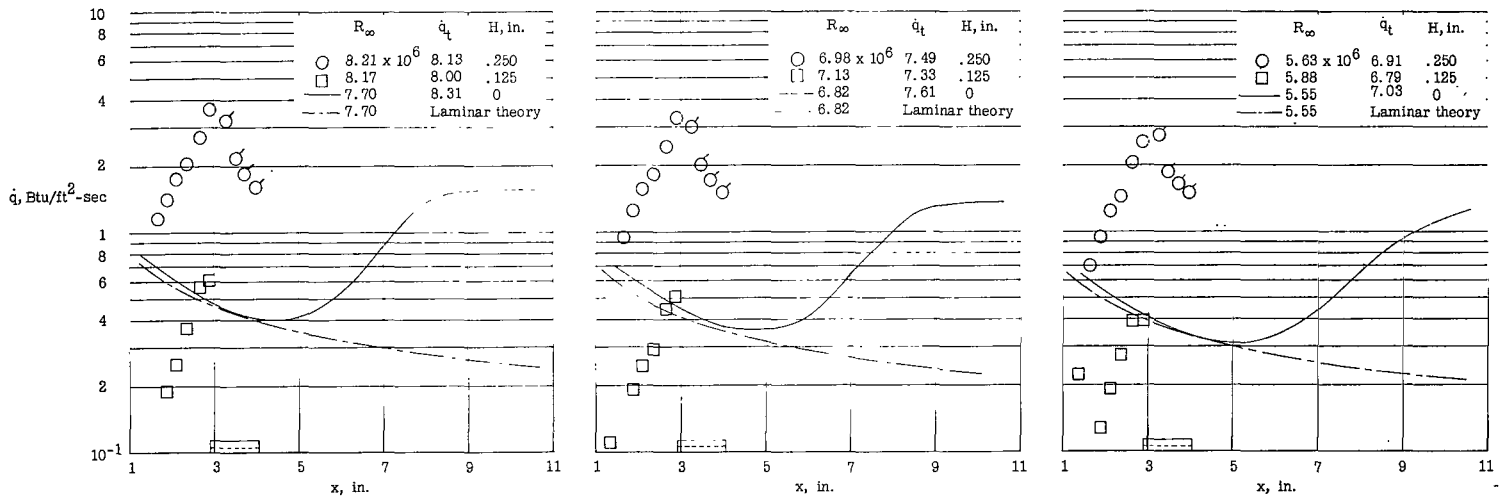

(a) $\alpha = 0^0$; $x_d = 2.94$ inches.

Figure 8.- Effect of step height on heat transfer within regions of separation and on the extent of separation for a sharp leading-edge model. t = 0.0015 inch; plate 1; tunnel 1, at three unit free-stream Reynolds numbers. Flagged symbols denote data on the upper step surface.

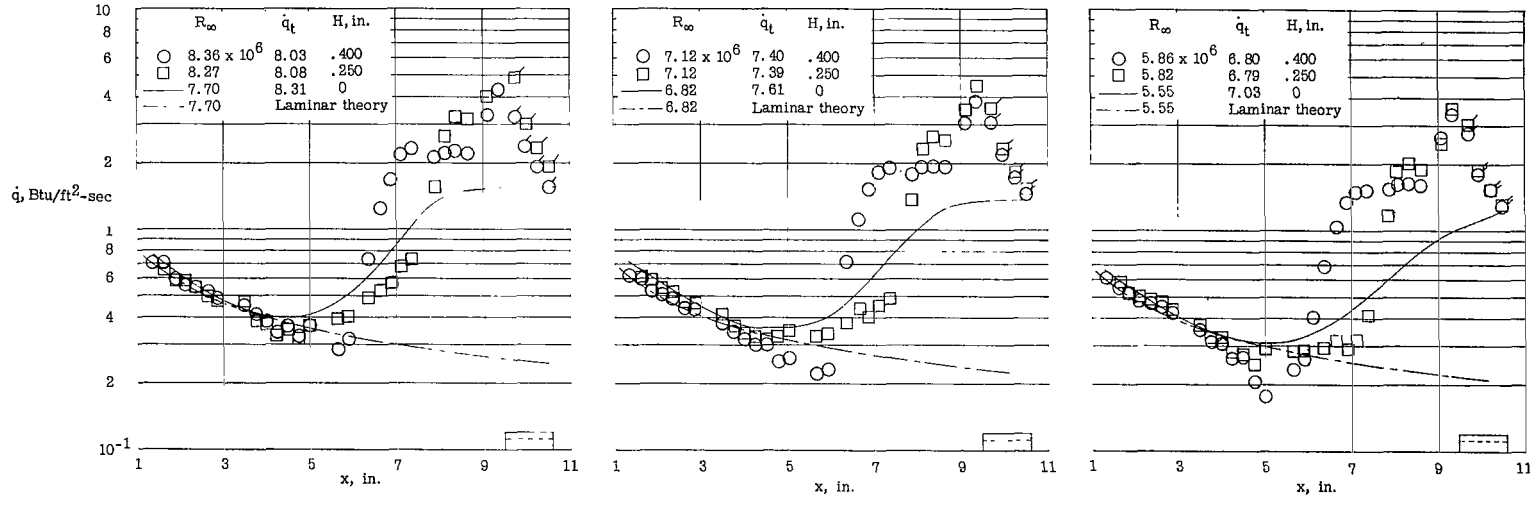

(b) $\alpha = 0^0$; $x_d = 9.44$ inches.

Figure 8.- Continued.

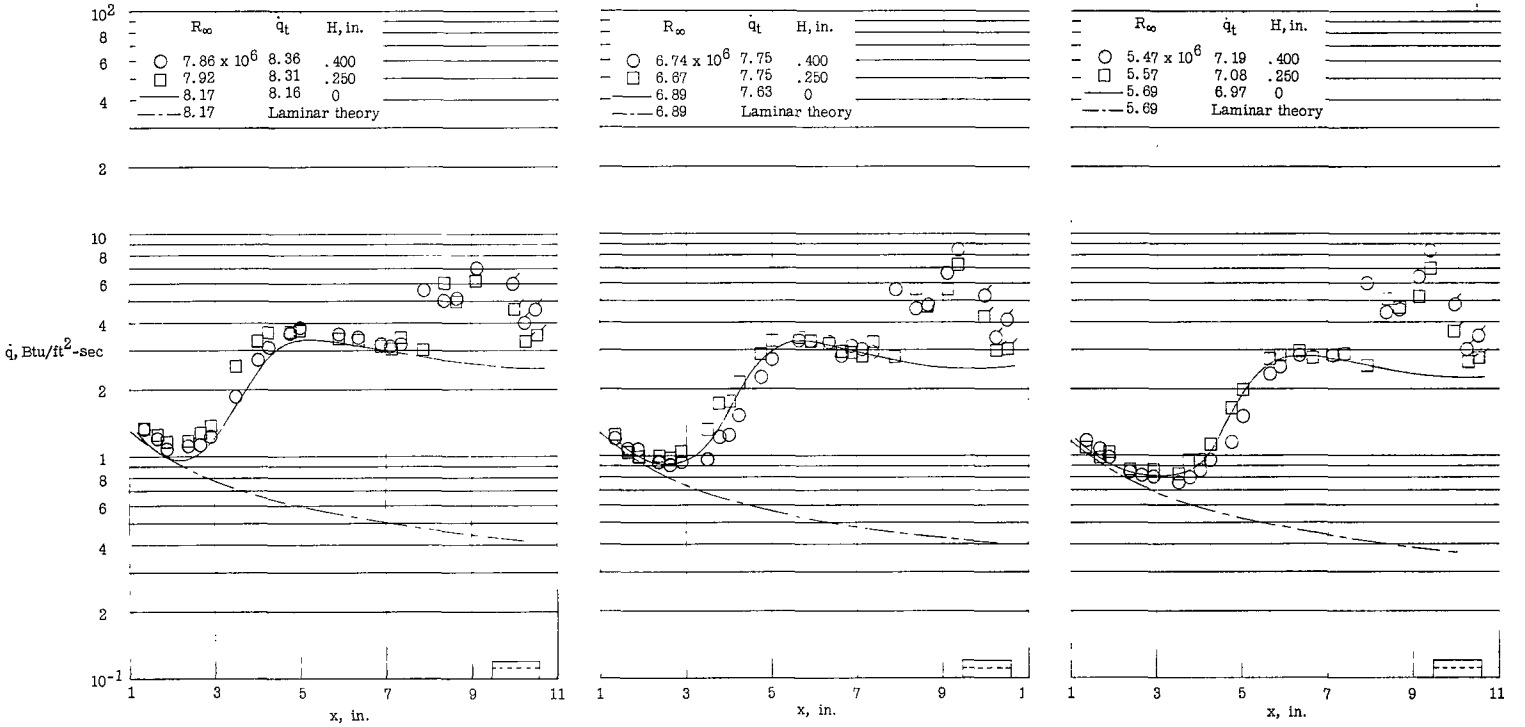

(c) $\alpha = 8^0$; $x_d = 9.44$ inches.

Figure 8.- Concluded.

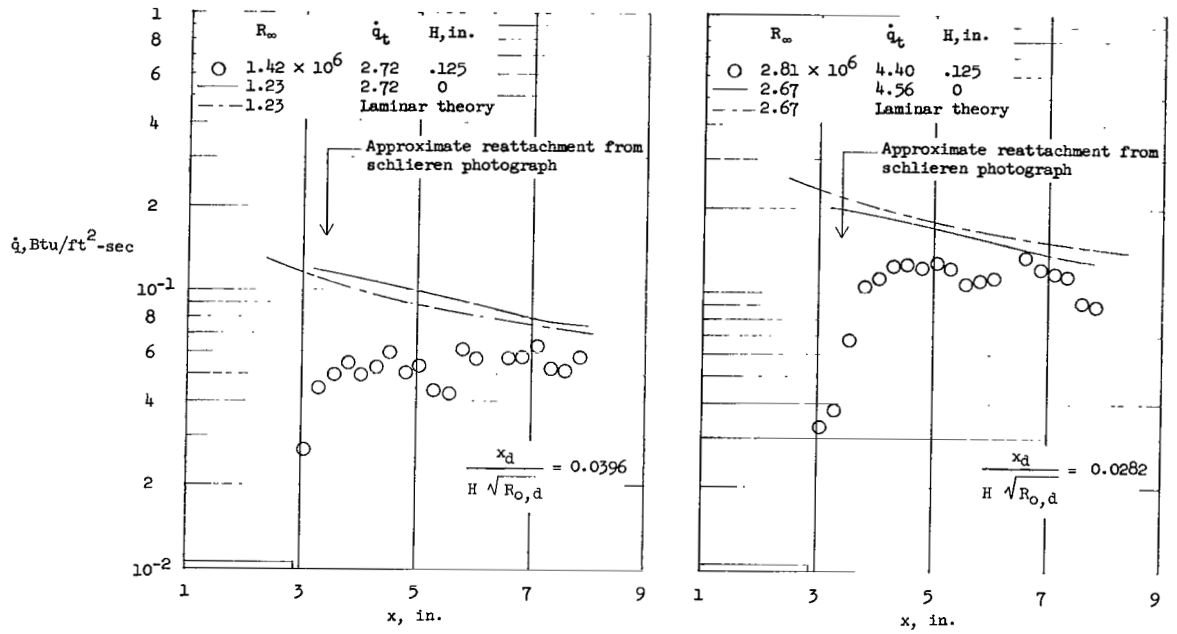

(a) H = 0.125 inch.

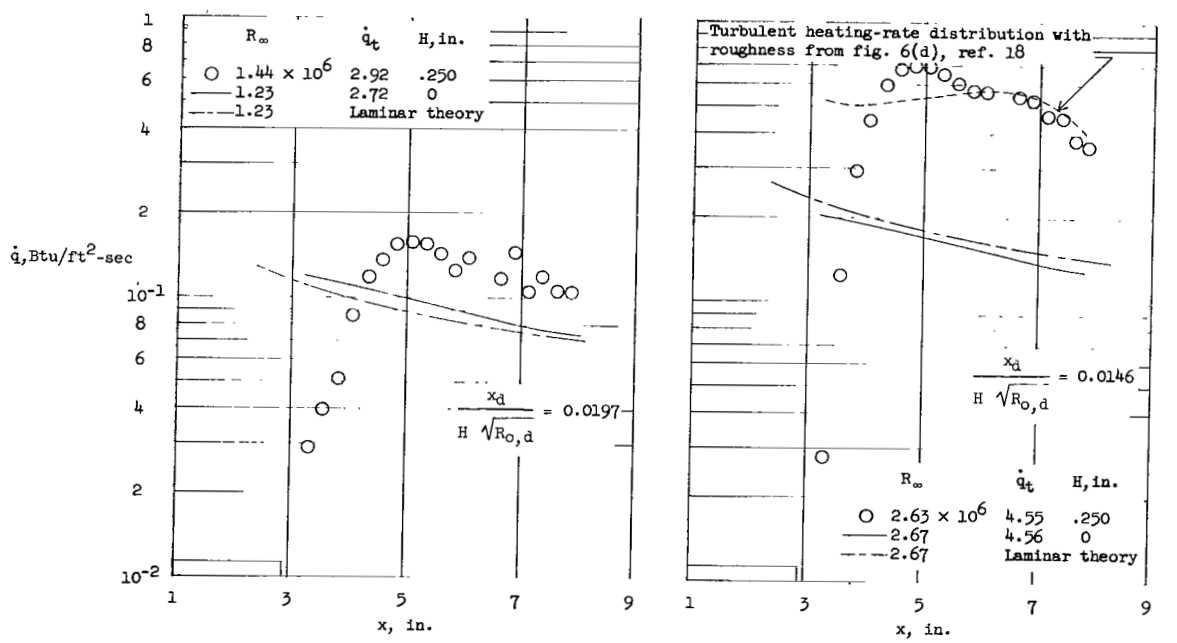

(b) H = 0.250 inch.

Figure 9.- Heat transfer behind rearward-facing steps on a sharp-leading-edge model at $R_\infty \approx 1.3 \times 10^6$ and 2.8×10^6 per foot. $\alpha = 0^0$; x_d = 2.90 inches; plate 2; and tunnel 2.

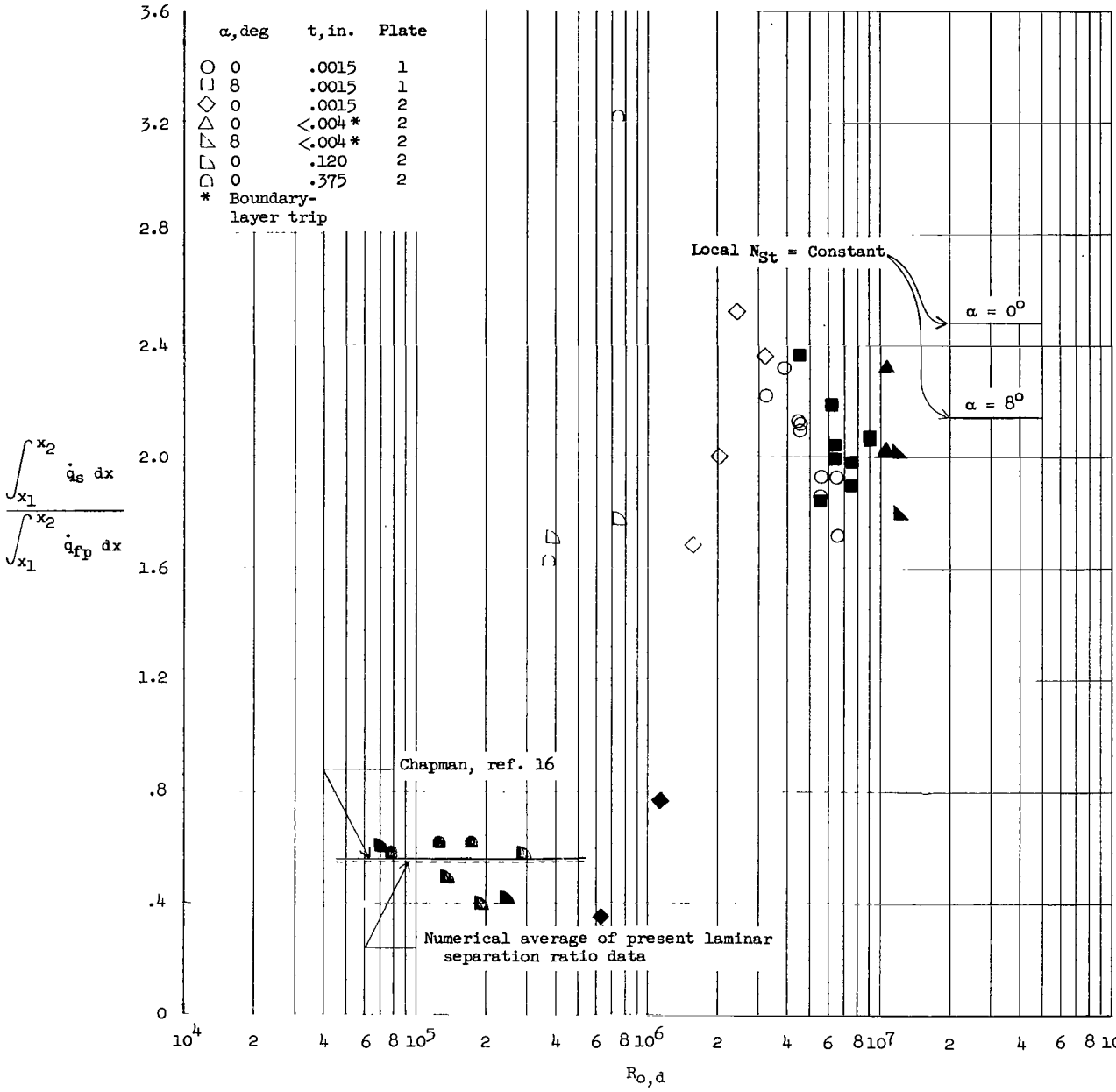

Figure 10.- Effects of Reynolds number variation on ratio of integrated heating rate in regions of separated flow forced by forward-facing steps to integrated heating rate in a similar region of attached flow. Solid symbols on left of figure and on right of figure denote laminar and turbulent separation results, respectively. Open symbols denote transitional separation results.

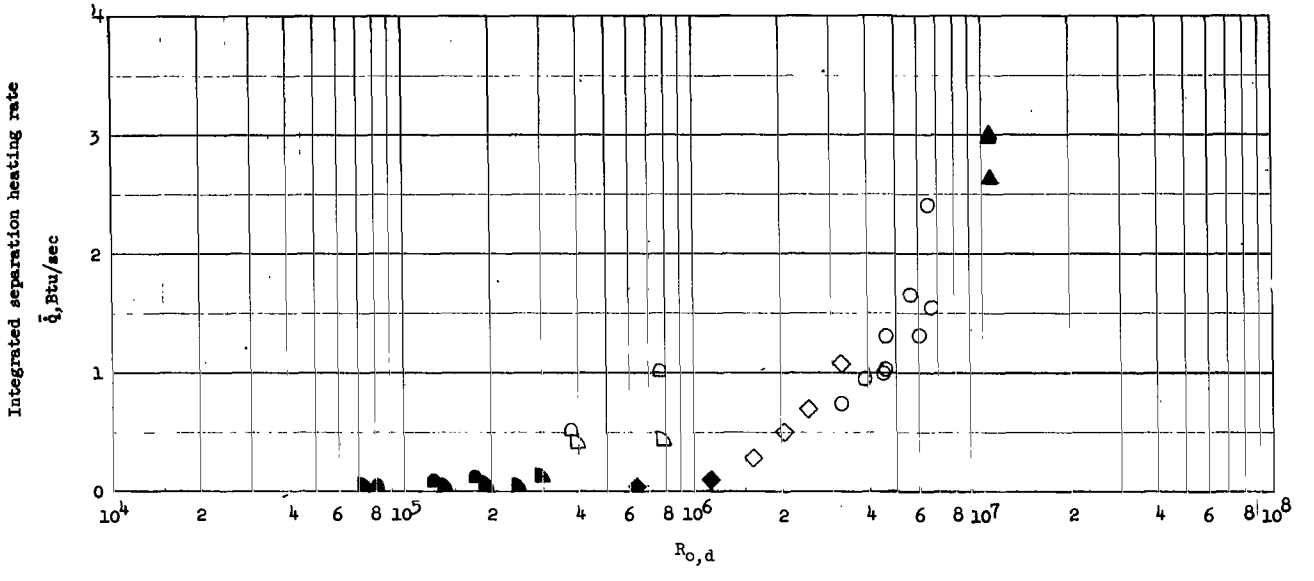

(a) $\alpha = 0^0$.

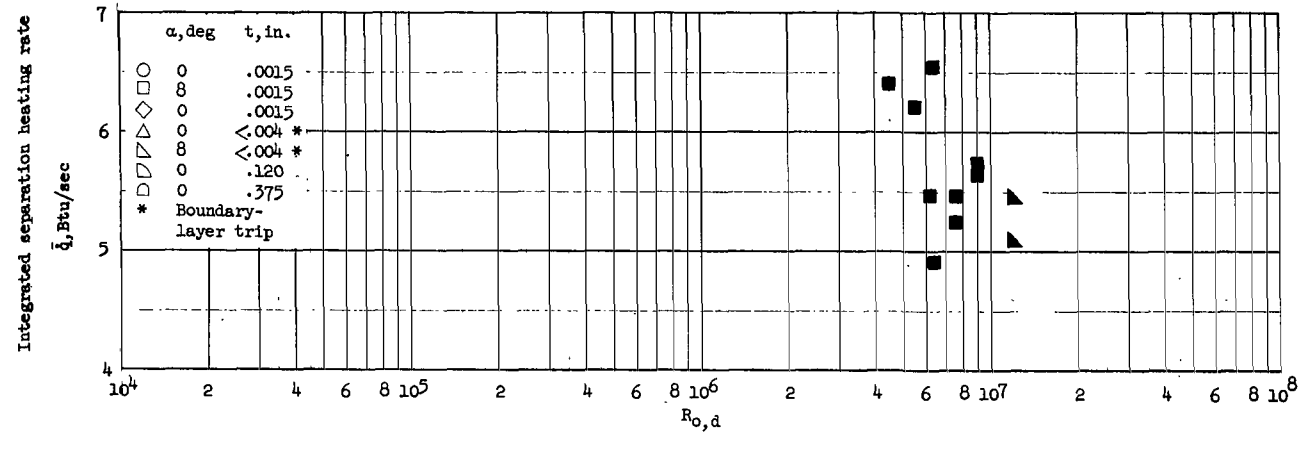

(b) $\alpha = 8^0$.

Figure 11.- Effects of Reynolds number variation of integrated heating rate in regions of separated flow forced by forward-facing steps. Solid symbols on left of figure and on right of figure denote laminar and turbulent separation results, respectively. Open symbols denote separation results.

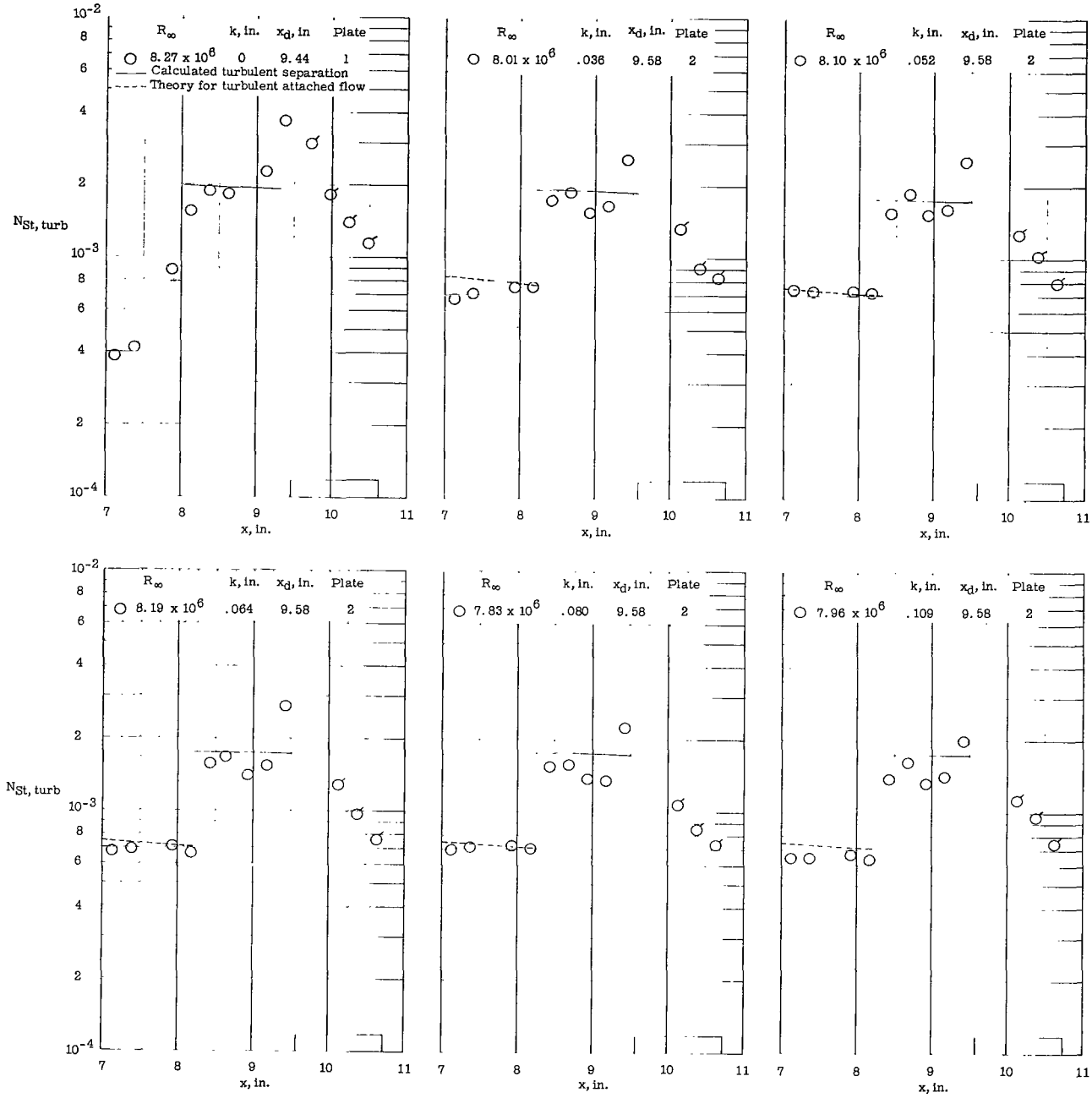

(a) $\alpha = 0^0$; H = 0.250 inch.

Figure 12.- Comparison of experimental Stanton number distributions in regions of turbulent separation forced by forward-facing steps with predictions for sharp-leading-edge models. Tunnel 1. Flagged symbols denote data on upper step surface.

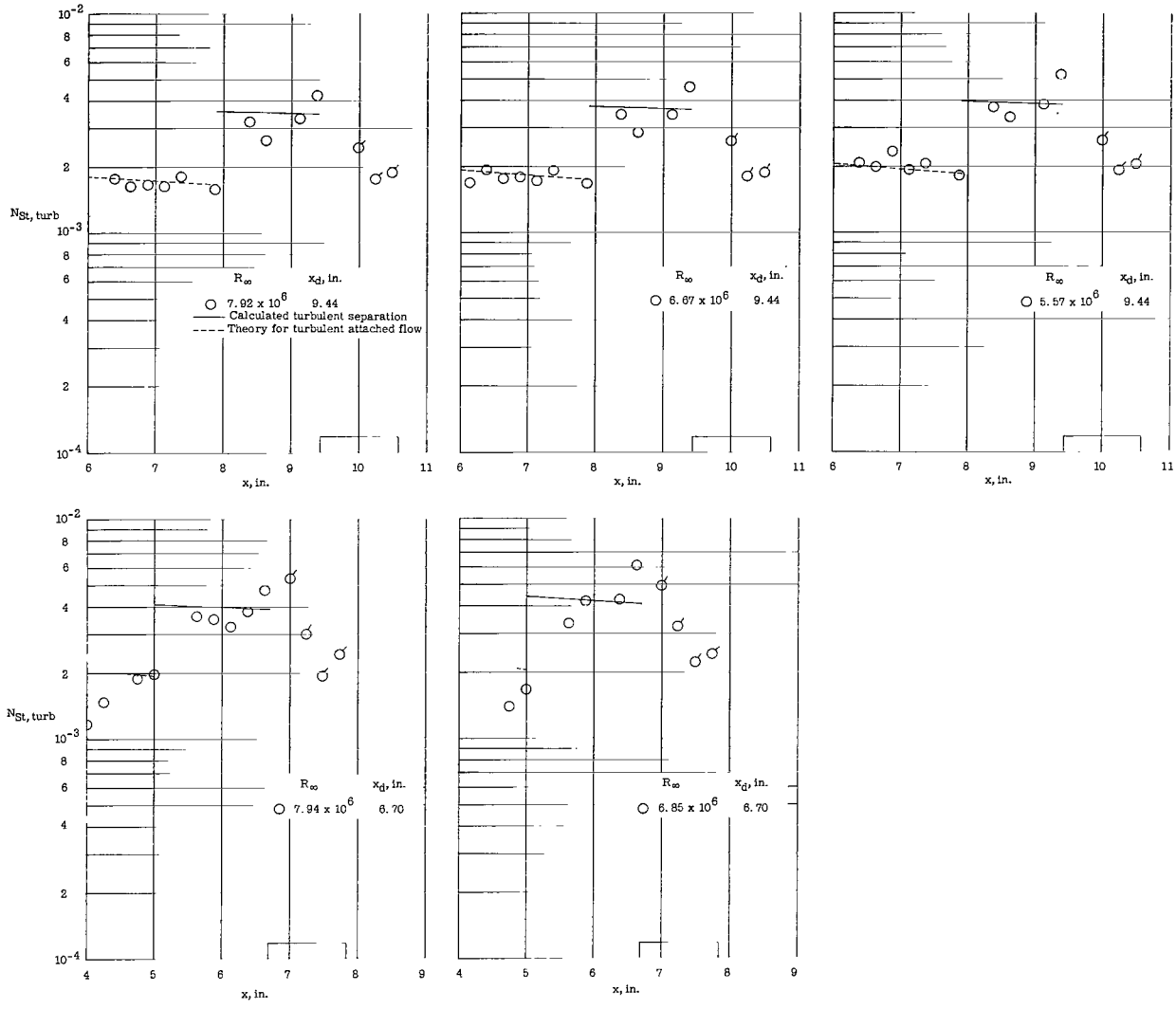

(b) $\alpha = 8^0$; H = 0.250 inch; plate 1.

Figure 12.- Continued.

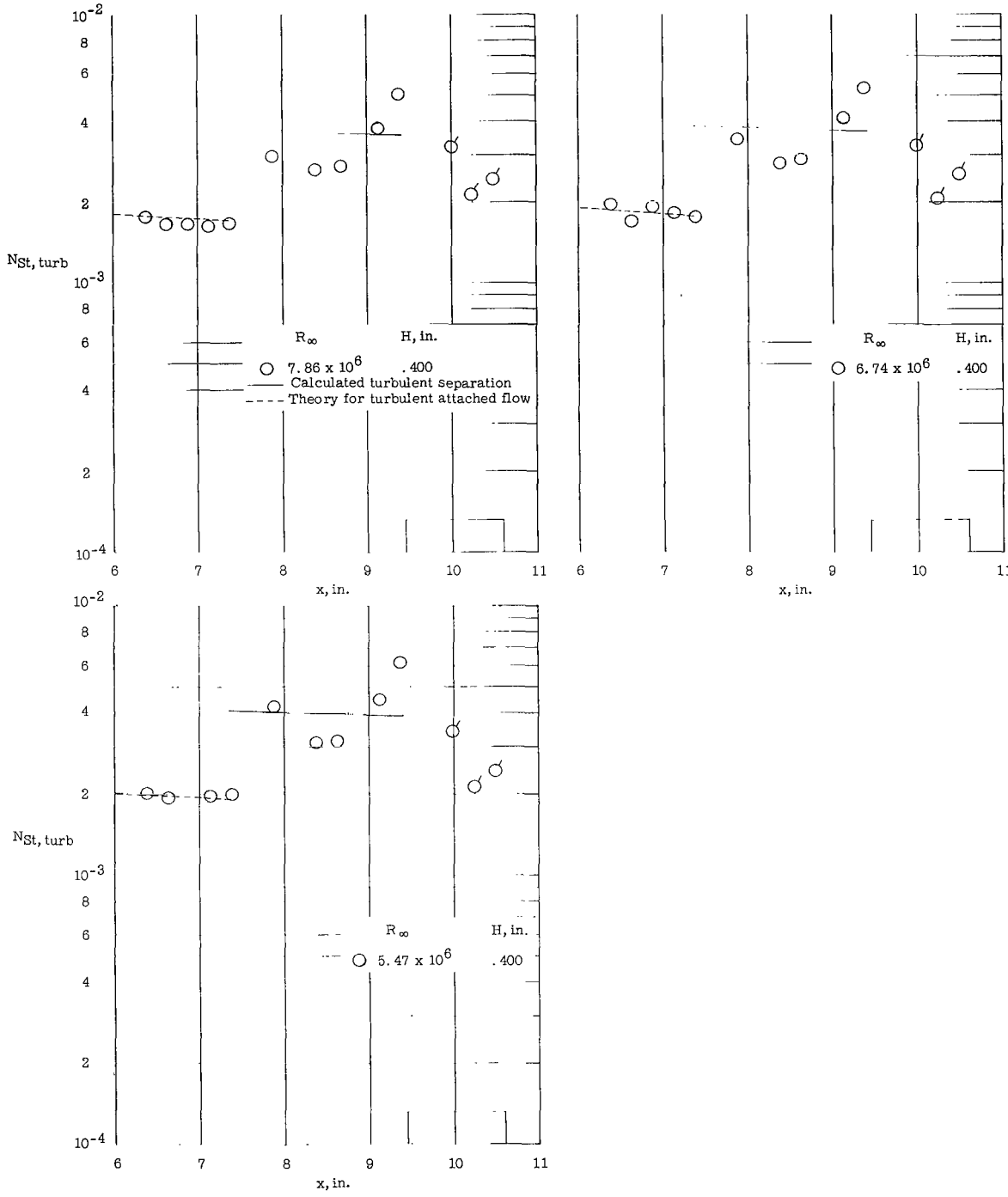

(c) $\alpha = 8^0$; $x_d = 9.44$ inches; plate 1.

Figure 12.- Continued.

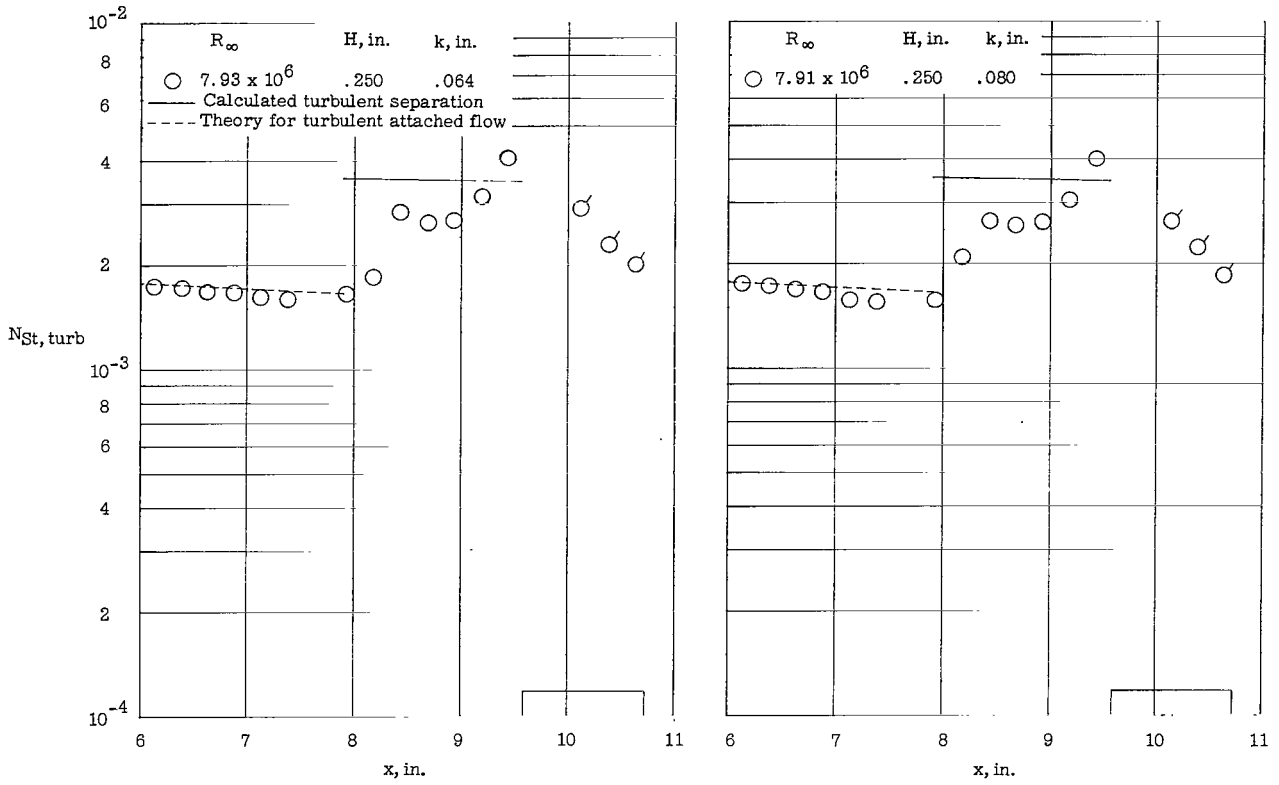

(d) $\alpha = 8^0$; $x_d = 9.58$ inches; plate 2.

Figure 12. - Concluded.

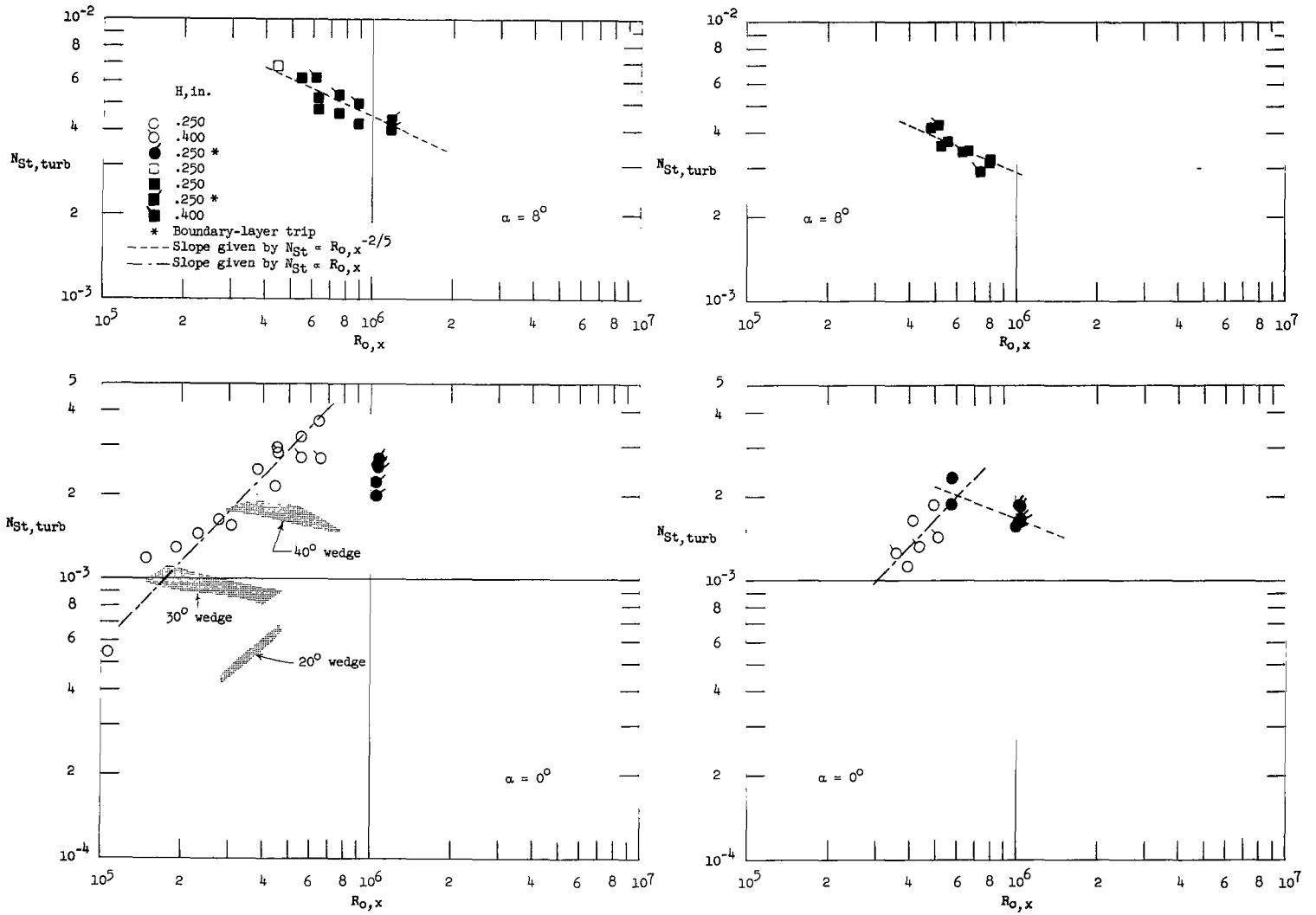

(a) Second peak heating in regions of transitional and turbulent separation for forward-facing steps.

(b) First peak heating in regions of turbulent separation and transitional separation with beginning of fully developed turbulence upstream of disturbance for forward-facing steps. (See fig. 3.)

Figure 13.- Effects of Reynolds number variation on peak Stanton numbers in regions of transitional and turbulent separation forced by forward-facing steps. t = 0.0015 inch; tunnel 1. (Open symbols denote transitional separation; solid symbols denote turbulent separation.)

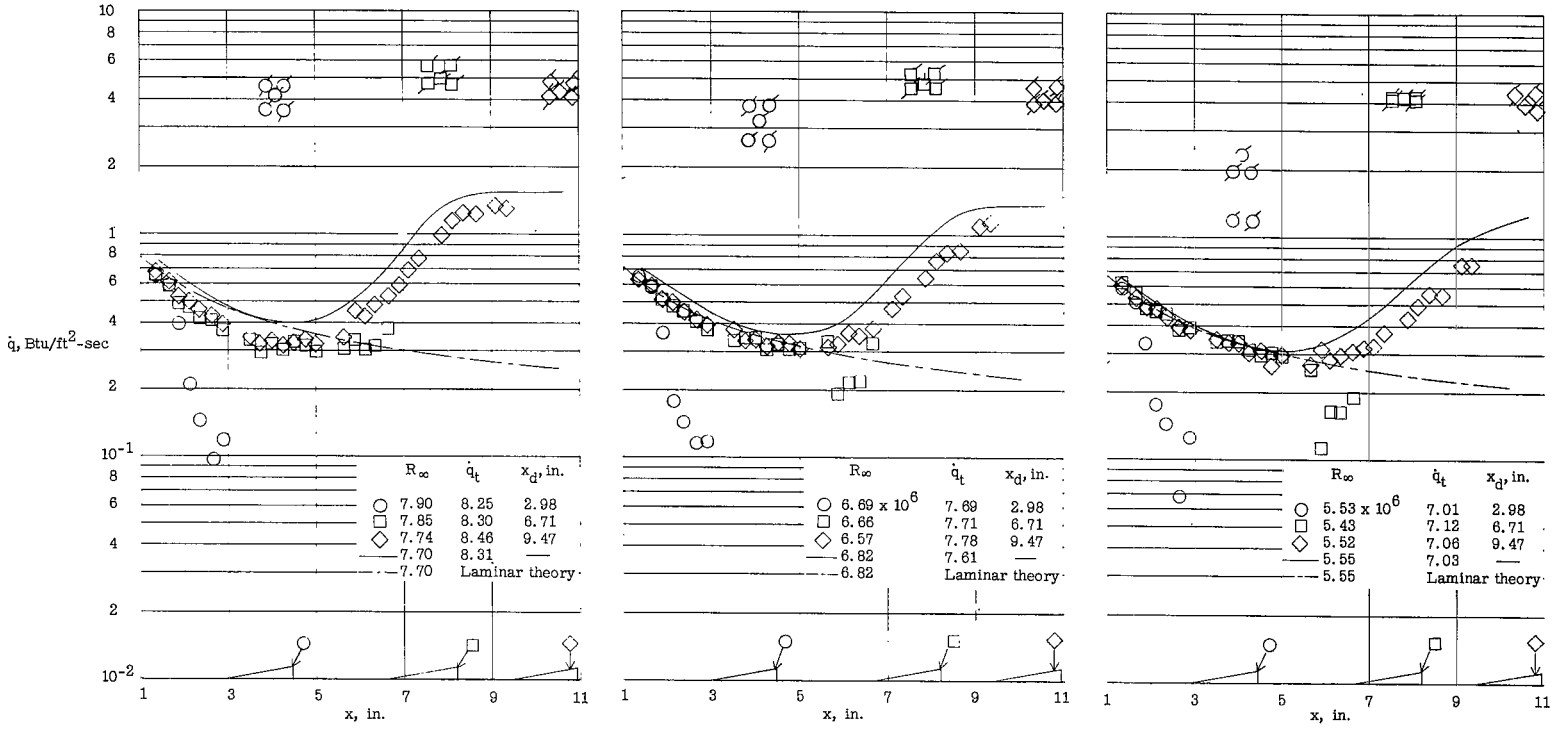

(a) Plate 1, tunnel 1.

Figure 14.- Effects of wedge location and free-stream Reynolds number variation on heat transfer on a sharp-leading-edge model (t = 0.0015 inch) with a 10° wedge at $\alpha = 0^{\circ}$. Flagged symbols denote data on wedge surface.

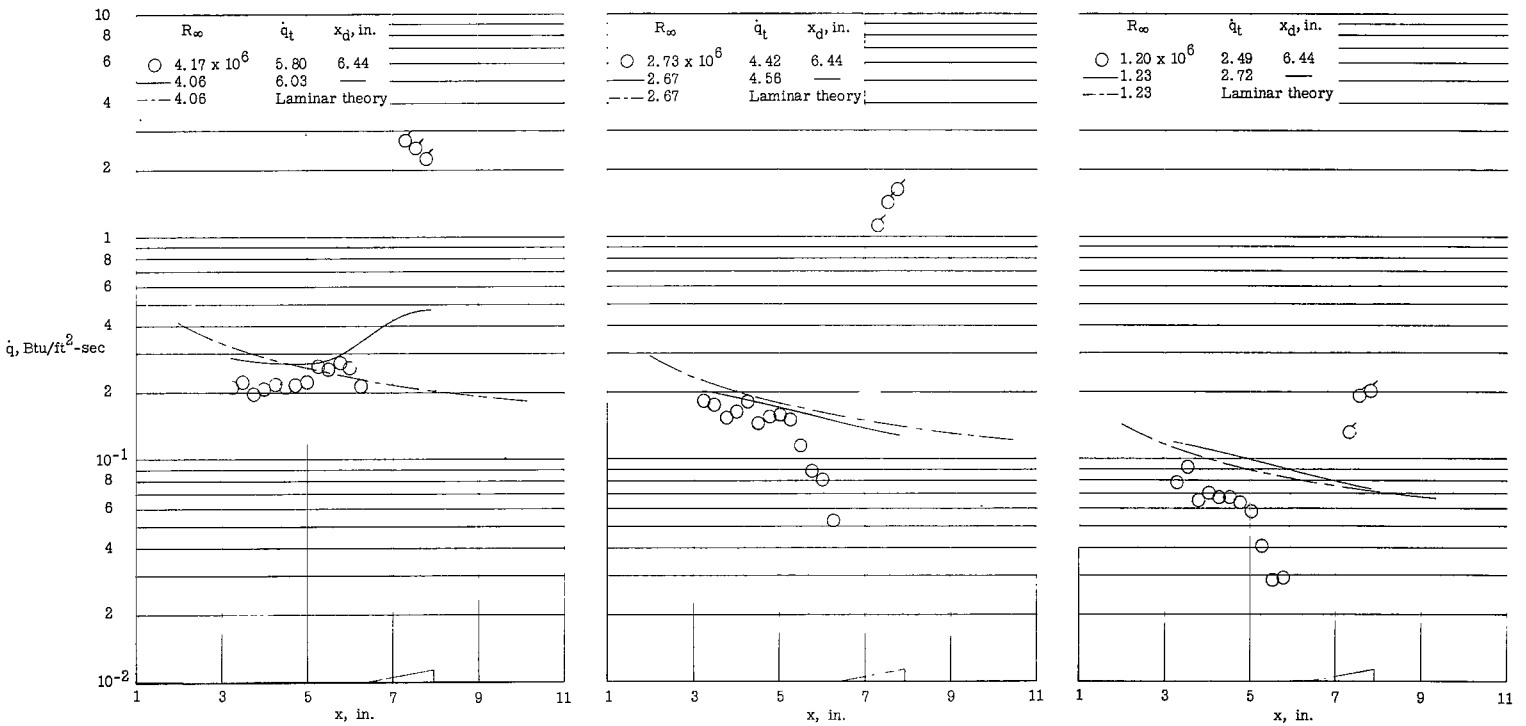

(b) Plate 2, tunnel 2.

Figure 14.- Concluded.

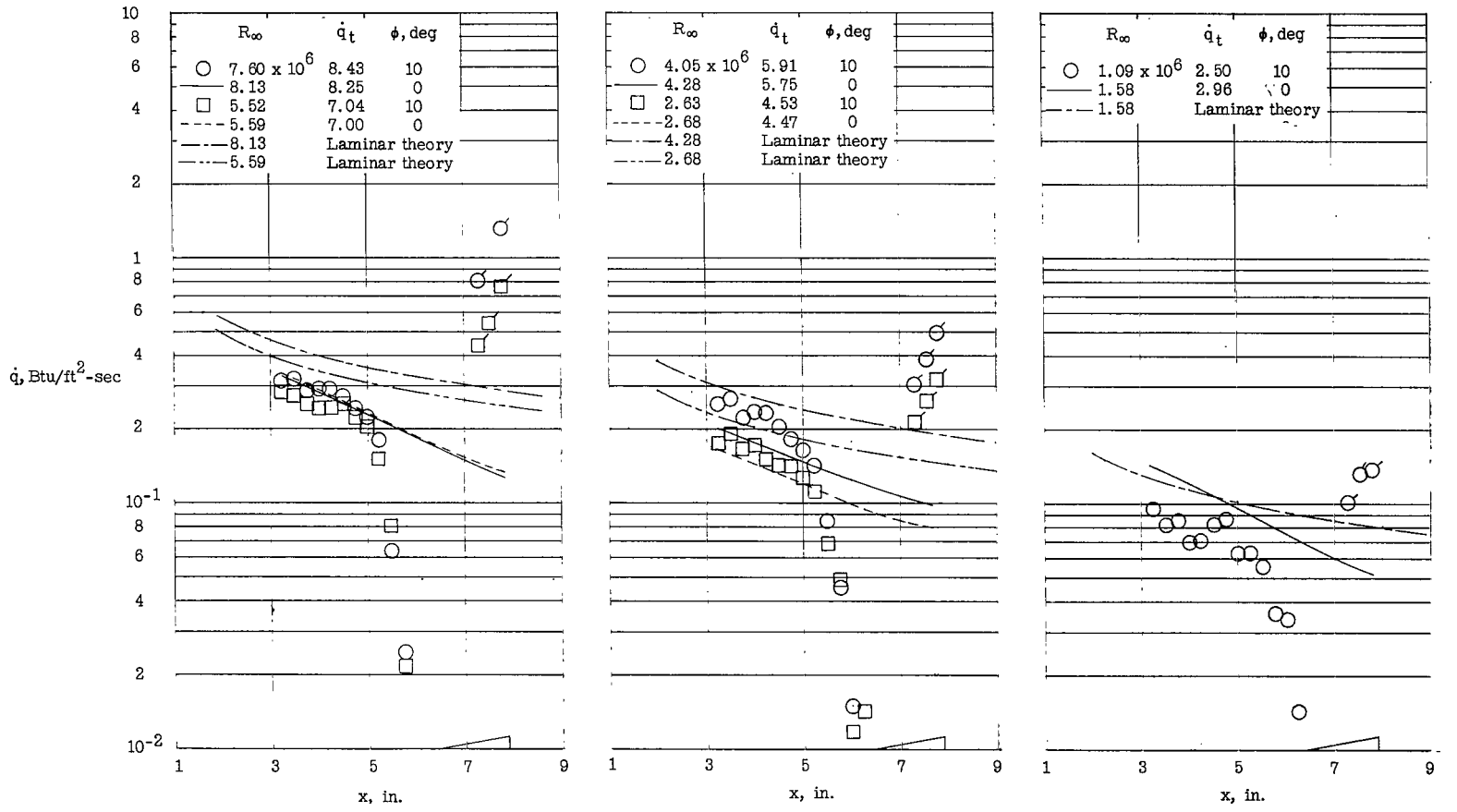

(a) t = 0.120 inch.

Figure 15.- Effects of free-stream Reynolds number variation on heat transfer on blunt-leading-edge models (t = 0.120 inch and t = 0.375 inch) with a 10° wedge at $\alpha = 0°$, and x_d = 6.44 inches; plate 2; tunnel 2. Flagged symbols denote data on wedge surface.

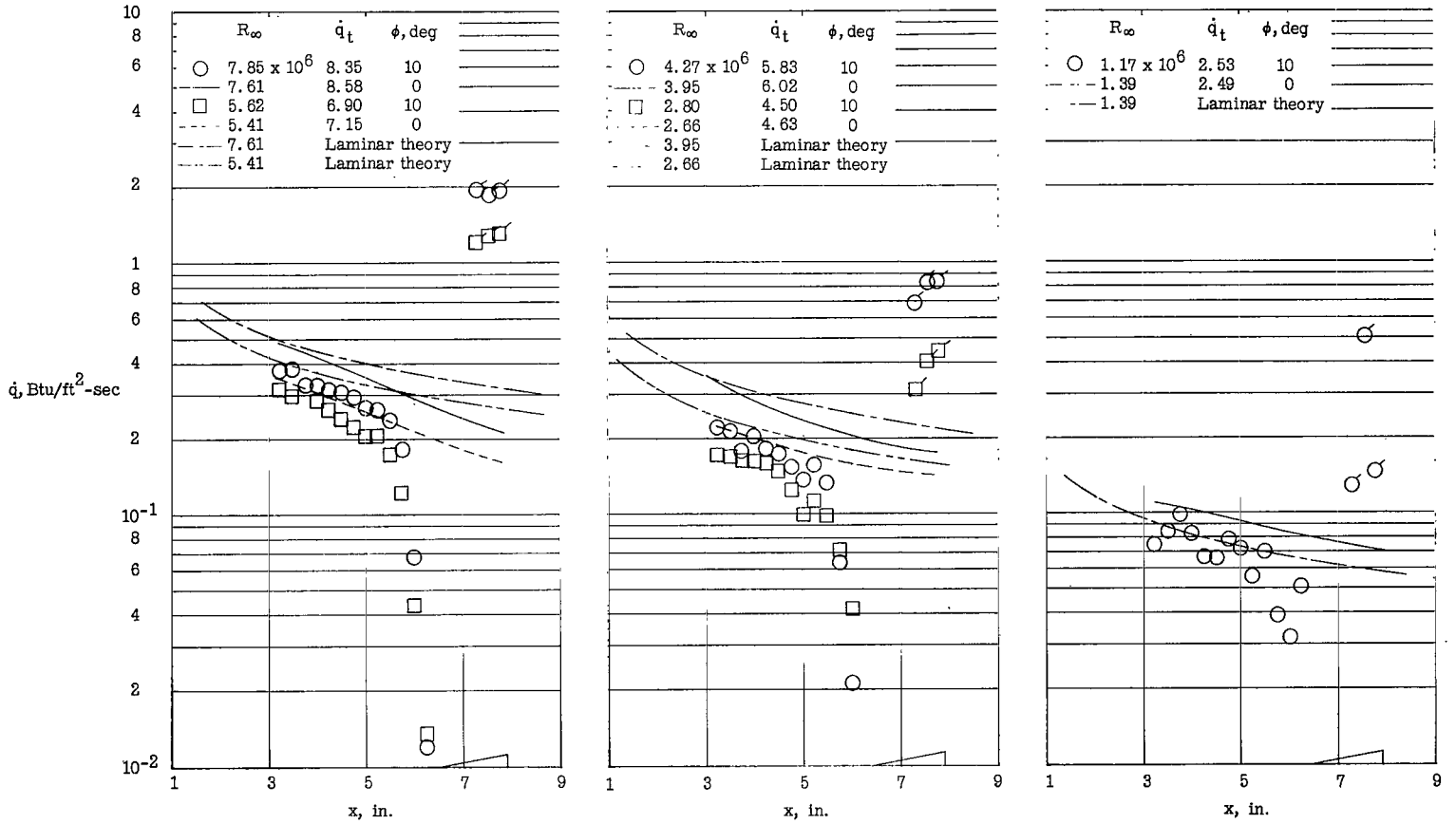

(b) t = 0.375 inch.

Figure 15.- Concluded.

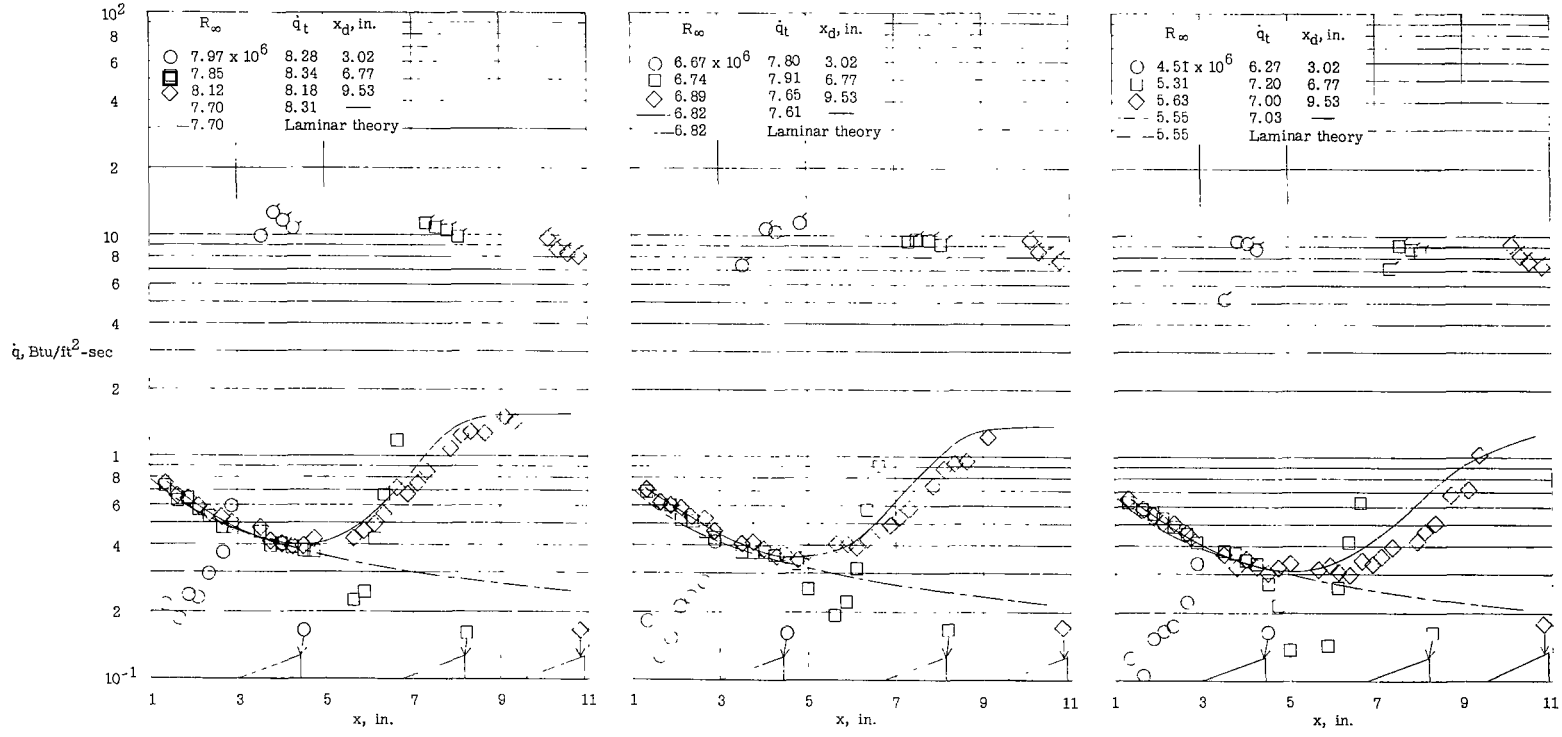

(a) Plate 1, tunnel 1.

Figure 16.- Effects of wedge location and free-stream Reynolds number variation on heat transfer on a sharp-leading-edge model (t = 0.0015 inch) with a 20^0 wedge at $\alpha = 0^0$. Flagged symbols denote data on wedge surface.

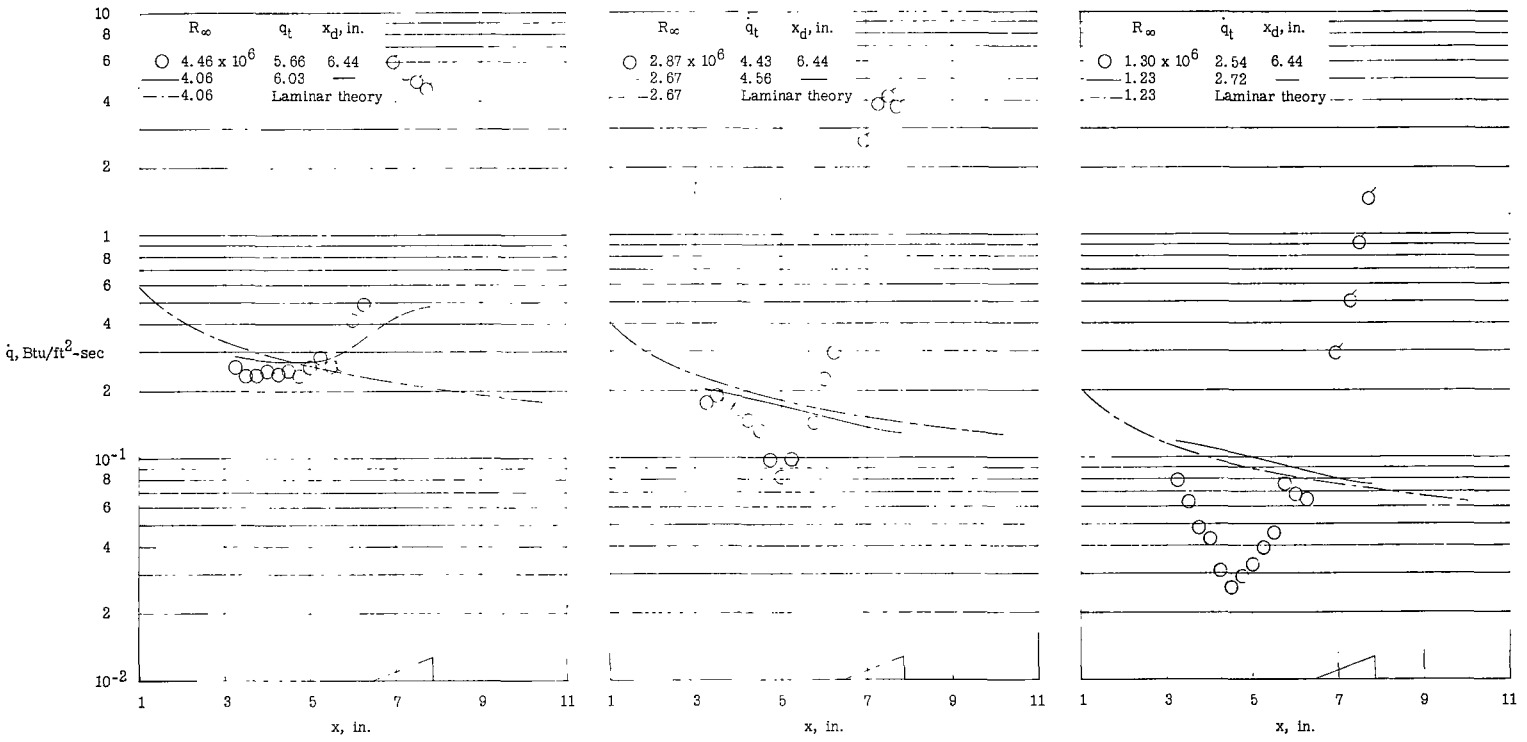

(b) Plate 2, tunnel 2.

Figure 16.- Concluded.

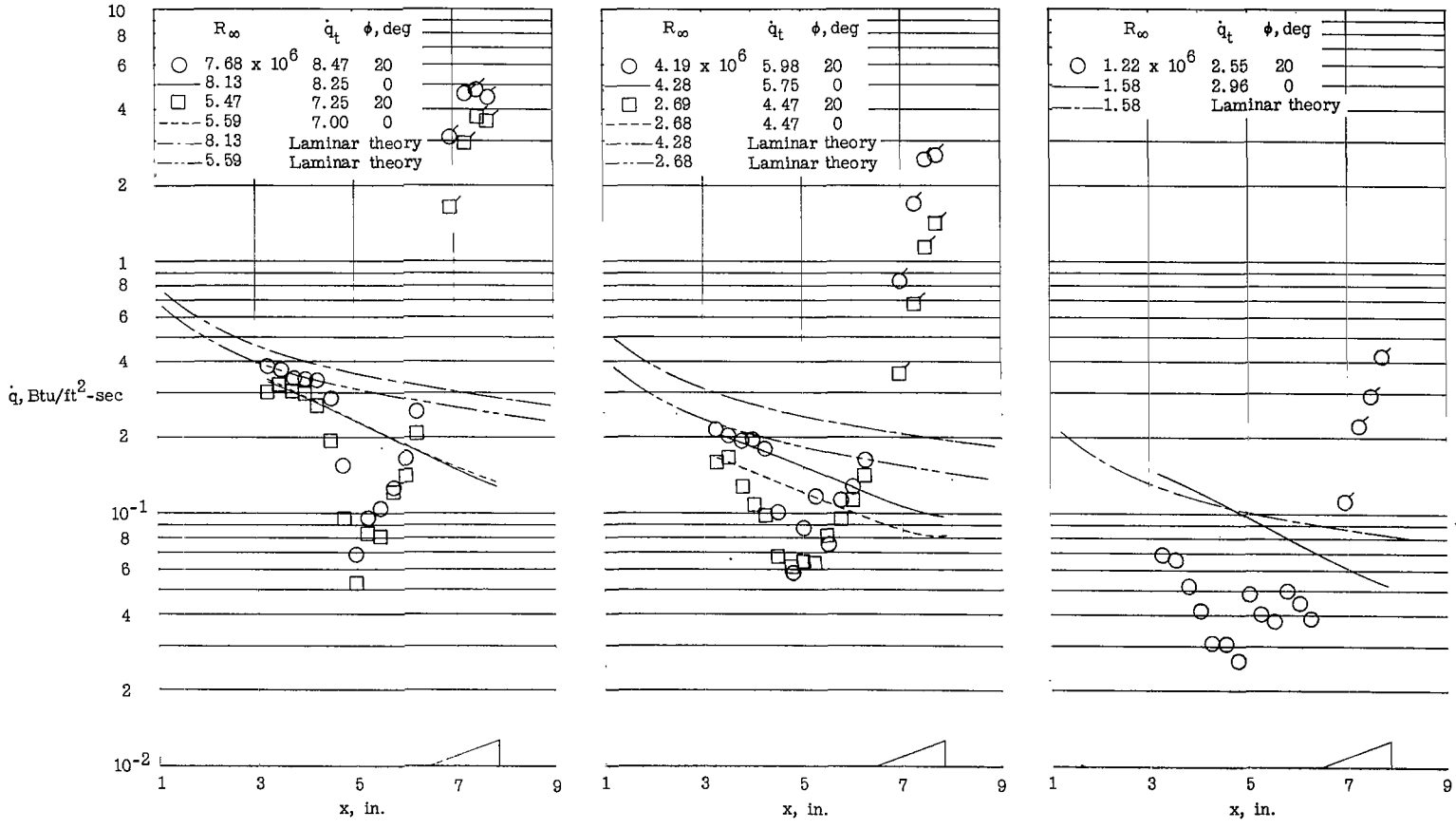

(a) t = 0.120 inch.

Figure 17.- Effects of free-stream Reynolds number variation on heat transfer on blunt-leading-edge models (t = 0.120 inch and t = 0.375 inch) with a 20° wedge at $\alpha = 0^0$; x_d = 6.44 inches; plate 2; tunnel 2. Flagged symbols denote data on wedge surface.

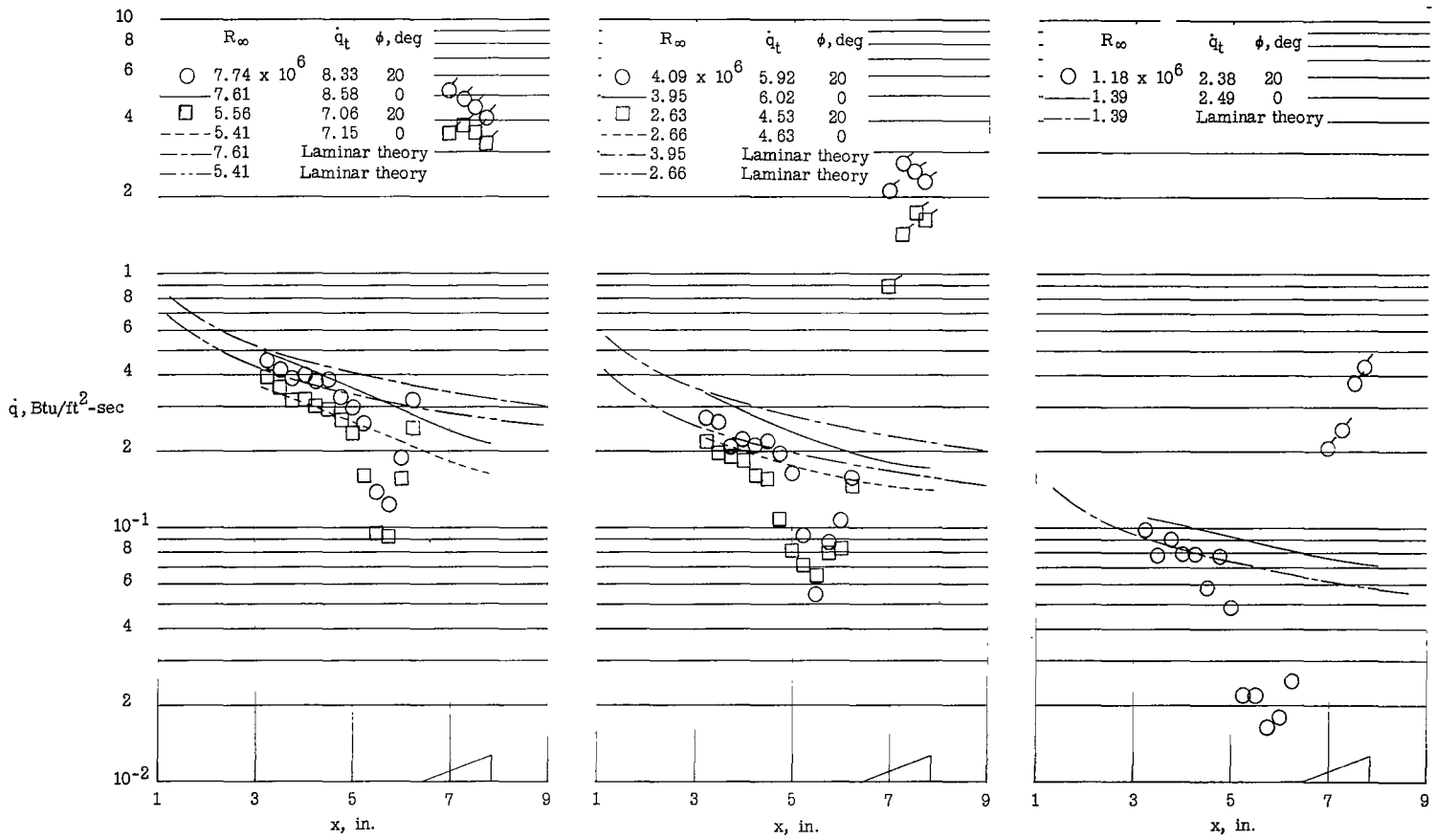

(b) t = 0.375 inch.

Figure 17.- Concluded.

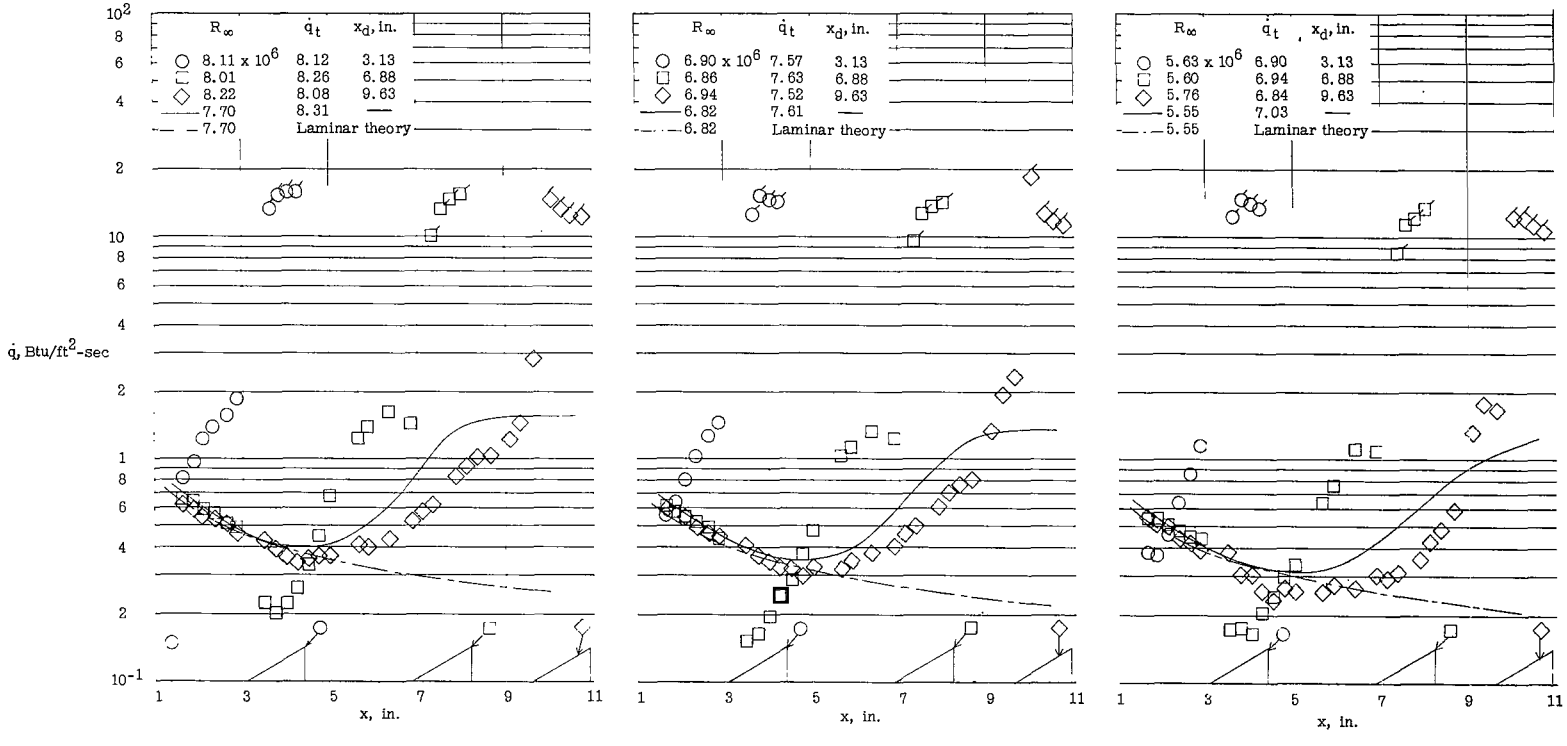

(a) Plate 1, tunnel 1.

Figure 18.- Effects of wedge location and free-stream Reynolds number variation on heat transfer on a sharp-leading-edge model (t = 0.0015 inch) with a 30° wedge at $\alpha = 0^0$. Flagged symbols denote data on wedge surface.

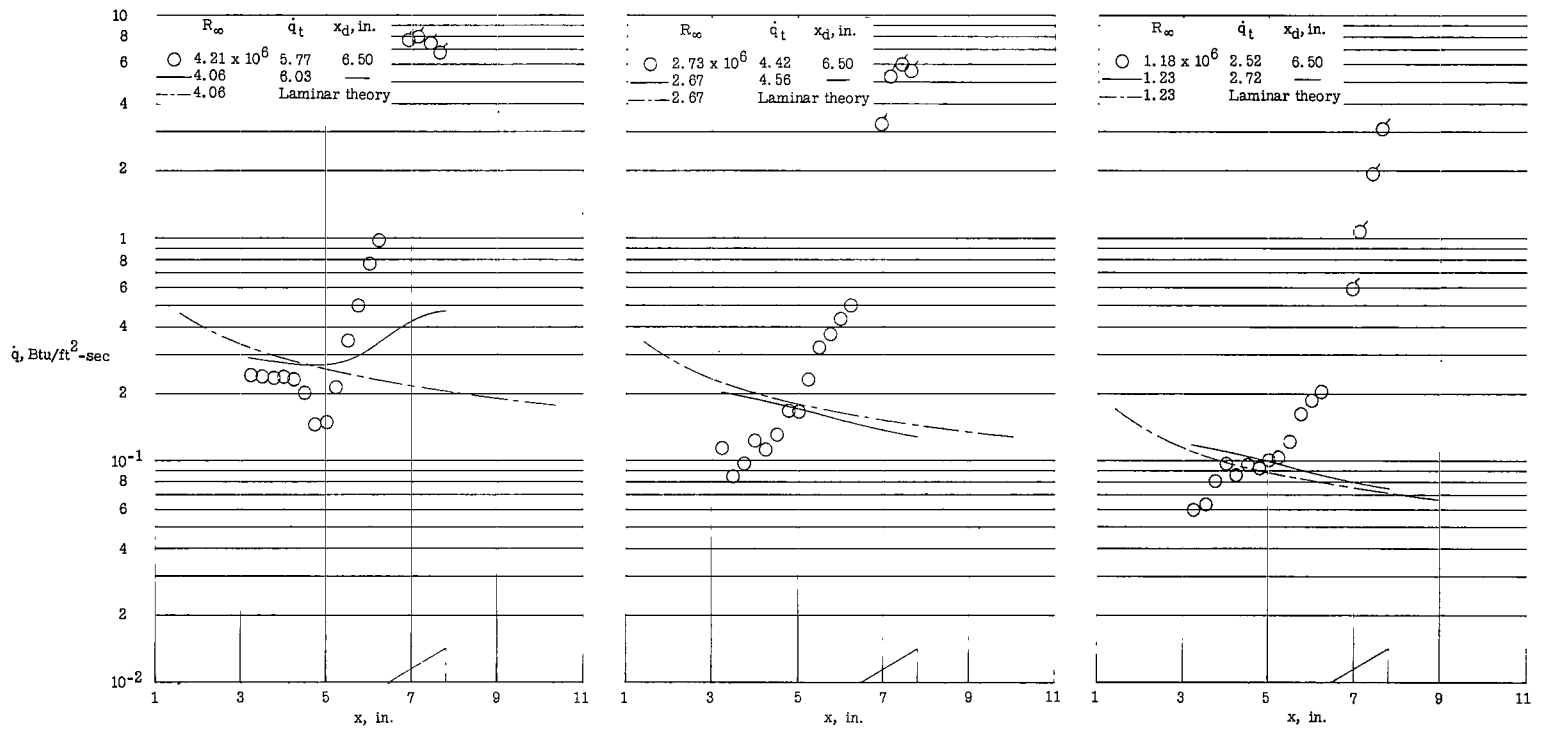

(b) Plate 2, tunnel 2.

Figure 18.- Concluded.

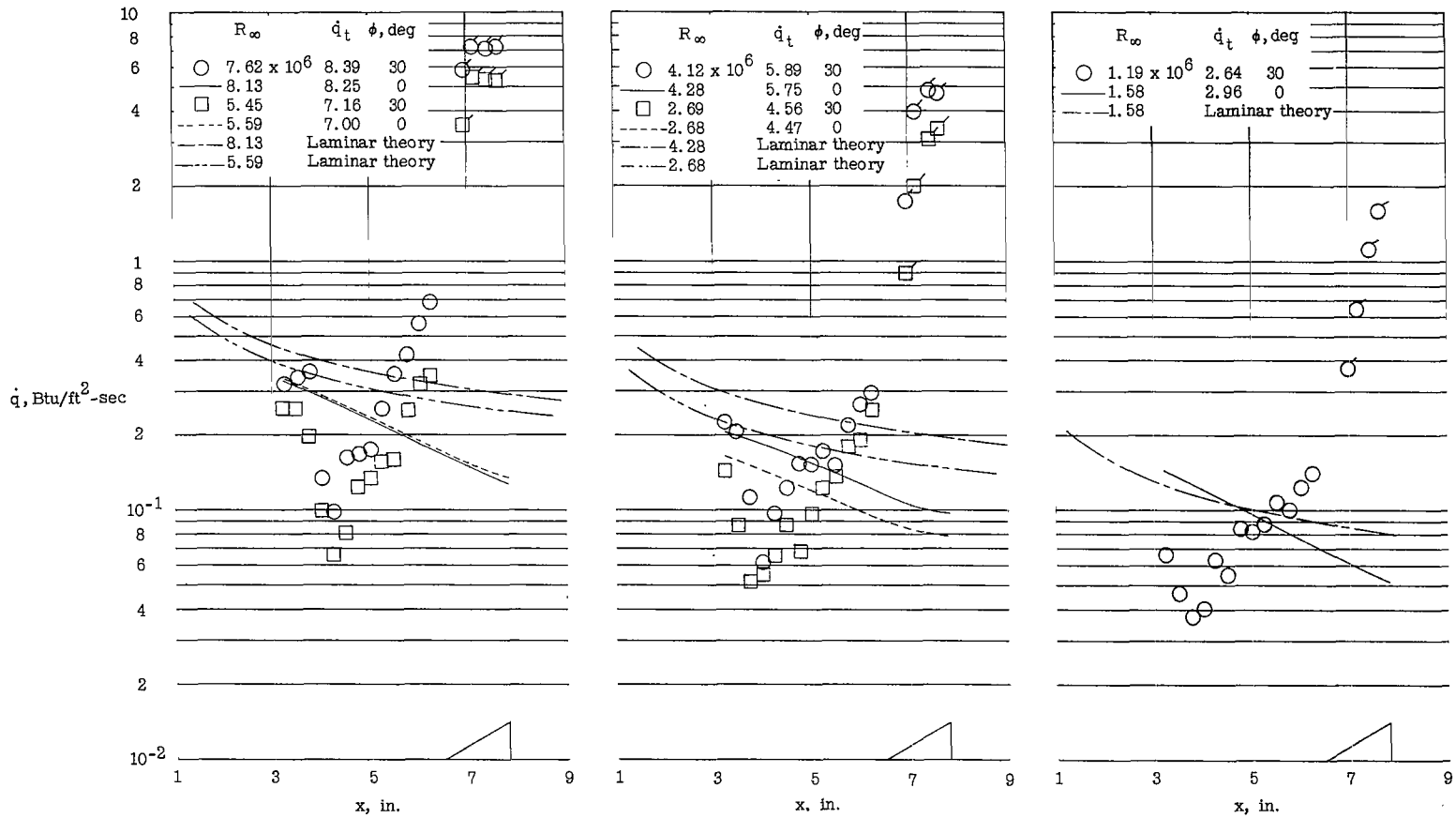

(a) t = 0.120 inch.

Figure 19.- Effects of free-stream Reynolds number variation on heat transfer on blunt-leading-edge models (t = 0.120 inch and t = 0.375 inch) with a 30° wedge at $\alpha = 0^0$; x_d = 6.50 inches; plate 2; and tunnel 2. Flagged symbols denote data on wedge surface.

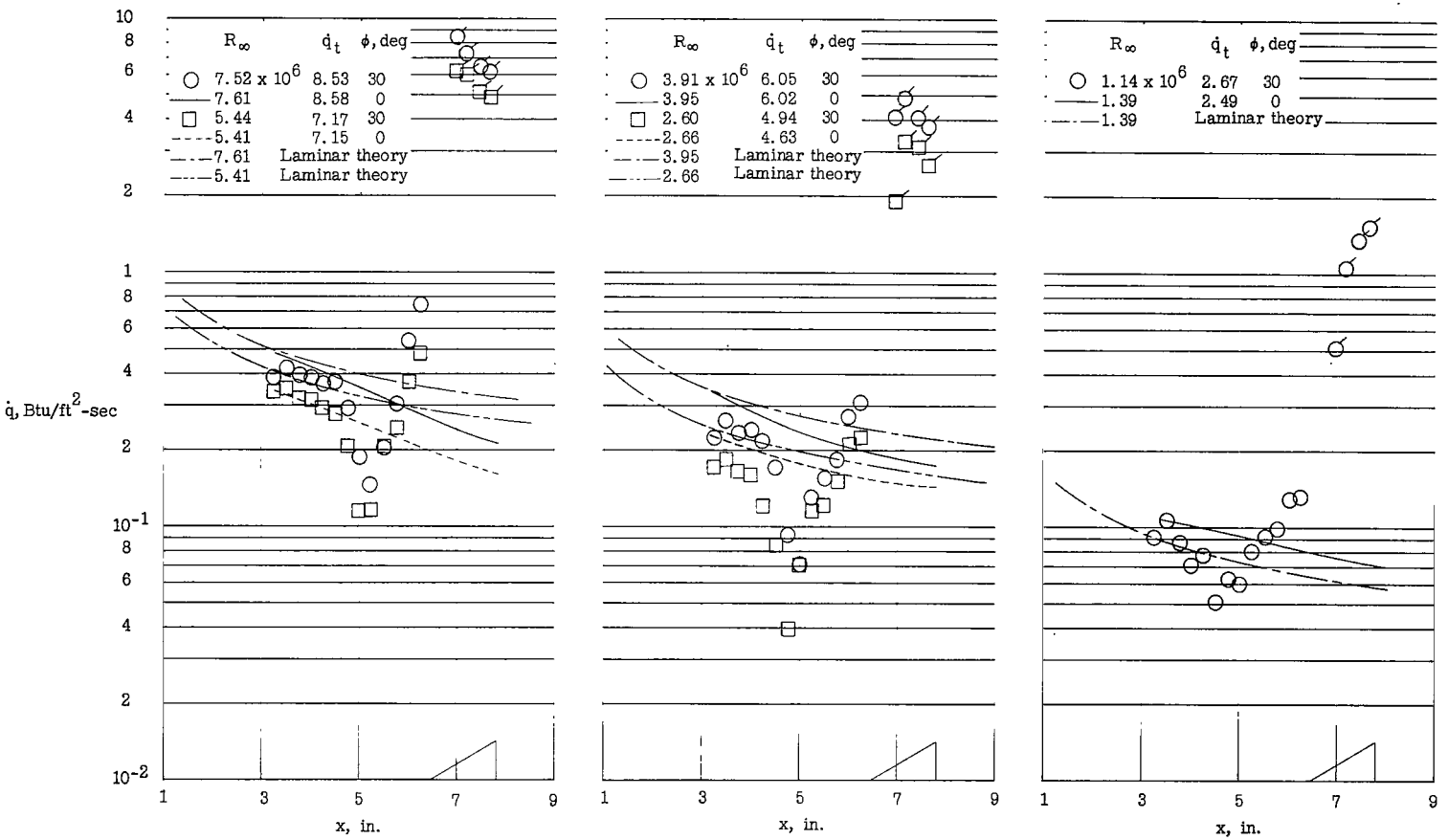

(b) t = 0.375 inch.

Figure 19.- Concluded.

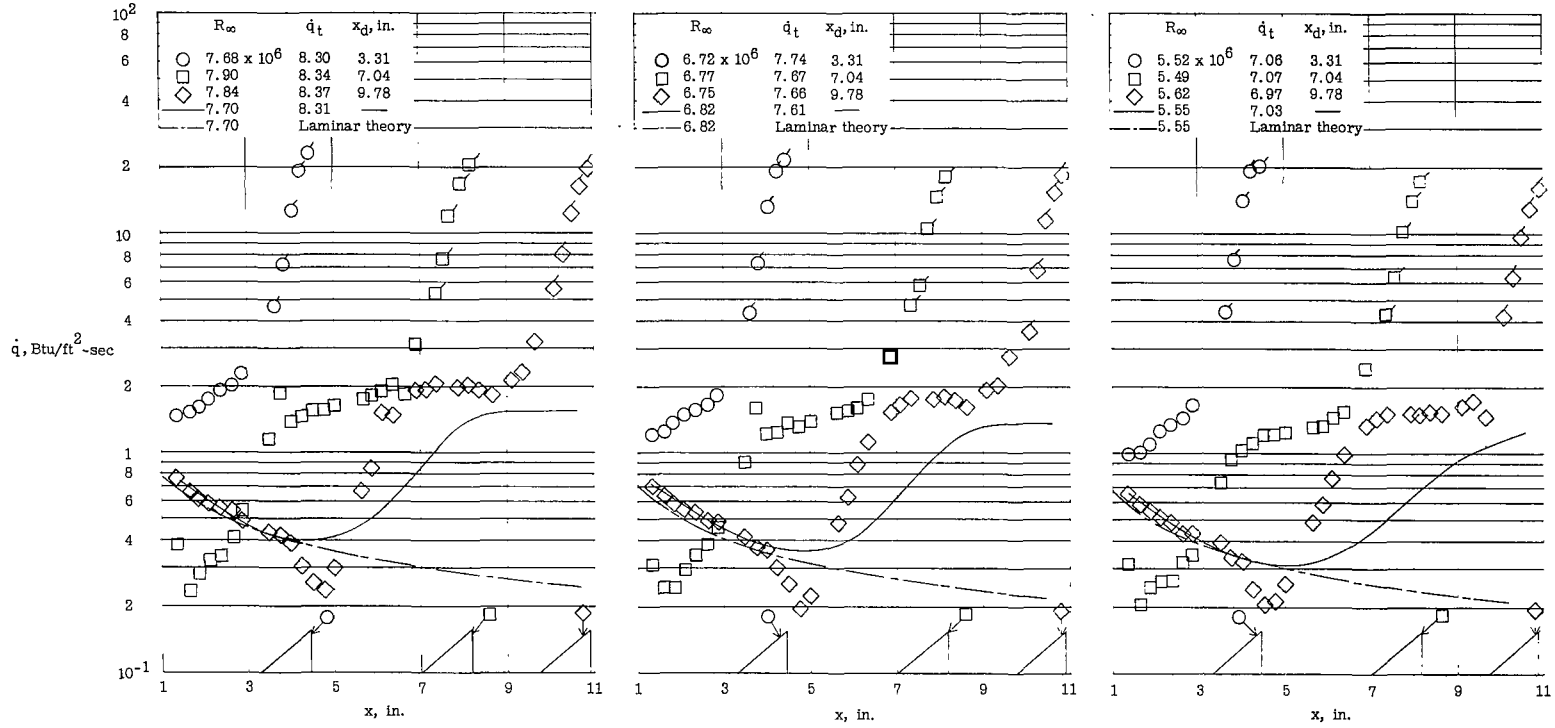

(a) Plate 1, tunnel 1.

Figure 20.- Effects of wedge location and free-stream Reynolds number variation on heat transfer on a sharp-leading-edge model (t = 0.0015 inch) with a 40° wedge at $\alpha = 0^0$. Flagged symbols denote data on the wedge surface.

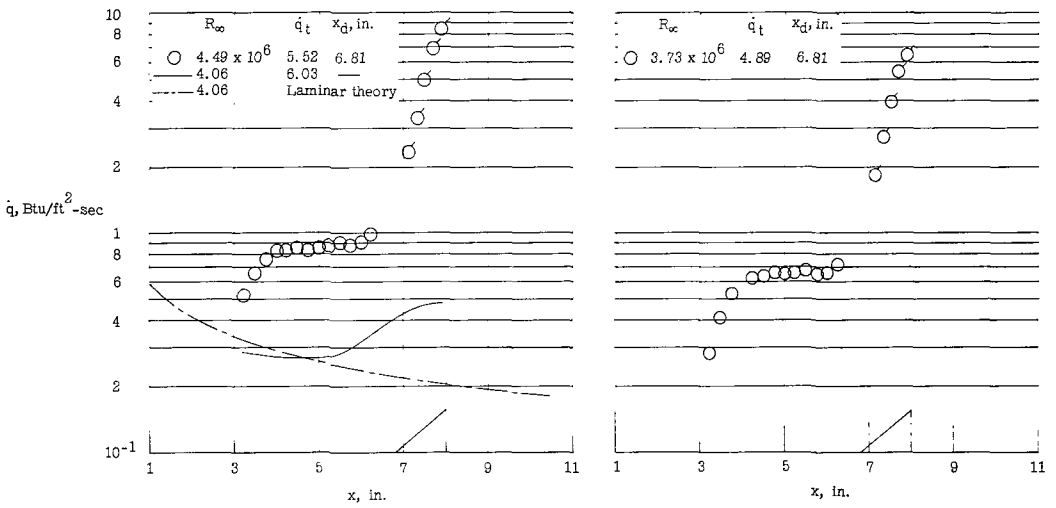

(b) Plate 2, tunnel 2.

Figure 20.- Concluded.

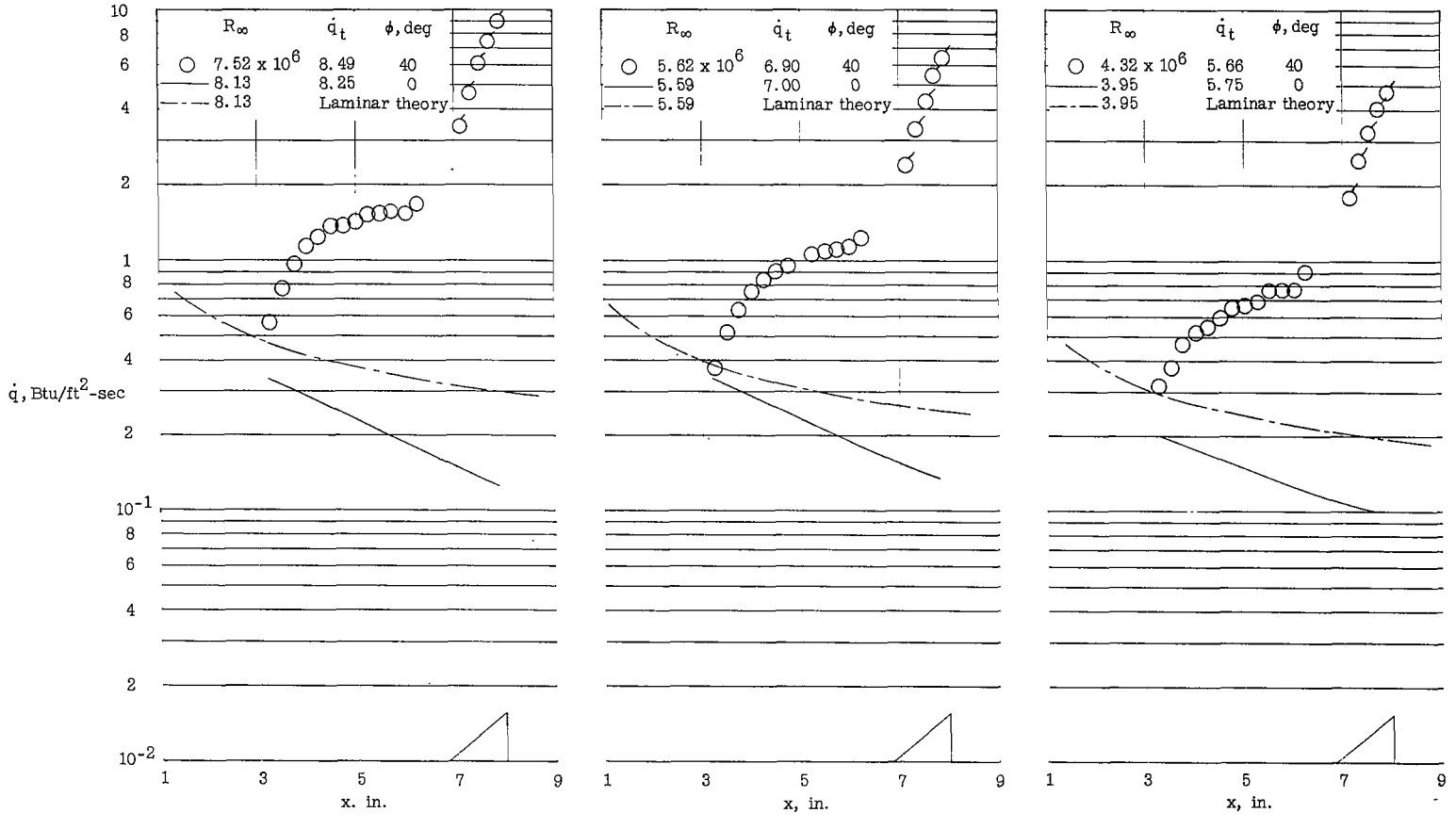

(a) t = 0.120 inch.

Figure 21.- Effects of free-stream Reynolds number variation on heat transfer on blunt-leading-edge models (t = 0.120 inch and t = 0.375 inch) with a 40° wedge at $\alpha = 0°$; x_d = 6.81 inches; plate 2; tunnel 2. Flagged symbols denote data on wedge surface.

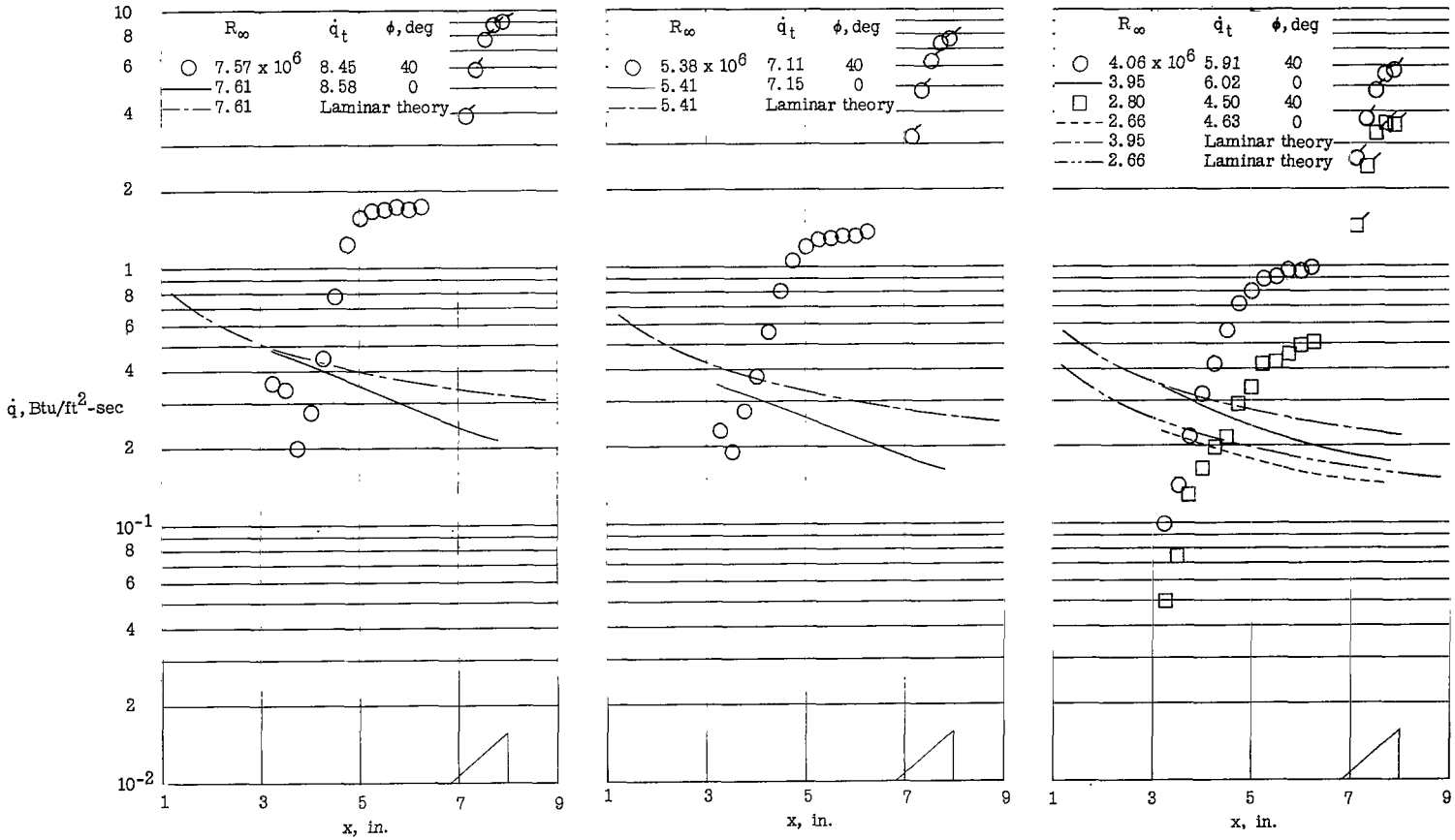

(b) t = 0.375 inch.

Figure 21.- Concluded.

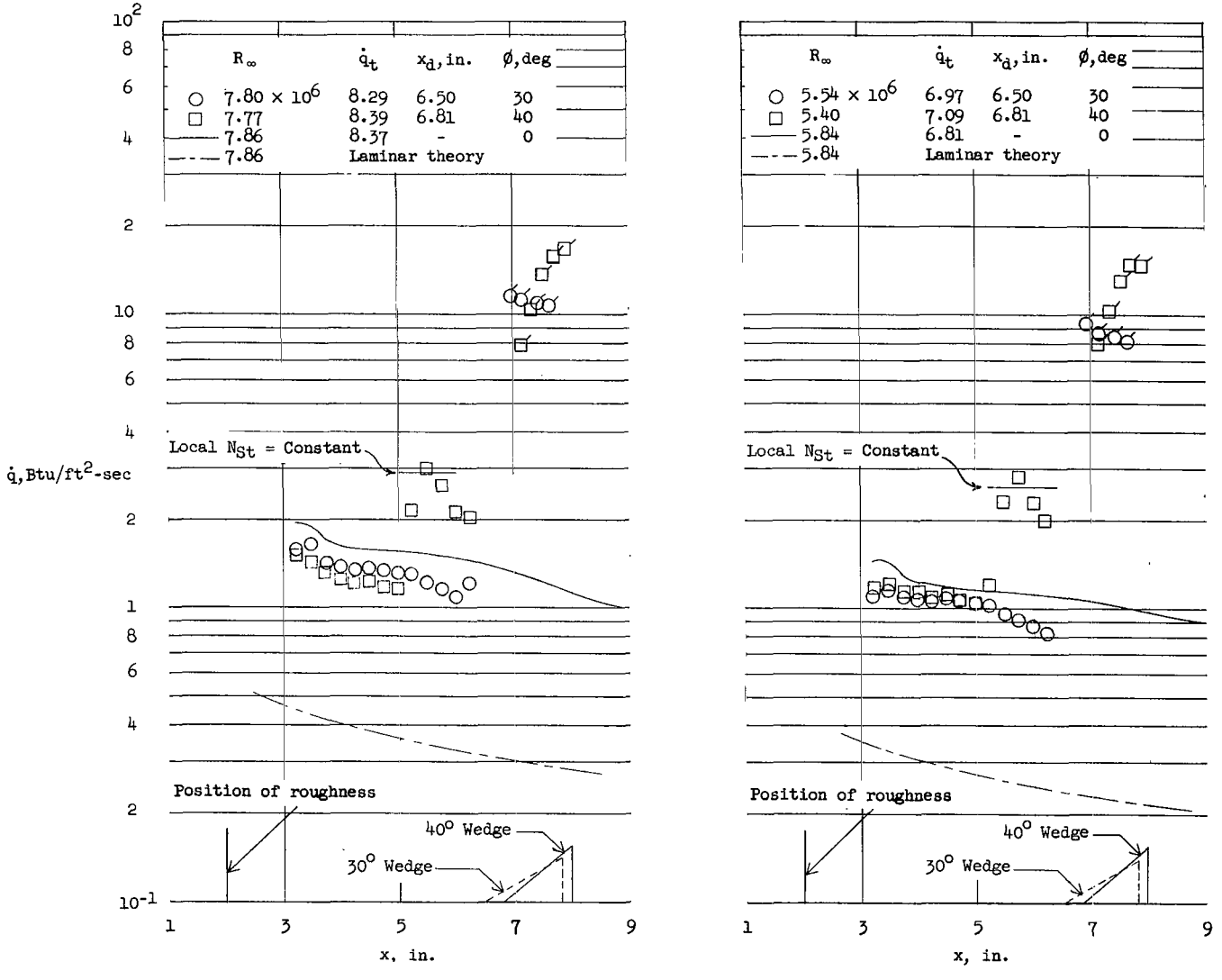

(a) $R_\infty \approx 7.8 = 10^6$.

(b) $R_\infty \approx 5.6 \times 10^6$.

Figure 22.- Heat transfer associated with 30° and 40° wedges with turbulent local flow obtained by tripping boundary layer at two free-stream Reynolds numbers. $\alpha = 0^0$; $t < 0.004$ inch; $k = 0.080$ inch; plate 2; and tunnel 2. Flagged symbols denote data on wedge surface.

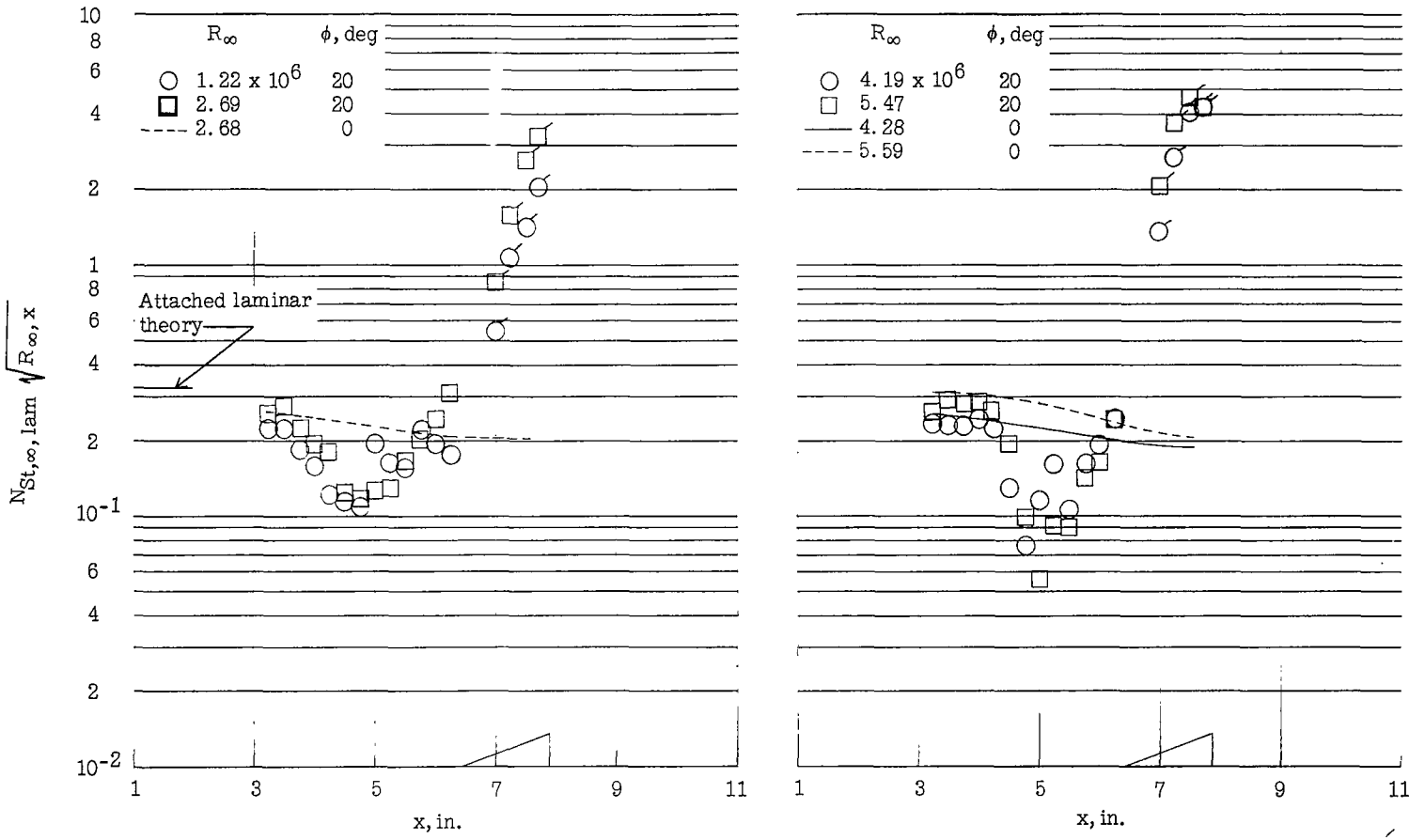

(a) 20^0 wedge; blunt leading edge; t = 0.120 inch.

Figure 23.- Local heat-transfer parameters on a flat plate with wedges for various Reynolds numbers. M_∞ = 6.0. Flagged symbols denote data on wedge surface.

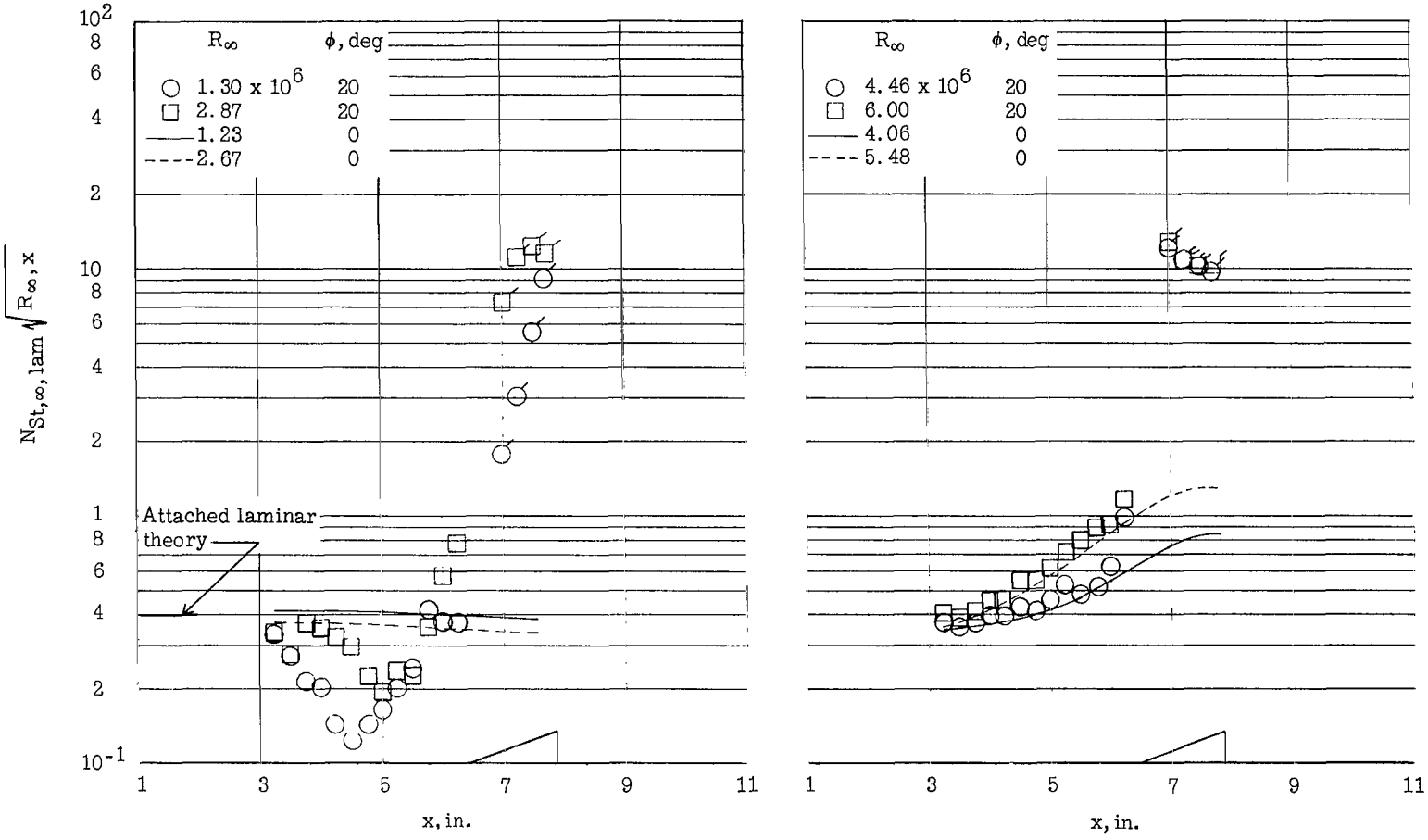

(b) 20^0 wedge; sharp leading edge; t = 0.0015 inch.

Figure 23.- Continued.

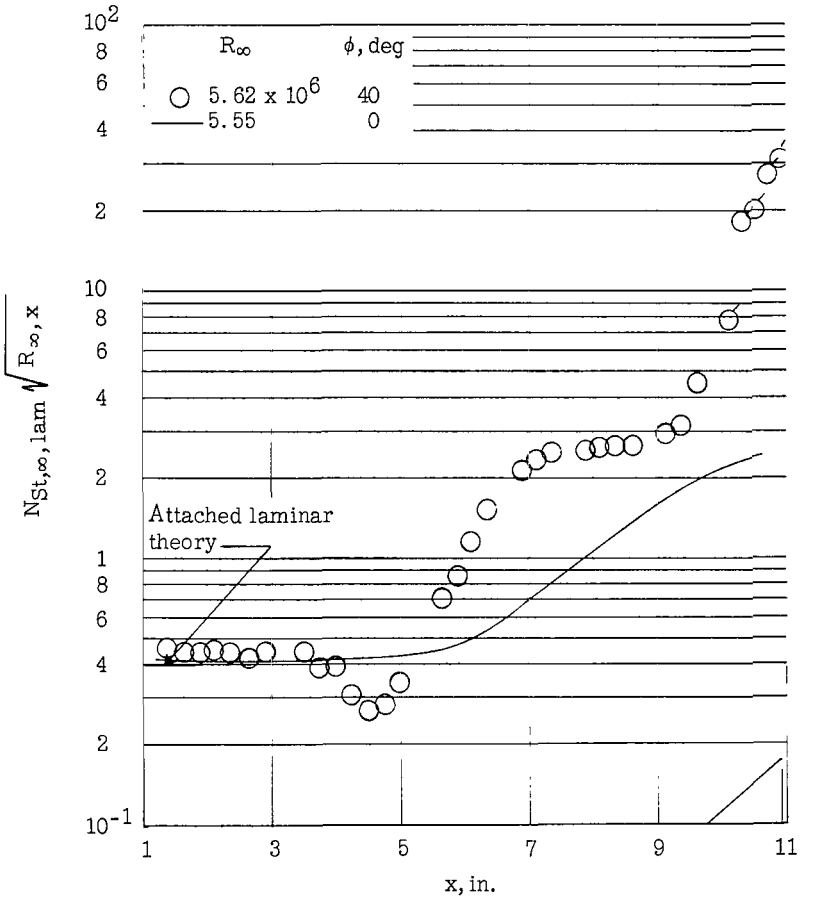

(c) 40^0 wedge; sharp leading edge; t = 0.0015 inch.

Figure 23.- Concluded.

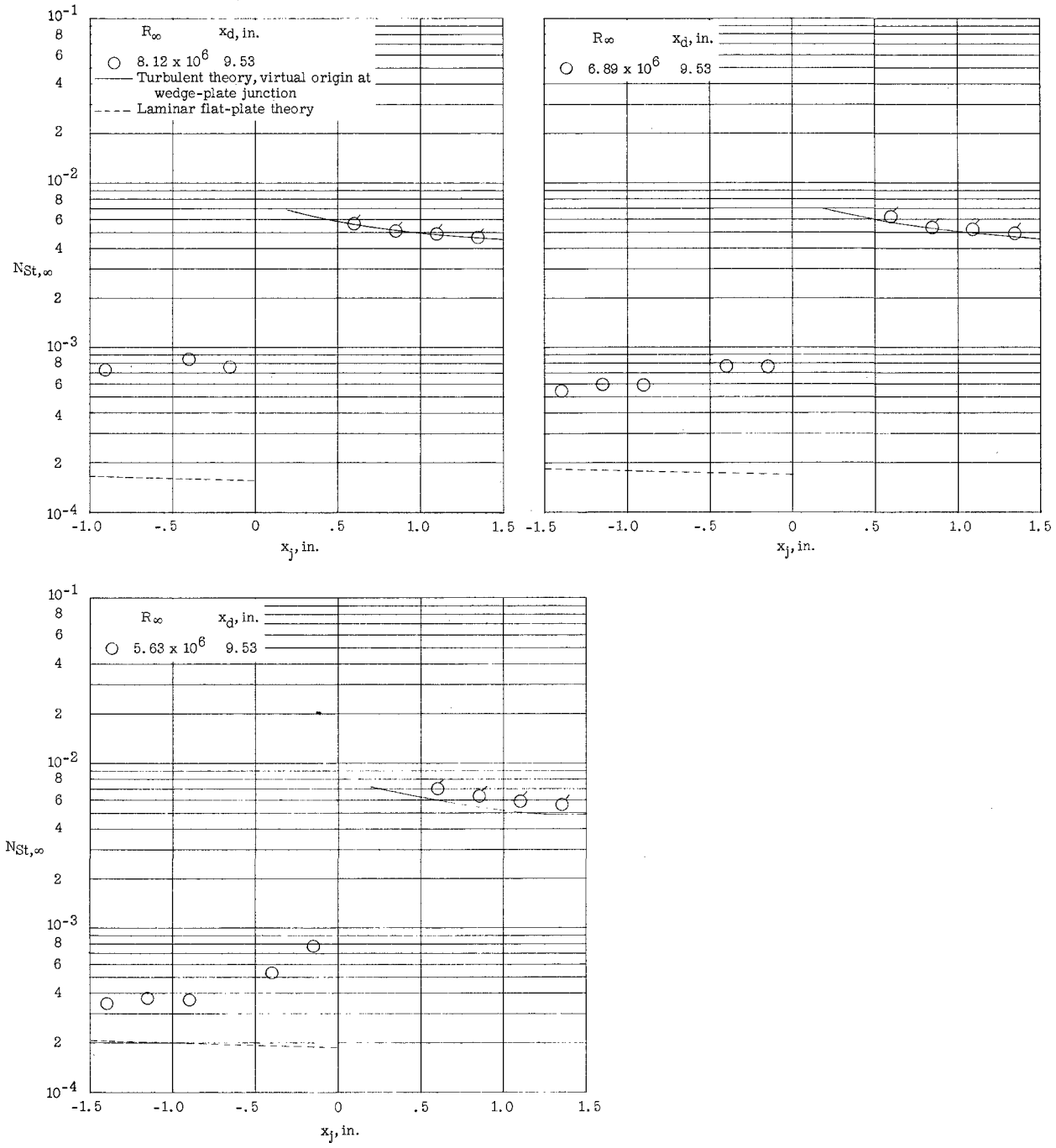

(a) 20^0 wedge; plate 1; tunnel 1.

Figure 24.- Comparison of experimental Stanton number distributions on wedges with theoretical prediction for sharp-leading-edge models at $\alpha = 0^0$. Flagged symbols denote data on wedge surface. Solid and open symbols indicate Stanton number based on laminar and turbulent recovery factors, respectively.

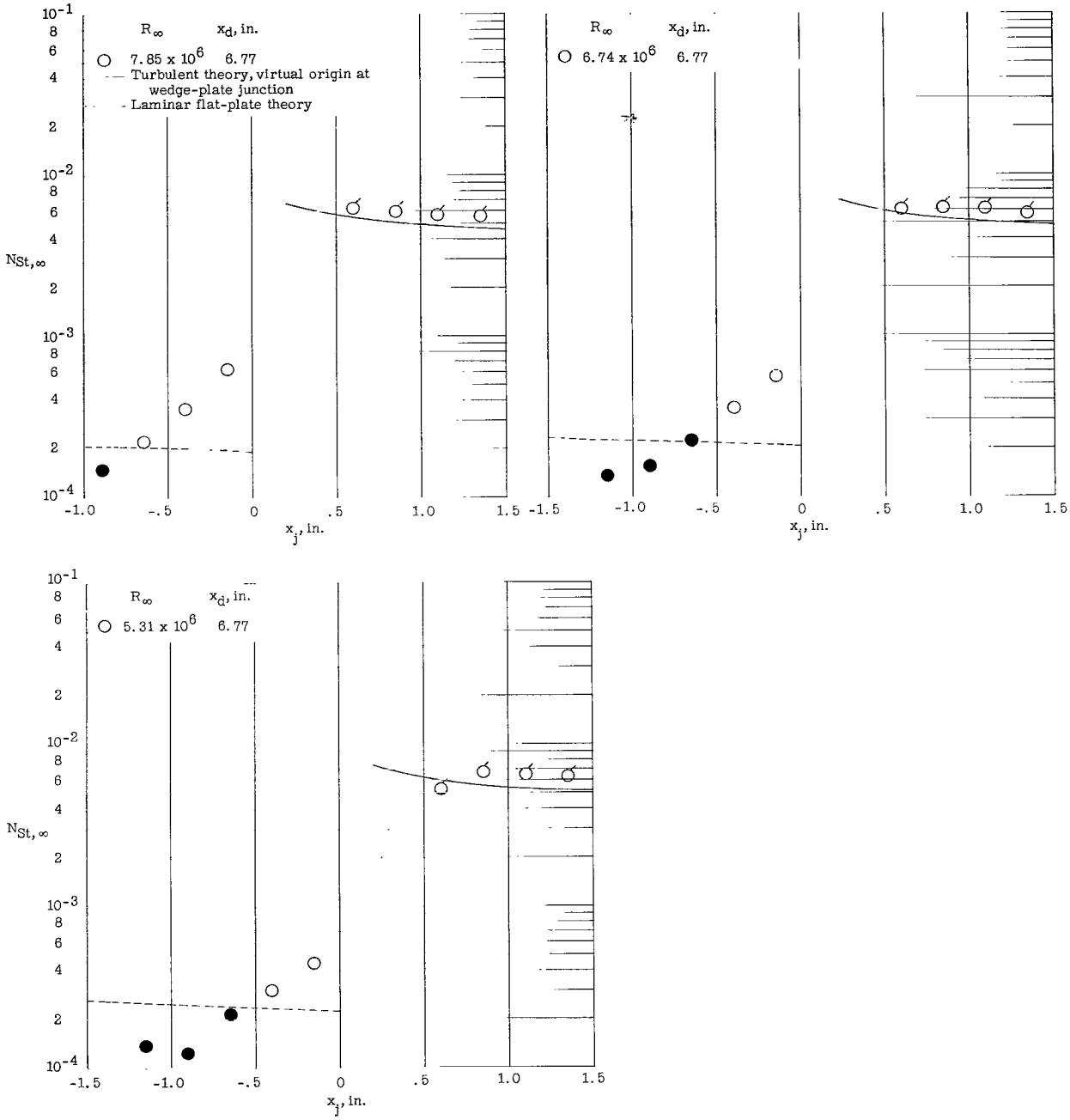

(a) Continued.

Figure 24.- Continued.

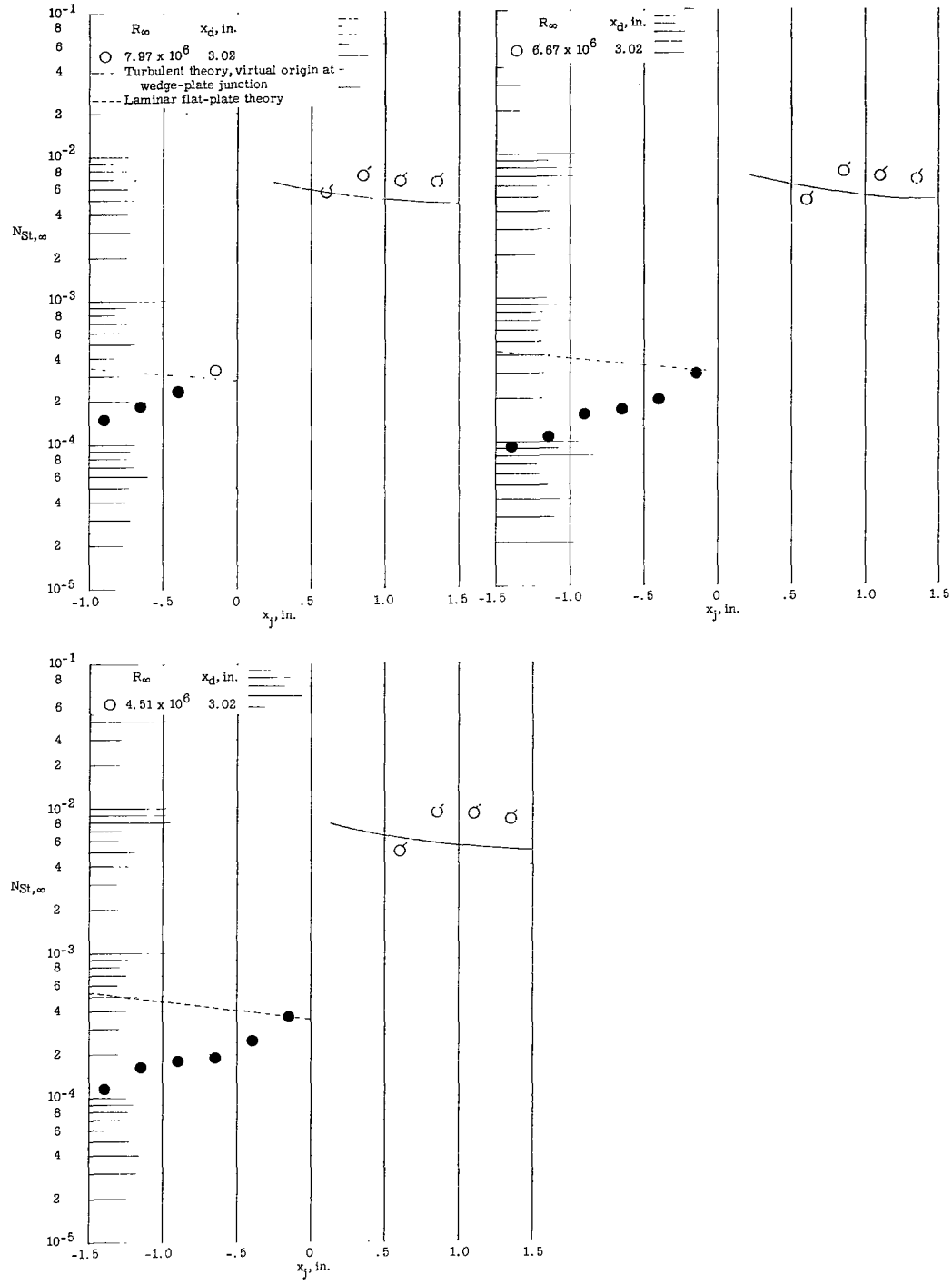

(a) Concluded.

Figure 24.- Continued.

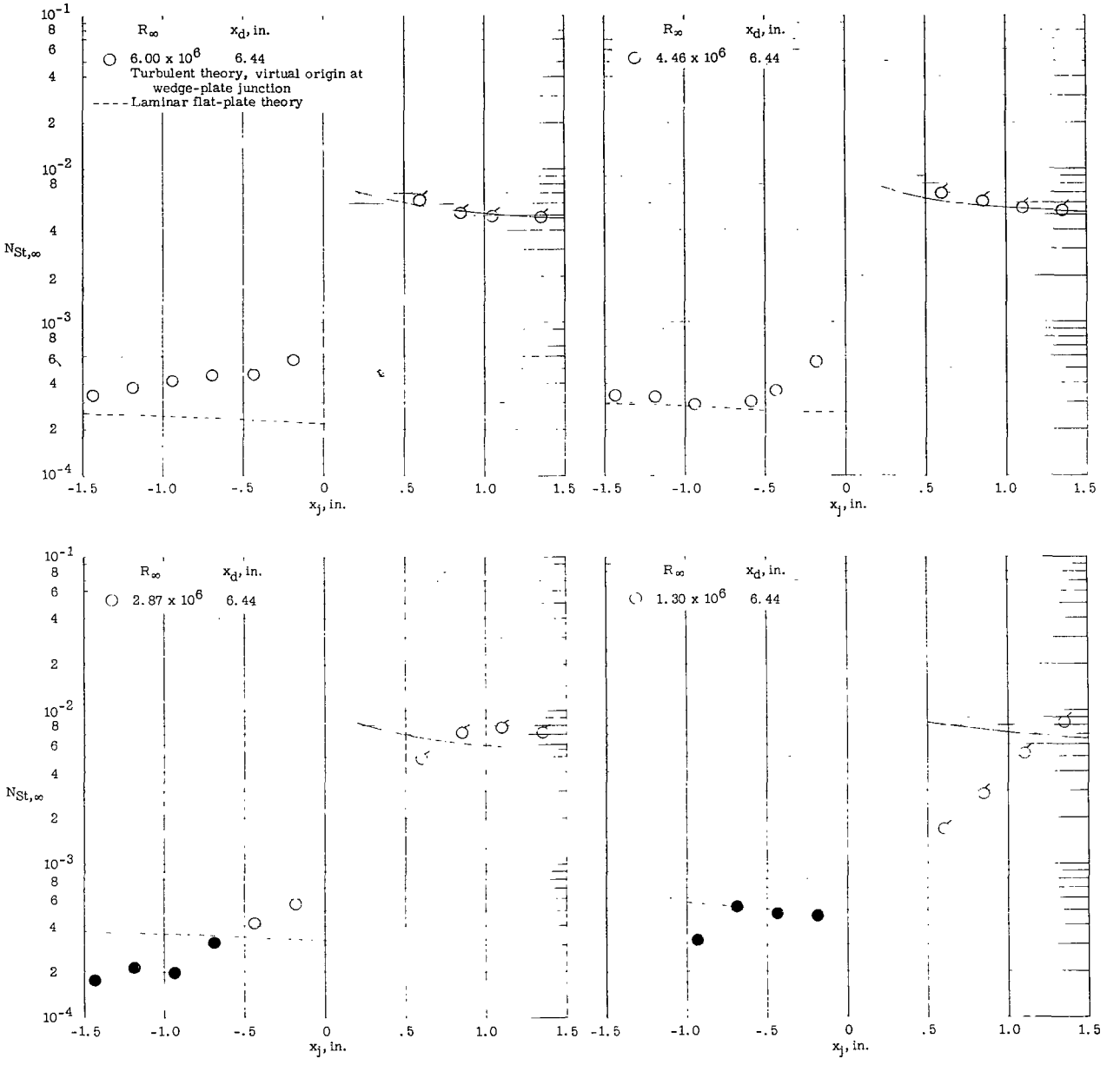

(b) 20^0 wedge; plate 2; tunnel 2.

Figure 24.- Continued.

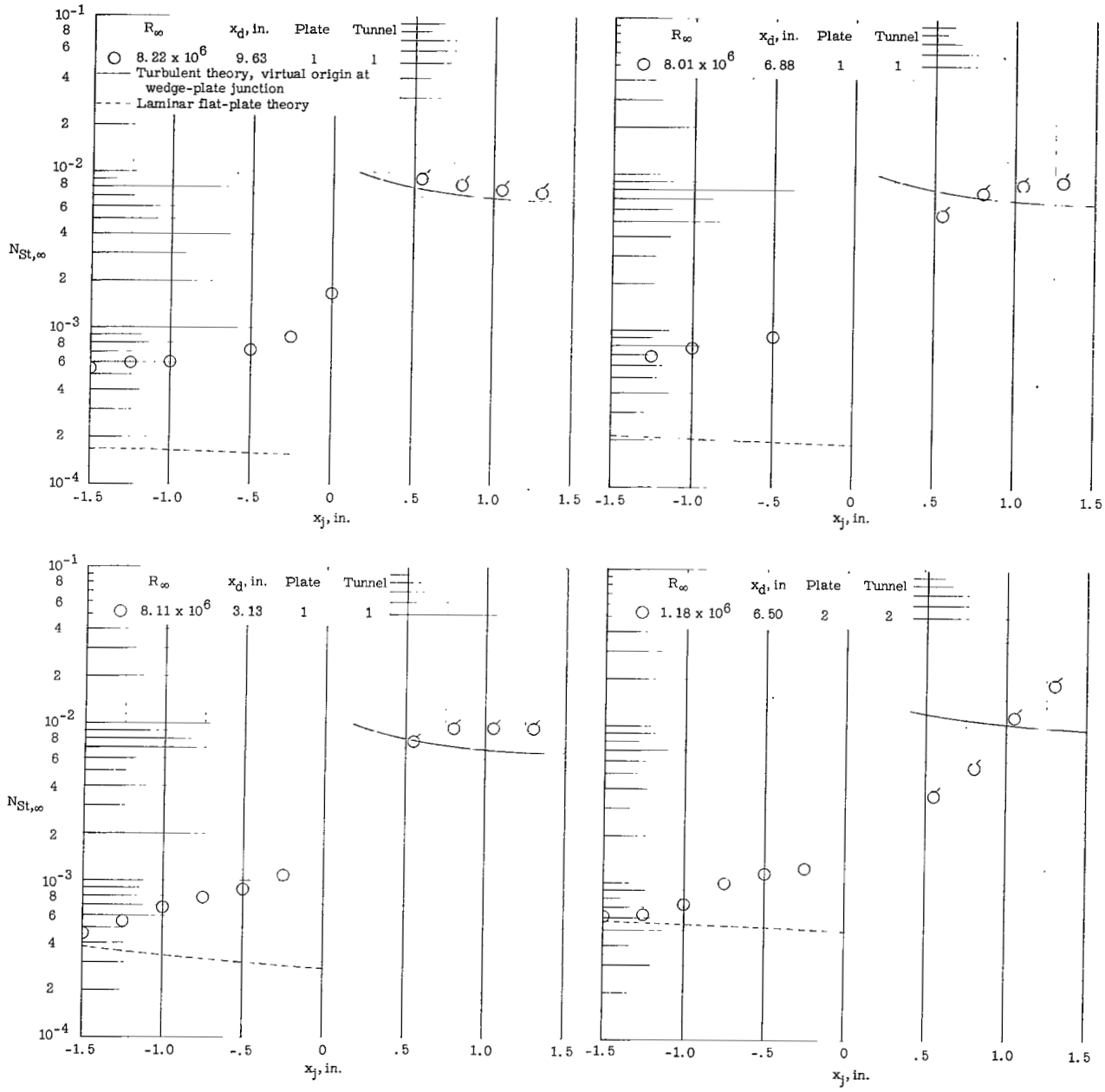

(c) 30^0 wedge.

Figure 24.- Continued.

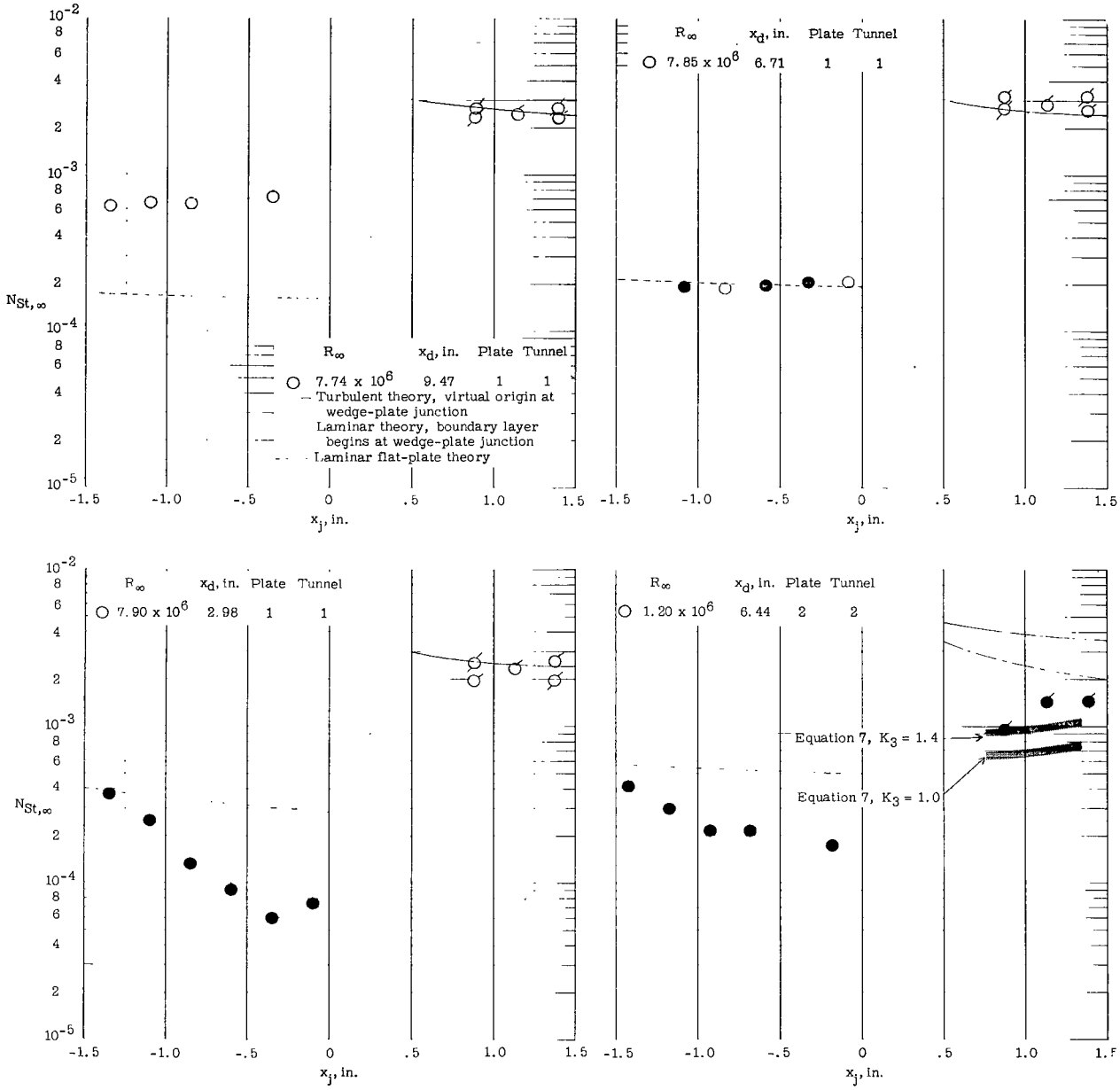

(d) 10^0 wedge.

Figure 24.- Continued.

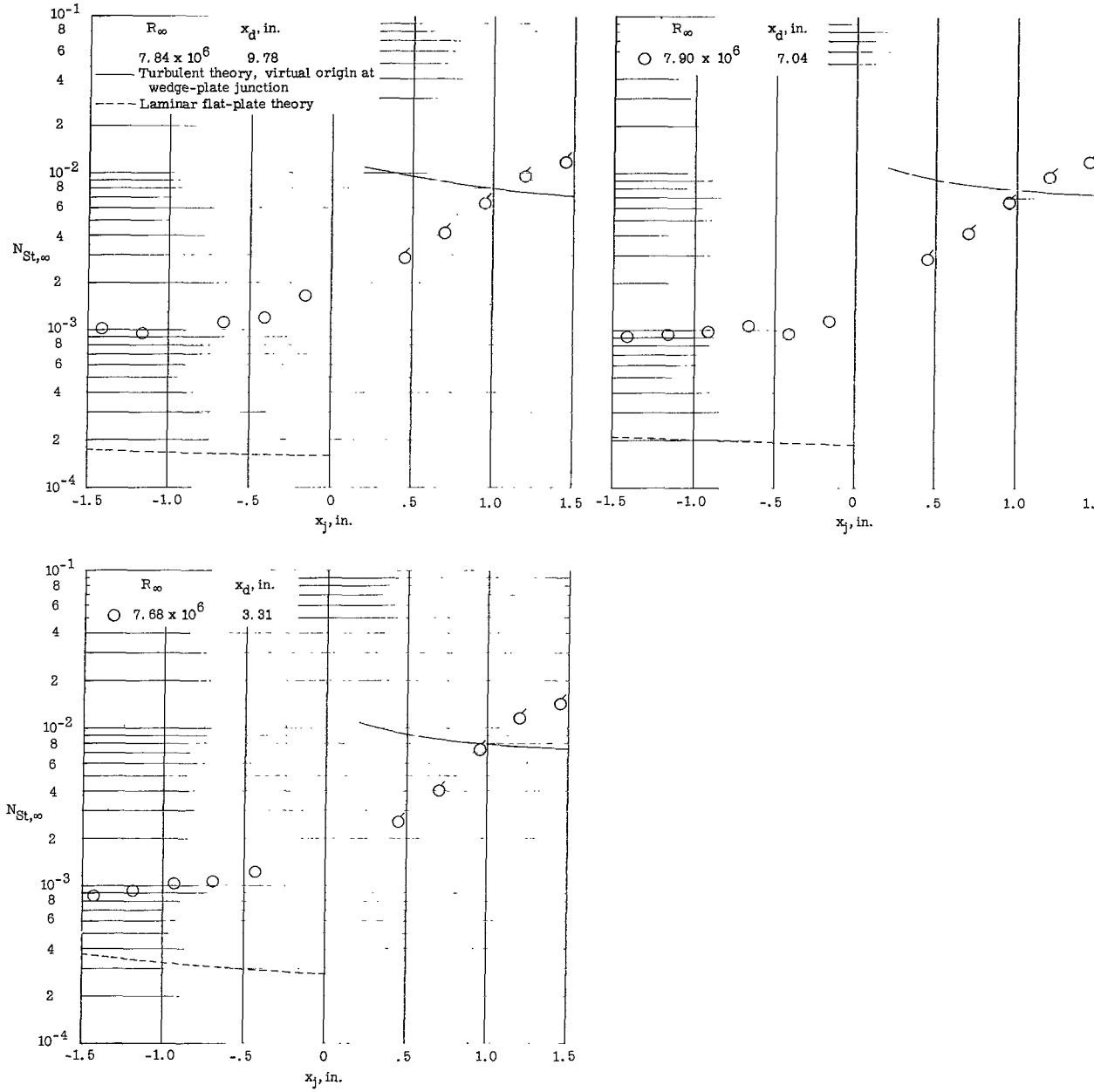

(e) 40° wedge plate; plate 1; tunnel 1.

Figure 24.- Concluded.

$\phi = 10^{\circ}$
$x_d = 2.98$ inches

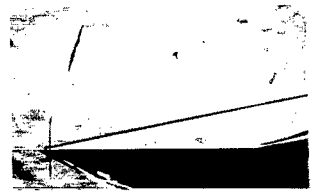

$\phi = 10^{\circ}$
$x_d = 6.71$ inches

$\phi = 20^{\circ}$
$x_d = 3.02$ inches

$\phi = 20^{\circ}$
$x_d = 6.77$ inches

$\phi = 30^{\circ}$
$x_d = 3.13$ inches

$\phi = 30^{\circ}$
$x_d = 6.88$ inches

$\phi = 40^{\circ}$
$x_d = 3.31$ inches

$\phi = 40^{\circ}$
$x_d = 7.04$ inches

L-65-158

Figure 25.- Schlieren photographs of flow over wedges for plate 1. $M_\infty = 6.0$; $R_\infty \approx 8 \times 10^6$ per foot. (Separation occurs for all cases as indicated by heat-transfer data except $\phi = 10^0$ and $x_d = 6.71$ inches.)

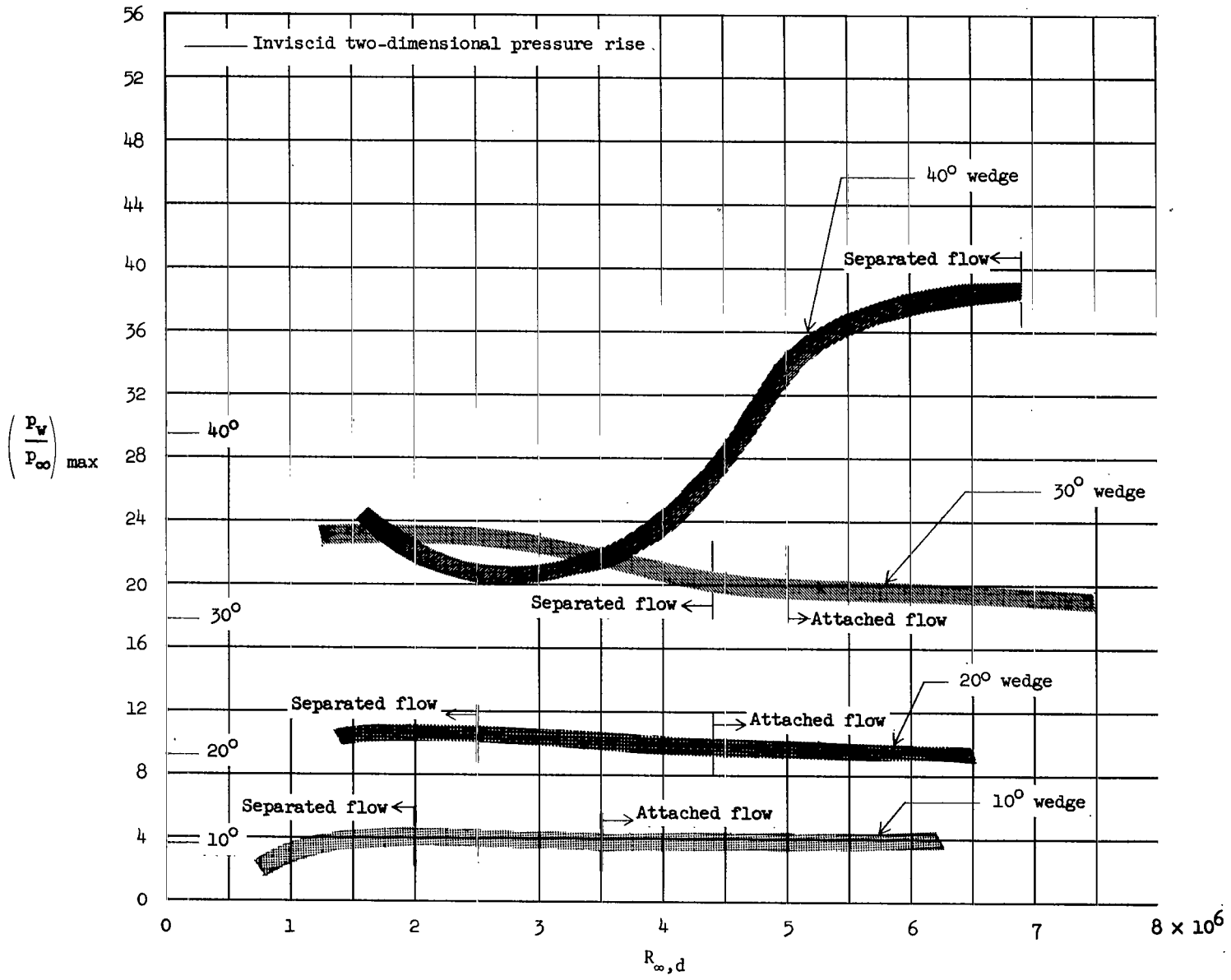

Figure 26.- Measured peak pressures on wedges for sharp-leading-edge model.

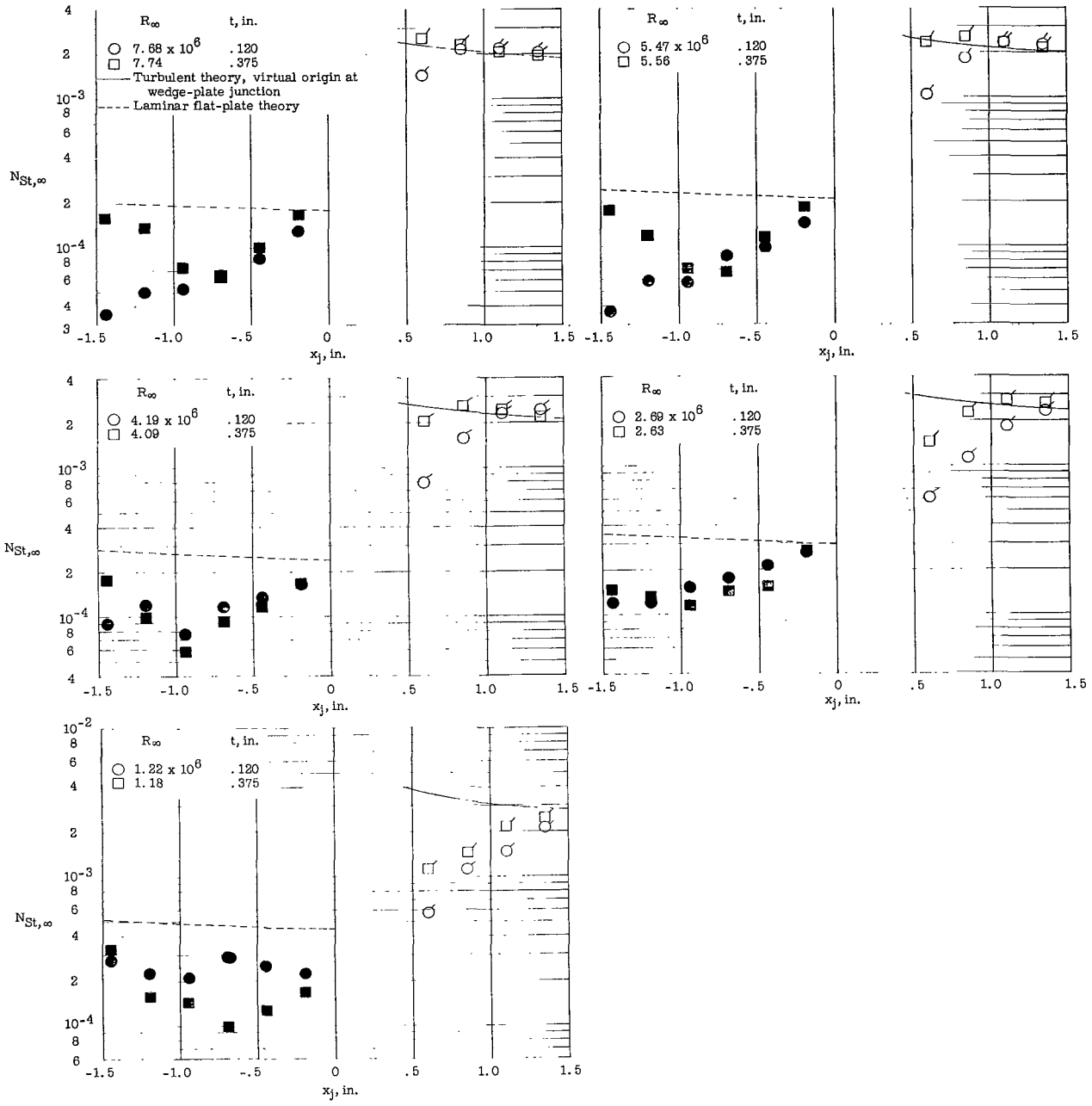

(a) 20° wedge; x_d = 6.44 inches.

Figure 27.- Comparison of experimental Stanton number distributions on wedges with theoretical predictions for blunt-leading-edge models. Plate 2; tunnel 2. Solid and open symbols indicate Stanton number based on laminar and turbulent recovery factors, respectively.

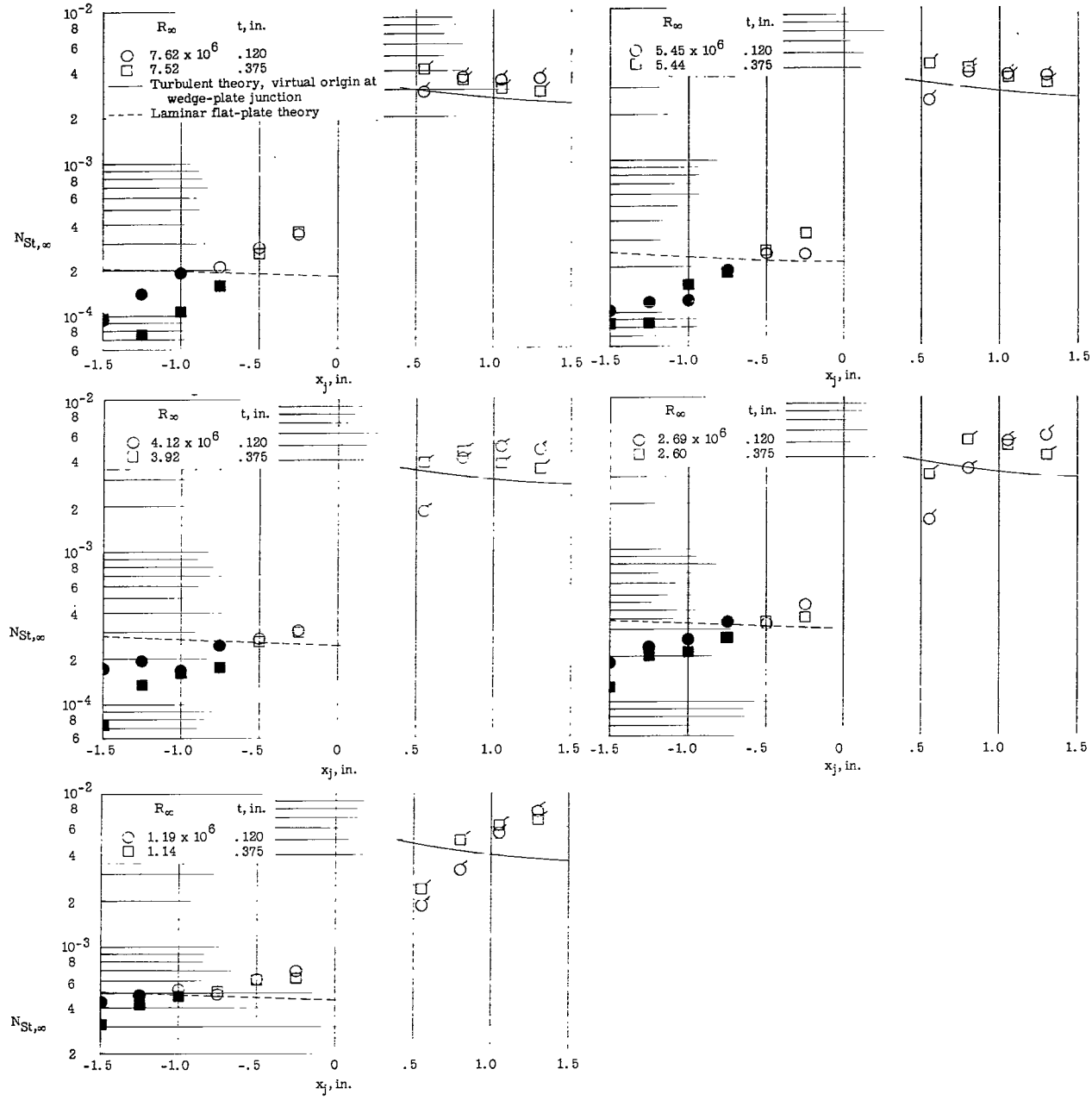

(b) 30^0 wedge; x_d = 6.50 inches.

Figure 27.- Continued.

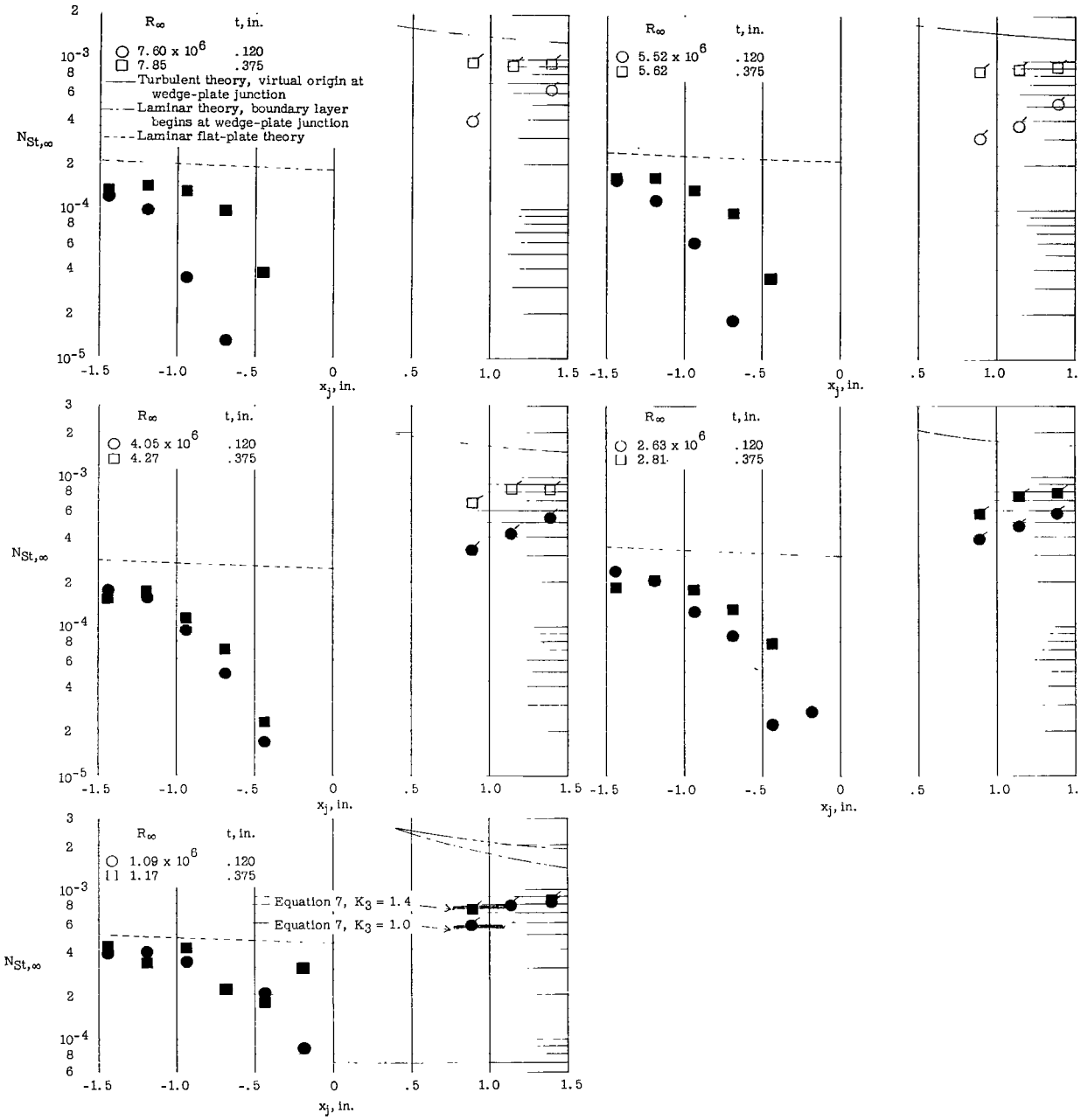

(c) 10^0 wedge; x_d = 6.44 inches.

Figure 27.- Concluded.

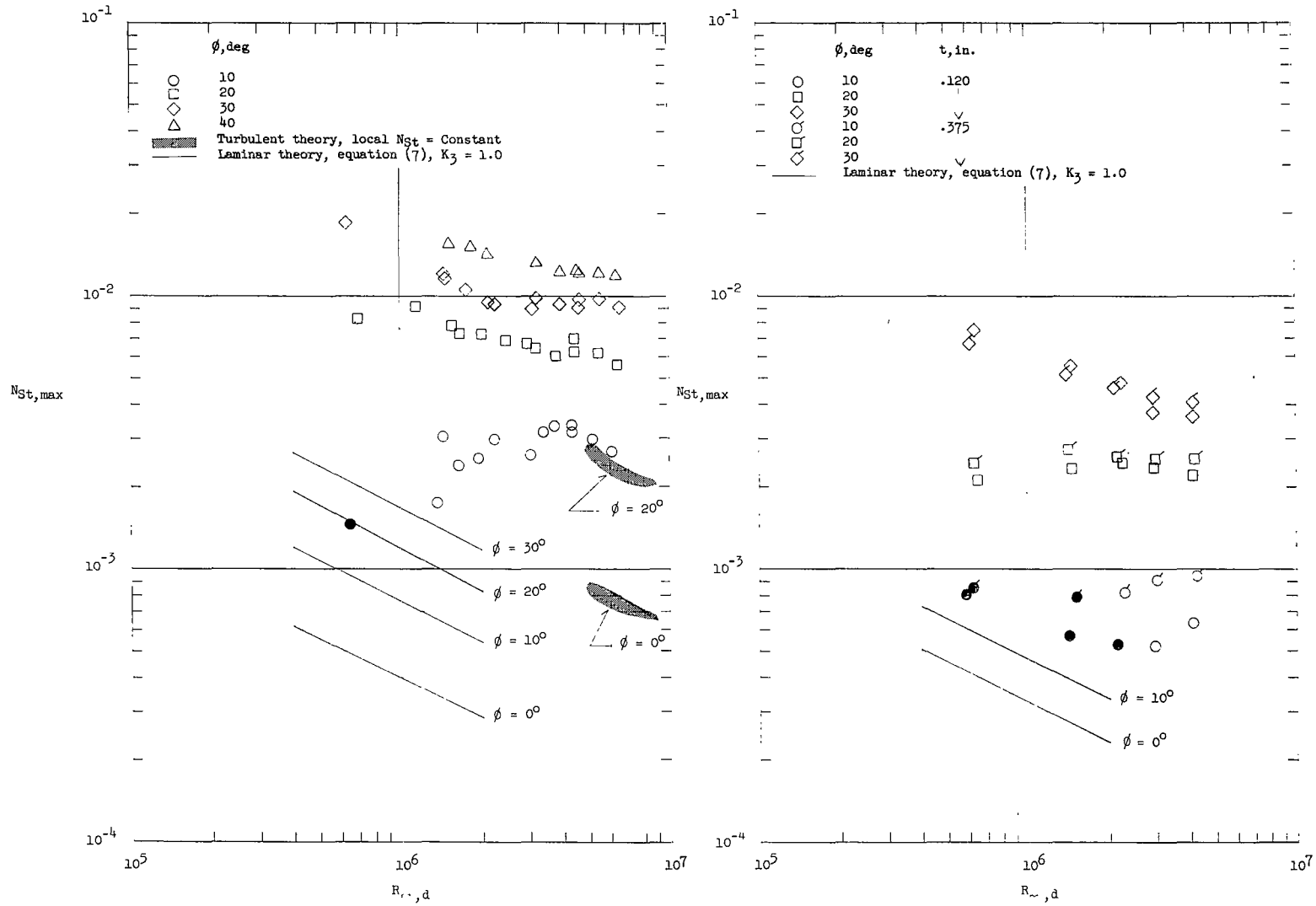

(a) Sharp leading edge.

(b) Blunt leading edge.

Figure 28.- Effects of Reynolds number variation on maximum Stanton number measured on wedges mounted on sharp- and blunt-leading-edge flat plate. Solid symbols denote approximate laminar conditions at end of wedge.

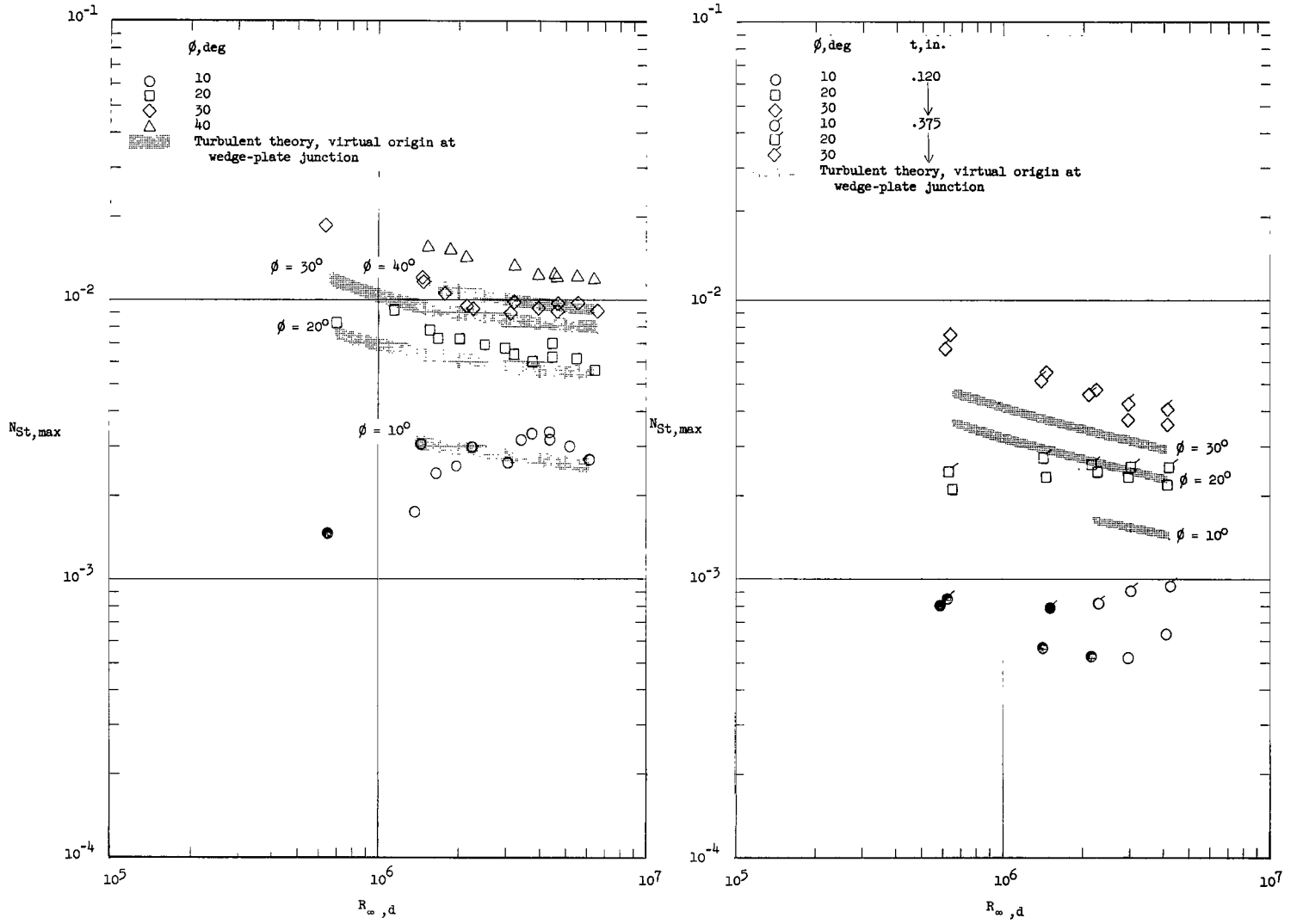

(a) Sharp leading edge.

(b) Blunt leading edge.

Figure 29.- Comparison of maximum Stanton number measured on wedges mounted on sharp- and blunt-leading-edge flat plates with turbulent theory ("virtual origin" at junction of wedge and plate). Solid symbols denote approximate laminar conditions at end of wedge.

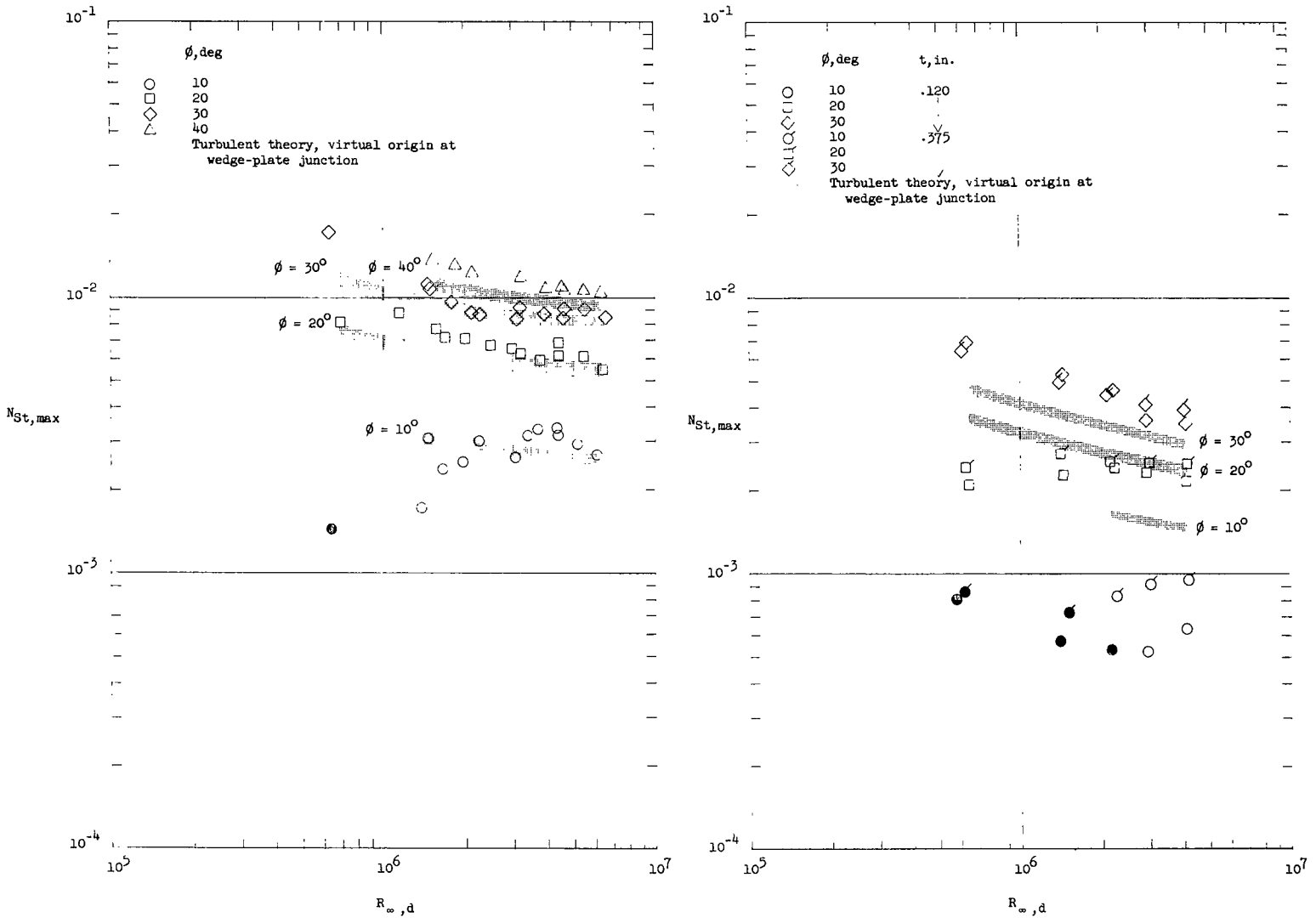

(a) Sharp leading edge.

(b) Blunt leading edge.

Figure 30.- Comparison of maximum Stanton number on wedges calculated from experimental data (with a local Mach number determined by a total pressure predicted by inviscid considerations and local measured pressures) with turbulent theory. Solid symbols denote laminar conditions at end of wedge.

3/18/87

"The aeronautical and space activities of the United States shall be conducted so as to contribute . . . to the expansion of human knowledge of phenomena in the atmosphere and space. The Administration shall provide for the widest practicable and appropriate dissemination of information concerning its activities and the results thereof."

—NATIONAL AERONAUTICS AND SPACE ACT OF 1958

NASA SCIENTIFIC AND TECHNICAL PUBLICATIONS

TECHNICAL REPORTS: Scientific and technical information considered important, complete, and a lasting contribution to existing knowledge.

TECHNICAL NOTES: Information less broad in scope but nevertheless of importance as a contribution to existing knowledge.

TECHNICAL MEMORANDUMS: Information receiving limited distribution because of preliminary data, security classification, or other reasons.

CONTRACTOR REPORTS: Technical information generated in connection with a NASA contract or grant and released under NASA auspices.

TECHNICAL TRANSLATIONS: Information published in a foreign language considered to merit NASA distribution in English.

TECHNICAL REPRINTS: Information derived from NASA activities and initially published in the form of journal articles.

SPECIAL PUBLICATIONS: Information derived from or of value to NASA activities but not necessarily reporting the results of individual NASA-programmed scientific efforts. Publications include conference proceedings, monographs, data compilations, handbooks, sourcebooks, and special bibliographies.

Details on the availability of these publications may be obtained from:

SCIENTIFIC AND TECHNICAL INFORMATION DIVISION

NATIONAL AERONAUTICS AND SPACE ADMINISTRATION

Washington, D.C. 20546